AD-A164 321 IMPROVEMENT OF END BOUNDARY CONDITIONS FOR OFF-AXIS 1/2
TENSION SPECIMEN USE(U) AIR FORCE INST OF TECH
WRIGHT-PATTERSON AFB OH SCHOOL OF ENGI... S M CRON
UNCLASSIFIED DEC 85 AFIT/GAE/AA/85D-3 F/G 20/11 NL

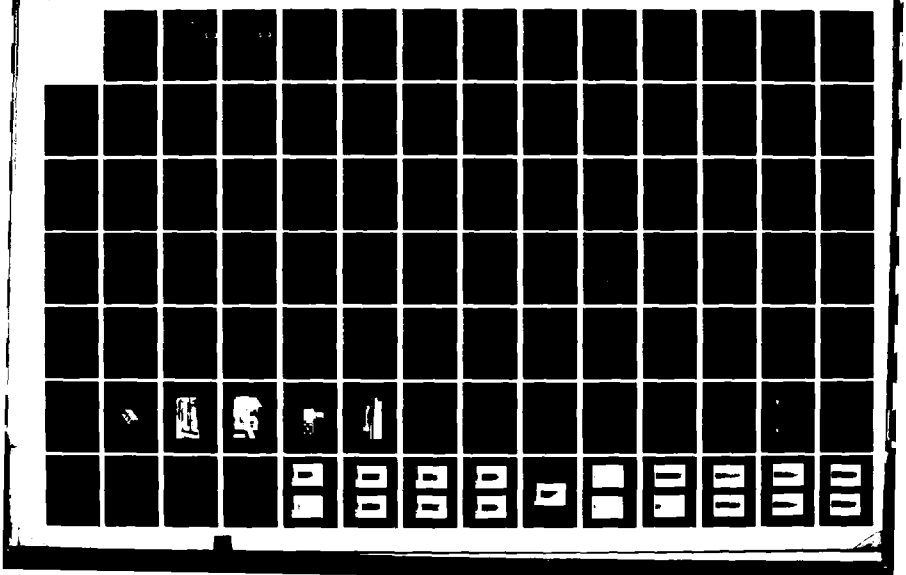

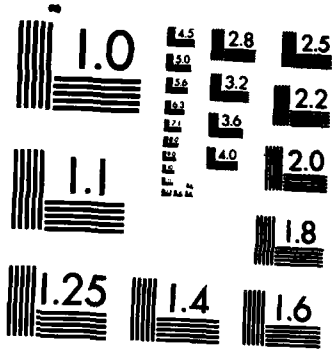

MICROCOPY RESOLUTION TEST CHART
NATIONAL BUREAU OF STANDARDS-1963-A

AD-A164 321

DTIC
ELECTE
FEB 14 1986
S D
D

"Original contains color plates: All DTIC reproductions will be in black and white"

IMPROVEMENT OF END BOUNDARY CONDITIONS FOR OFF-AXIS TENSION SPECIMEN USE

THESIS

Steven M. Cron
Second Lieutenant, USAF

AFIT/GAE/AA/85D-3

DTIC FILE COPY

"Original contains color plates: All DTIC reproductions will be in black and white"

DEPARTMENT OF THE AIR FORCE
AIR UNIVERSITY
AIR FORCE INSTITUTE OF TECHNOLOGY

Wright-Patterson Air Force Base, Ohio

86 2 14 01

AFIT/GAE/AA/85D-3

DTIC
ELECTE
FEB 1 4 1986
S D
D

IMPROVEMENT OF END BOUNDARY CONDITIONS FOR OFF-AXIS TENSION SPECIMEN USE

THESIS

Steven M. Cron
Second Lieutenant, USAF

AFIT/GAE/AA/85D-3

Original contains color plates: All DTIC reproductions will be in black and white

Approved for public release; distribution unlimited

AFIT/GAE/AA/85D-3

IMPROVEMENT OF END BOUNDARY CONDITIONS FOR OFF-AXIS TENSION SPECIMEN USE

THESIS

Presented to the Faculty of the School of Engineering
of the Air Force Institute of Technology
Air University
In Partial Fulfillment of the
Requirements for the Degree of
Master of Science in Aeronautical Engineering

Steven M. Cron, B.S.
Second Lieutenant, USAF

December 1985

Accesion For
NTIS CRA&I ☒
DTIC TAB ☐
Unannounced ☐
Justification .....
By .....
Dist ibution /
Availability Codes
Dist | Avail and / or Special
A-1

Approved for public release; distribution unlimited

QUALITY INSPECTED 3

Acknowledgments

I would like to express my gratitude to my thesis advisor Professor A. N. Palazotto for his expert advice and genuine concern, manifested throughout the course of this effort. I would also like to express my thanks to Dr. R. S. Sandhu of the Flight Dynamics Laboratory for supplying not only the idea for this study but much of the inspiration and insight needed to carry it through to completion. I would also like to thank John Pappas of the Flight Dynamics Laboratory for helping in the experimental phases of the study.

Finally, I wish to thank my wonderful wife Teresa for her loving concern and understanding attitude, without which I would have been at a great loss.

Steven M. Cron

Table of Contents

	Page
Acknowledgments	ii
List of Figures	v
List of Tables	viii
Abstract	ix
1. Introduction	1
1.1 Background	1
1.2 Purpose	7
2. Theory	8
2.1 Introduction	8
2.2 Machromechanical Behavior of the Off-Axis Specimen	8
2.3 Linear Finite Element Theory	15
2.4 Nonlinear Finite Element Theory	18
2.5 Failure Criteria	27
3. Analysis	31
3.1 Introduction	31
3.2 Specimen Geometry	31
3.3 Finite Element Modeling	36
3.4 Parametric Analysis	40
3.5 Nonlinear Analysis	49
4. Experimentation	51
4.1 Introduction	51
4.2 Specimen Fabrication	51
4.3 Basic Material Property Tests	56
4.4 Off-Axis Tension Tests	58
5. Results and Discussion	67
5.1 Introduction	67
5.2 Results of Linear Parametric Study	67
5.3 Qualitative Assessment of Stress Uniformity	72
5.4 Results of the Nonlinear Analysis	90
5.5 Comparison of Analytical and Experimental Stress-Strain Responses	92

Page

5.6 Comparison of Analytical and Experimental Failure Data 98

6. Conclusions 107

Appendix A: Stiffness and Compliance Matrices . . . 109

Appendix B: Experimental Stress-Strain Curves . . . 111

Appendix C: Engineering Elastic Constants 120

Bibliography 121

Vita 123

List of Figures

Figure		Page
2.1	Deformed Shape of the Off-Axis Specimen	9
2.2	Constant Strain Triangle Element	16
2.3	Graphical Illustration of One-Dimensional Nonlinear Response	23
2.4	Strain (ε_2) Under Biaxial Stress Field (σ_1,σ_2) .	26
2.5	Comparison of Various Strength Theories	30
3.1	Specimen Geometry	32
3.2	Shear Coupling Ratio, η_{xy}	34
3.3	Fine Mesh Finite Element Model with Typical Applied Displacements	39
3.4	Finite Element Models used for Convergence . . .	41
3.5	Plot of Axial Stress Along Specimen Centerline to Show Convergence	42
3.6	Plan View of End of Specimen	43
3.7	Differential Stress, $\Delta\sigma_x$, versus Pin Position, D_p, for the 10° Off-Axis Specimen	46
3.8	Differential Stress, $\Delta\sigma_x$, versus Pin Position, D_p, for the 14° Off Axis Specimen	47
3.9	Minimum Differential Stress, $\Delta\sigma_x$, for Given Amount of Clamping	48
4.1	0°, 90°, and ±45° Tension Test Specimens	54
4.2	Off-Axis Tension Specimens	55
4.3	Rosette Strain Gage Numbering and Orientation .	57
4.4	Off-Axis Test Fixture	59
4.5	Fixture and Specimen in Instron Machine	60
4.6	Close Up of Pin and Clamp	61

Page

4.7 Close up of Clamp and Specimen 62

4.8 Fixture for Aligning Clamp and Specimen While Being Tightened 63

5.1 Displaced Finite Element Model with $D_c = D_p = 1.75"$ 70

5.2 Displaced Finite Element Model with $D_c = 1.0"$, $D_p = 0.25"$ 71

5.3 Axial Stress, σ_x, Contours 73

5.4 14° Specimens Coated with Photoelastic Plastic at Various Loads 76

5.5 10° Specimens Coated with Photoellastic Plastic at Various Loads 81

5.6 Failed 10° Off-Axis Specimens 88

5.7 Failed 14° Off-Axis Specimens 89

5.8 Variation in $\Delta\sigma_x$ as Load is Applied 91

5.9 Experimental-Analytical Stress-Strain Curves for 10° Off-Axis 93

5.10 Experimental-Analytical Stress-Strain Curves for 14° Off-Axis 94

5.11 Experimental-Analytical Shear Stress-Strain Curves 97

5.12 Location of First Elements Predicted to Fail . . 101

5.13 Effect of Variation in m Parameter on Failure Criteria for 10° Off-Axis Specimen 102

5.14 Effect of Variation in m Parameter on Failure Criteria for 14° Off-Axis Specimen 103

5.15 Effect of Variation in $\bar{R}_6$ on Failure Criteria for 10° Off-Axis Specimen 105

5.16 Effect of Variation in $\bar{R}_6$ on Failure Criteria for 14° Off-Axis Specimen 106

Page

B.1 Experimental σ_1 vs. ε_1 for graphite/epoxy 112

B.2 Experimental σ_2 vs. ε_2 for graphite/epoxy 113

B.3 Experimental τ_{12} vs. γ_{12} for graphite/epoxy . . . 114

B.4 Experimental ν_{12} vs. ε_1 for graphite/epoxy . . . 115

B.5 Experimental σ_1 vs. ε_1 for glass/epoxy 116

B.6 Experimental σ_2 vs. ε_2 for glass/epoxy 117

B.7 Experimental τ_{12} vs. γ_{12} for glass/epoxy 118

B.8 Experimental ν_{12} vs. ε_1 for glass/epoxy 119

List of Tables

Table		Page
2.1	Stress-Strain Curves and Corresponding Experimental Tests	19
4.1	Stress-Strain Curves and Corresponding Experimental Tests	53
5.1	Analytical and Experimental Strains at the Experimental Failure Loads	99

AFIT/GAE/AA/85D-3

Abstract

Inaccuracies in using the off-axis tension test are caused by the nonuniform stresses produced by the end constraints. The purpose of this ~~study~~ is to show that these nonuniformities can be virtually eliminated by adjusting the amount of tab clamping and selectively locating the point about which the clamp may rotate. A second phase of the study is to conduct a limited verification of a strain energy failure criteria that can account for the material nonlinearity found in composites.

Determination of the ideal amount of clamping and point of rotation was carried out using a linear finite element method. The nonlinear behavior of the specimen was simulated using a nonlinear finite element method. The failure criteria was used in conjunction with the nonlinear finite element algorithm in determining failure. Experimentation was also carried out to verify the finite element solutions.

The results indicate that a nearly uniform state of stress can be produced with ideal tab clamping and rotation. The results indicate that the nonlinear behavior of the specimen was accurately predicted by the nonlinear finite element method but that the failure state predicted by the failure criteria was in error. Suggestions are made for improving the accuracy of the failure criteria.

IMPROVEMENT OF END BOUNDARY CONDITIONS FOR OFF-AXIS TENSION SPECIMEN USE

CHAPTER 1

INTRODUCTION

1.1. Background

In the off-axis tension test specimen, unidirectional composite material fibers are oriented at an angle that is neither 0° nor 90° to the specimen axis. If the load is introduced uniaxially with respect to the specimen axis, normal and shearing stresses will develop in the specimen relative to the material axes 1 and 2. Thus, it would seem, the off-axis tension test is a very simple means of testing fiber-reinforced composites under a biaxial state of stress. Furthermore, since available experimental data confirm the assumption that unidirectional composites are orthotropic i.e. normal and shear stresses are uncoupled, the off-axis test would appear to be a very convenient

method for testing the intralaminar (in-plane) shear properties of composites.

The usefulness of the off-axis tension test is somewhat diminished when one attempts to load an off-axis specimen with a truly uniform axial load. Since the off-axis specimen is anisotropic with respect to the specimen axes, a uniform axial stress, σ_x, causes not only normal and transverse strains but also shearing strains relative to the specimen axes. Consequently, any resistance to deformation due to end constraints such as tabs or clamps will cause the axial stress, σ_x, to become nonuniform. This, of course, also causes the biaxial stress field to become nonuniform. Thus, any test results obtained using an off-axis specimen will most likely be influenced by this nonuniformity. Though the influence of end constraints is present to some extent in all tensile tests, it is magnified in the case of off-axis specimens because of the rotational tendency caused by the shear coupling effects (1). Various techniques aimed at eliminating this difficulty have been suggested. These techniques will be discussed in the next few paragraphs in approximately chronological order.

Tsai (2 & 3) used off-axis specimens to experimentally verify his strength criteria. The criteria is based on the assumption that the axial stress, σ_x, be uniform. He found that specimens of uniform cross section and low fiber

orientation angles had a tendency to fail under the rigid grips used to apply the load. To insure that failure occurred in the test section, he reduced the test section in a "dog-bone" fashion. In a later effort, Lauraitis (4) used off-axis specimens to verify a strength criteria based on linear elastic fracture mechanics. For the same reasons given by Tsai, she reduced the test section cross section using a continuous large radius of curvature.

Pagano and Halpin (5) presented analytical and experimental evidence of the adverse effect of conventional (non-rotating) clamping devices on the stress field in an off-axis specimen. In the study, they presented a solution to a boundary value problem that approximated the off-axis specimen. Experiments with nylon reinforced rubber were also carried out to qualitatively verify the analytical results. The study showed that significant nonuniform in-plane bending stresses are produced in the off-axis specimen due to end constraints. After allowing limited rotation of the clamps, they concluded that the gripping restraint was the dominant factor in perturbing the stress field and that clamp rotation was of little importance. They also concluded that increasing the length of the specimen would produce a sufficiently uniform state of stress to obtain elastic moduli. To obtain strength data, however, they pointed out that some modification of the ends of the specimen would be required.

Rizzo (1) used the finite element method to investigate the effect on the off-axis specimen stress field of completely rigid clamping with and without end rotation. He observed a marked improvement in stress uniformity when clamp rotation was permitted. He also restated the observation made by Halpin and Pagano that for long specimens (length/width > 10) the stress field at the center of the specimen is uniform regardless of the end clamping arrangement. Two additional, somewhat subtle, observations made were that resistance to Poisson type contraction near the tabs has a major influence on the test's inaccuracies and that changing the pivot point may alter the above situtation significantly. No analytical or experimental data was given, however, to support these last two observations.

Wu and Thomas (6) designed a test fixture which allowed rotation of the end clamps about a point centered at the edge of the clamp area. With this fixture, they tested 15° off-axis specimens with length to width ratios of 5, 4, and 2.5. They acquired strain data from nine strain gages spaced relatively evenly across the specimen. They concluded from their investigation that with their rotating clamp fixture and within the length to width ratios used, the state of strain at low stress levels appeared to be relatively uniform. They also suggested that putting a compliant material between the specimen and

the clamp could reduce the restraining effect of the rigid clamps and that whether or not the fixture could provide the desired degree of uniformity at the high stress levels required in strength testing remained to be established.

Richards et. al. (7) conducted tests using 45° specimens with three inch tapered tabs, length to width ratios of 12, and loaded without any end rotation allowed, which verified the findings of Halpin and Pagano concerning the effect of large length to width ratios on uniformity.

Cole and Pipes (8) examined the off-axis tensile test in order to determine its utility as a biaxial characterization specimen for boron epoxy. Attempting to insure a uniform test section stress field, they used long specimens with the fiber orientation of highly tapered end tabs the same as the specimen fibers. The choice of tab fiber orientation was supported only by a simple intuitive argument. A very important discovery made in the course of their study was the fact that the normal and shear responses of boron epoxy remain uncoupled through the nonlinear regime. This observation prompted the advocation of the off-axis specimen for use in determining shear stress-strain response. Chamis and Sinclair (9) analyzed the 10° specimen explicitly for that purpose. Their test fixture allowed rotation of the end-clamps about points past the ends of the specimen. Chang et. al. (10) tested a modified version of the Chamis and Sinclair fixture which

had the clamp rotation point centered at the tapered edge of the tab. This modification appeared to improve stress uniformity.

Sandhu and Sendeckyj (11) conducted an extensive parametric study to determine a tab fiber orientation and tab inclination angle which produced the most uniform state of stress in off-axis specimens with off-axis angles ranging from 4° to 80°. The study was carried out with a linear finite element program for both rotating and non-rotating clamps. They found that matching the tab fiber orientation with the specimen fiber orientation, as suggested in Ref. (8), did in fact reduce the nonuniformity of the stress field. They also found that, using an optimized tab fiber angle and tab inclination angle along with rotating clamps, a nearly uniform state of stress could be attained. It is important to note that the specimen design in their study did not rely on large length to width ratios for achieving a uniform state of stress. To verify the results of the parametric study, experiments with the above optimized tab parameters were carried out. The results of the experiments were then plotted against the response predicted by a nonlinear finite element program incorporating appropriate boundary conditions.

1.2. Purpose

The purpose of this study is to show that a state of nearly uniform stress can be produced in a standard geometry off-axis specimen by adjusting the amount of tab clamping and selectively locating the point about which the clamp will rotate. Since in the analysis phase of the study, a uniform state of stress in the entire gage length (area between the tabs) will be the design objective, this study will result in a test method that will be useful not only for obtaining elastic moduli but also for conducting strength tests.

A secondary purpose of this study is a limited verification of the strain energy failure criteria presented by Sandhu in Ref. (12 & 13).

The present study will be an extension of the work done by Sandhu and Sendeckyj. The essential difference between the two studies is the parameters that are allowed to vary. In Sandhu and Sendeckyj's work, the parameters were fiber orientation angle and tab inclination angle whereas in the present study the parameters are the amount of clamping and the point about which the clamped area will rotate.

CHAPTER 2

THEORY

2.1. Introduction

In this section, the theory used to describe the response of composite laminates, as it relates to the off-axis specimen, will be discussed. Second, a formulation of the finite element methods used (linear and nonlinear) will be presented. Finally, the failure criteria to be verified will be presented.

2.2. Macromechanical Behavior of the Off-Axis Specimen

If a uniform axial stress, σ_x, is applied to an off-axis specimen, as shown in Fig. 2.1, normal and transverse stresses will develop relative to the material axis system. Recalling from elementary mechanics of materials, the transformation equations relating the stresses in an

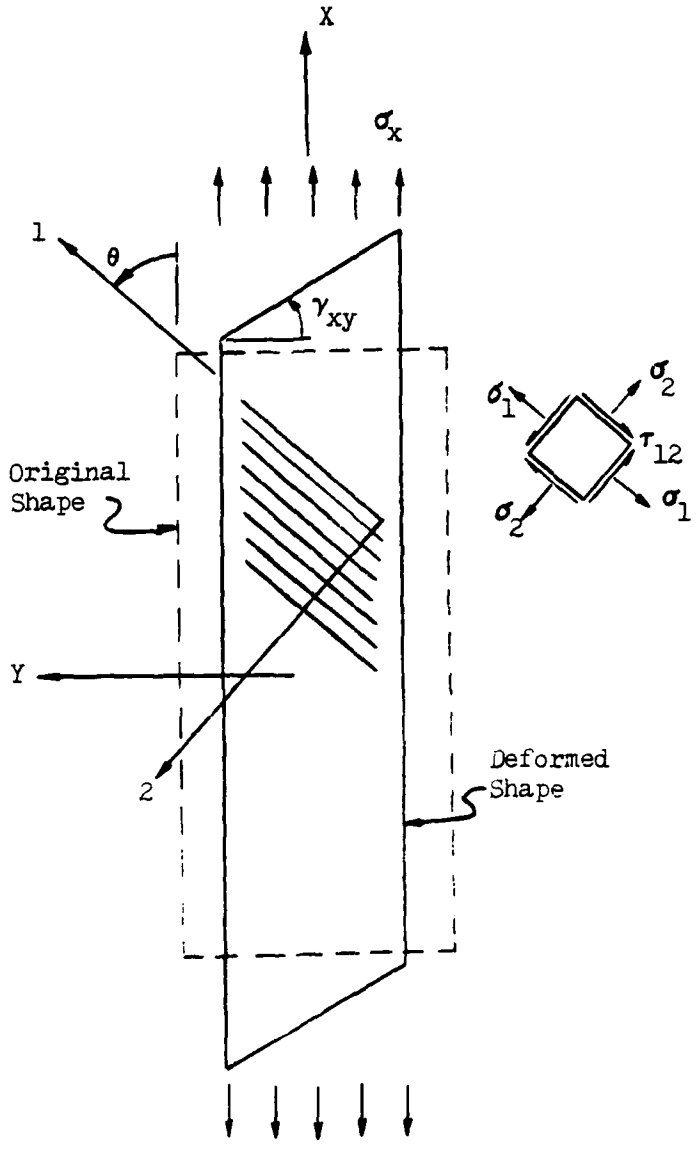

Fig. 2.1 Deformed Shape of the Off-Axis Specimen

X,Y coordinate system to the stresses in a 1,2 coordinate system,

$$\begin{Bmatrix} \sigma_1 \\ \sigma_2 \\ \tau_{12} \end{Bmatrix} = \begin{bmatrix} m^2 & n^2 & 2nm \\ n^2 & m^2 & -2nm \\ -nm & nm & m^2 - n^2 \end{bmatrix} \begin{Bmatrix} \sigma_x \\ \sigma_y \\ \tau_{xy} \end{Bmatrix} \qquad (2.1)$$

or,

$$\{\sigma\} = [T]\{\bar{\sigma}\} \qquad (2.2)$$

where,

$$n = \sin\theta \quad \text{and} \quad m = \cos\theta \qquad (2.3)$$

We find for the uniaxially loaded off-axis specimen,

$$\sigma_y = \tau_{xy} = 0$$

giving,

$$\begin{aligned} \sigma_1 &= m^2\sigma_x \\ \sigma_2 &= n^2\sigma_x \\ \tau_{12} &= -nm\sigma_x \end{aligned} \qquad (2.4)$$

Obviously then, if we can find a way to load the off-axis specimen with a truly uniform axial stress, we will have a very convenient method of testing unidirectional composite materials under a uniform biaxial state of stress.

Note however (see Fig. 2.1), that a shearing strain γ_{xy} is induced relative to the specimen axes when σ_x is applied. This is due to the fact that the off-axis specimen is anisotropic with respect to the specimen axes, i.e.,

$$\begin{Bmatrix} \varepsilon_x \\ \varepsilon_y \\ \gamma_{xy} \end{Bmatrix} = \begin{bmatrix} \bar{S}_{11} & \bar{S}_{12} & \bar{S}_{16} \\ \bar{S}_{12} & \bar{S}_{22} & \bar{S}_{26} \\ \bar{S}_{16} & \bar{S}_{26} & \bar{S}_{66} \end{bmatrix} \begin{Bmatrix} \sigma_x \\ \sigma_y \\ \tau_{xy} \end{Bmatrix} \qquad (2.5)$$

It should be pointed out that the stress-strain response is not anisotropic with respect to the material axes, rather it is orthotropic, i.e.,

$$\begin{Bmatrix} \varepsilon_1 \\ \varepsilon_2 \\ \gamma_{12} \end{Bmatrix} = \begin{bmatrix} S_{11} & S_{12} & 0 \\ S_{12} & S_{22} & 0 \\ 0 & 0 & S_{66} \end{bmatrix} \begin{Bmatrix} \sigma_1 \\ \sigma_2 \\ \tau_{12} \end{Bmatrix} \qquad (2.6)$$

Thus, the anisotropic behavior observed relative to the specimen axes is due solely to the transformation of the orthotropic stress-strain relations through an angle θ,

$$[\bar{S}] = [T]^T[S][T] \qquad (2.7)$$

where, [S] and [T] are as given above. All the terms of the $[\bar{S}]$ and [S] matrices are given explicitly in appendix A.

In order to physically load a specimen to the high load levels required for most testing, some sort of clamping device (such as thosse found in an Instron or MTS machine) will undoubtedly be used. Furthermore, the ends of the specimen may be reinforced by tabs of one sort or another. If the loading device and end-tabs provide any resistance to the natural deformations associated with a

uniform σ_x, the axial and biaxial stress fields will become nonuniform.

The shear coupling ratio (14:22),

$$\eta_{xy} = \bar{S}_{16}/\bar{S}_{11} \tag{2.8}$$

gives a measure of the degree to which end-rotation will occur as a function of off-axis angle. The greater the possible rotation, the greater the effect of the clamp. If we set the derivative of η_{xy} with respect to the off-axis angle equal to zero, we can solve for the angle for which shear coupling is a maximum.

$$d\eta_{xy}/d\theta = (\bar{S}_{11}\bar{S}'_{16} - \bar{S}_{16}\bar{S}'_{11})/(\bar{S}_{11})^2 = 0 \tag{2.9}$$

where the primes denote differentiation with respect to θ. The terms in Eq. (2.9) are,

$$\begin{aligned}
\bar{S}_{11} &= m^4S_{11} + m^2n^2(2S_{12}+S_{66}) + n^4S_{22} \\
d\bar{S}_{11}/d\theta &= 2mn^3(2S_{22}-2S_{12}-S_{66}) - 2m^3n(2S_{11}-2S_{12}-S_{66}) \\
\bar{S}_{16} &= nm^3(2S_{11}-2S_{12}-S_{66}) - n^3m(2S_{22}-2S_{12}-S_{66}) \\
d\bar{S}_{16}/d\theta &= m^4(2S_{11}-2S_{12}-S_{66}) - 6n^2m^2(S_{11}+S_{22}-2S_{12}-S_{66}) \\
&\qquad + n^4(2S_{22}-2S_{12}-S_{66})
\end{aligned} \tag{2.10}$$

Since $(\bar{S}_{11})^2$ is positive and finite, we need only solve

$$\bar{S}_{11}\bar{S}'_{16} - \bar{S}_{16}\bar{S}'_{11} = 0 \tag{2.11}$$

for θ. This equation will be used subsequently to determine the off-axis angle that maximizes the shear

coupling ratio for the material used in this study.

The work done by Sandhu (12) and Daniel (15) and reported by Whitney et. al. (14:192) indicate that the off-axis specimen does not yield as much of the shear stress-strain curve as does the (±45) laminate commonly used for obtaining shear stress-strain curves for graphite/epoxy. A possible reason for this phenomenon is that the method of load introduction (rigid clamps with little or no rotation) cause stress concentrations near the grips that in turn cause premature failure. In this study it will be observed if the near elimination of such stress concentrations will allow the off-axis specimen to yield a shear stress-strain curve closer to that of the (±45) laminate.

Refs. (9) and (11) point out that the fiber orientation of an off-axis specimen used for obtaining shear stress-strain curves must be chosen such that the contribution made by the normal stresses towards failure is a minimum or equivalently, the contribution made by shear stresses is a maximum. If we look at the Tsai-Hill failure criteria,

$$(\sigma_1/X)^2 + \sigma_1\sigma_2/(X)^2 + (\sigma_2/Y)^2 + (\tau_{12}/S)^2 = 1 \quad (2.12)$$

where X, Y, and S are the normal, transverse, and shear strengths in tension, respectively, we see that the contribution made by shear is,

$$Z_s = (\tau_{12}/S)^2 \quad (2.13)$$

Recalling from Eq. 2.4,

$$\tau_{12} = -nm\sigma_x \qquad \sigma_1 = m^2\sigma_x \qquad \sigma_2 = n^2\sigma_x \qquad (2.14)$$

we can rewrite Eq. (2.12) as,

$$\sigma_x^2 = 1/(m^4/X^2 + (1/S^2 - 1/X^2)m^2n^2 + n^4/Y^2) \qquad (2.15)$$

Thus, substituting Eq. (2.15) into Eq. (2.13) we obtain,

$$Z_s = 1/((S\ \cot\theta/X)^2 + (1 - (S/X)^2) + (S\ \tan\theta/Y)^2) \qquad (2.16)$$

Now Z_s attains a maximum value when,

$$dZ_s/d\theta = 0 \qquad (2.17)$$

which, on simplification leads to,

$$\tan\theta' = \sqrt{(Y/X)} \qquad (2.18)$$

where θ' is the off-axis angle for which Z_s attains a maximum. This equation will be used subsequently to determine the value of θ' for the material used in this study.

It is important to note that all of the derivations to this point have been based on the assumption that the material under consideration remains linearly elastic to failure. This is not the case, however. In reality, the shear response of graphite/epoxy, the material system used in this study, is highly nonlinear. Ref. (11) showed, using a fully nonlinear finite element technique, that the value of θ' corresponding to maximum shear contribution to failure was 13° whereas, using the linear analysis shown above, the value of θ' was 11.38°. This adjustment must be

taken into consideration when using Eq. (2.18).

2.3. Linear Finite Element Theory

The linear finite element program used in this study is based on the constant strain triangle (see Fig. 2.2 for coordinates). The assumed element displacement field is linear in x and y:

$$\begin{Bmatrix} u(x,y) \\ v(x,y) \end{Bmatrix} = \begin{bmatrix} 1 & x & y & 0 & 0 & 0 \\ 0 & 0 & 0 & 1 & x & y \end{bmatrix} \begin{Bmatrix} a_1 \\ a_2 \\ a_3 \\ a_4 \\ a_5 \\ a_6 \end{Bmatrix} \tag{2.19}$$

The strain are expressed by,

$$\{\bar{\varepsilon}\} = \begin{Bmatrix} \varepsilon_x \\ \varepsilon_y \\ \gamma_{xy} \end{Bmatrix} = [B]\{d\} = [B] \begin{Bmatrix} u_1 \\ v_1 \\ u_2 \\ v_2 \\ u_3 \\ v_3 \end{Bmatrix} \tag{2.20}$$

where {d} is the nodal displacement vector and,

$$[B] = 1/2A \begin{bmatrix} (y_2-y_3) & 0 & (y_3-y_1) & 0 & (y_1-y_2) & 0 \\ 0 & (x_3-x_2) & 0 & (x_1-x_3) & 0 & (x_2-x_1) \\ (x_3-x_2) & (y_2-y_3) & (x_1-x_3) & (y_3-y_1) & (x_2-x_1) & (y_1-y_2) \end{bmatrix} \tag{2.21}$$

where A is the area of the triangle and x_i and y_i are the x

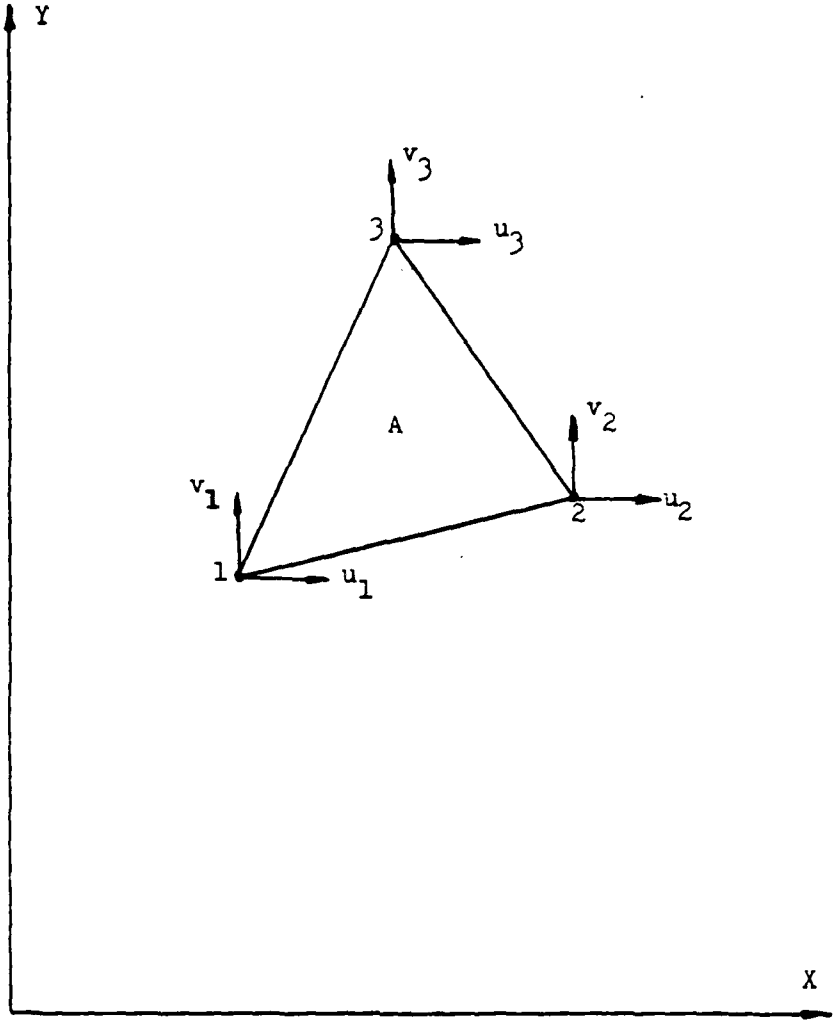

Fig. 2.2 Constant Strain Triangle Element

and y coordinates of the ith node.

For an orthotropic lamina whose principal direction is oriented at an angle θ to the X and Y directions, the stresses are related to the strains by,

$$\begin{Bmatrix} \sigma_x \\ \sigma_y \\ \tau_{xy} \end{Bmatrix} = [\bar{Q}] \begin{Bmatrix} \varepsilon_x \\ \varepsilon_y \\ \gamma_{xy} \end{Bmatrix} \tag{2.22}$$

where,

$$[\bar{Q}] = [T][Q][[T]^{-1}]^T \tag{2.23}$$

where [Q] are the orthotropic plane stress stiffness coefficients.

We can now write the element stiffness matrix for the constant strain triangle,

$$[k] = \int_A [B]^T[\bar{Q}][B]t\,dA \tag{2.24}$$

Since the thickness and all of the terms of [B] and $[\bar{Q}]$ are constants, the integral reduces to,

$$[k] = [B]^T[\bar{Q}][B]tA \tag{2.25}$$

Now allowing for n layers of orthotropic material through the thickness we can express the equivalent element stiffness matrix as,

$$[k_{eq}] = A \sum_{i=1}^{n} [B]^T[\bar{Q}]_i[B]t_i \tag{2.26}$$

where i denotes the ith layer. Thus, loads and displacements are related, on an element basis by,

$$\{f\} = [k_{eq}]\{d\} \tag{2.27}$$

Note that even though multiple layers have been allowed through the thickness of the element, the layers have common nodes and thus no strain or displacement variation is being permitted through the thickness.

2.4. Nonlinear Finite Element Theory

The effect of material nonlinearity on the uniformity of the off-axis specimen stress field is analyzed using a nonlinear finite element technique based on the constant strain element described in the preceding section. A complete development of the technique is given in Ref. (12). In this technique,

$$d\{f\} = [k(\varepsilon)_{eq}]d\{d\} \tag{2.28}$$

where $d\{f\}$, $d\{d\}$, and $[k(\varepsilon)_{eq}]$ are the increments of load and displacement and the current stiffness matrix, respectively. As shown, the stiffness matrix depends on the current strain level. This dependence comes about through the $[\bar{Q}]$ matrix. Recall the equation for $[k_{eq}]$, (Eq. 2.26),

$$[k_{eq}] = A \sum_{i=1}^{n} [B]^T[\bar{Q}]_i[B]t_i \tag{2.29}$$

One can see that $[k_{eq}]$ is calculated using $[\bar{Q}]_i$ (See appendix A for the terms of $[\bar{Q}]$). If the material being analyzed exhibits material nonlinearity, the lamina

material properties (E_1, E_2, G_{12}, ν_{12}) will vary with strain. It follows then, since $[\bar{Q}]_i$ is calculated from these properties, that $[\bar{Q}]_i$ and hence $[k_{eq}]$ will vary with strain as well.

As implied, the material property curves for the material(s) being analyzed are obtained from the experimental stress-strain curves of unidirectional lamina. The curves, and corresponding experimental tests, required for each material, are shown in Table 2.1.

Curve	Experiment
σ_1 vs. ε_1	0° tension
σ_1 vs. ε_1	0° compression
σ_2 vs. ε_2	90° tension
σ_2 vs. ε_2	90° compression
τ_{12} vs. γ_{12}	$\pm 45^\circ$ tension
ν_{12} vs. ε_1	0° tension
ν_{12} vs. ε_1	0° compression

Table 2.1 Stress-Strain Curves and Corresponding Experimental Tests

To make the experimental curves usable by the computer program, they are represented analytically by cubic spline interpolation functions. The material properties curves are thus represented as functions of strain by simple polynomials. With the stress-strain curves in this form,

the tangent moduli (E_1, E_2, G_{12}) can be readily obtained, as functions of strain, by differentiating the appropriate cubic spline functions with respect to strain.

Obviously, the load cannot be applied in a truly continuous manner using a computer program. As indicated in Eq. (2.28), it is applied incrementally. This presents a slight dilemma, however, since $[k_{eq}]$ may vary during a load increment. To overcome this difficulty, a predictor-corrector iterative procedure is utilized. In this procedure $[k_{eq}]$ is initially calculated using material properties that correspond to the state of strain existing at the end of the previous load increment. For the very first increment, engineering linear elastic constants are used.

Having calculated $[k_{eq}]$, corresponding to the end of the previous load increment, a new increment of the load is applied and an increment of displacement, $d\{d\}$, is calculated using Eq. (2.28). Note that when a given load increment is first applied, Eq. (2.28) will take the form,

$$d\{f\}_{n+1} = [k(\varepsilon)_{eq}]_n d\{d\}_{n+1} \qquad (2.30)$$

where n denotes the nth load increment.

$d\{d\}$ can then be used to calculate an increment of strain using a slightly modified version of Eq. (2.20),

$$d\{\bar{\varepsilon}\} = [B]d\{d\} \qquad (2.31)$$

The increment of stress can be calculated from,

$$d\{\bar{\sigma}\}_i = [\bar{Q}]_i d\{\bar{\varepsilon}\} \tag{2.32}$$

were i denotes the ith layer as defined in section 2.3.

Notice that in this last equation it has been assumed that

a. The increment of stress depends upon the strain state and the increment of strain; and

b. The increment of strain is proportional to the increment of stress.

Note that the stress and strain increments in Eqs. (2.31) and (2.32) are relative to the specimen axes X and Y. To obtain the stress and strain increments relative to the material axes, 1 and 2, Eq. (2.1) must be used,

$$d\{\sigma\} = [T]d\{\bar{\sigma}\} \tag{2.33}$$

$$d\{\varepsilon\} = [T]d\{\bar{\varepsilon}\} \tag{2.34}$$

Having computed the increments of stress and strain, new levels of stress and strain are determined by adding the new increments to the levels existing at the end of the previous increment.

A mean level of strain is then computed by averaging the new level of strain with the level of strain existing at the end of the previous load increment. These "average" strains are then used to determine a new set of material properties since, as mentioned above, they are readily obtainable as functions of strain through the cubic spline

functions. This concept will be discussed graphically in a subsequent paragraph.

With the new elastic properties in hand, $[\bar{Q}]$ and hence $[k_{eq}]$ are recalculated. The load increment is then reapplied and the increment of displacement and strain, is recalculated. Note that the same load increment has been reapplied, not an additional one. This procedure is continued, for a given load increment, until the ratio of the change of the strain increment to the strain increment is less that 0.001, i.e.,

$$(d\{\varepsilon\}_{n+1} - d\{\varepsilon\}_n)/d\{\varepsilon\}_n < 0.001 \qquad (2.35)$$

where n denotes the nth reapplication of a given load increment. When Eq. (2.35) is satisfied, a new load increment is applied. The repetitive use of the procedure outlined above generates the predicted stress-strain response of the laminate under consideration.

In Fig. 2.3 an attempt has been made to graphically display how the above procedure is carried out. For clarity a simple case of one-dimensional loading in shear is shown. As shown, an initial strain γ_0 is assumed to exist due to a previous load increment. An increment of the load is then applied and the resulting strain, γ_1, is calculated based on the tangent modulus at point 0. A new modulus is now determined, corresponding to the average of γ_1 and γ_0 (point A). The load is then reapplied and the

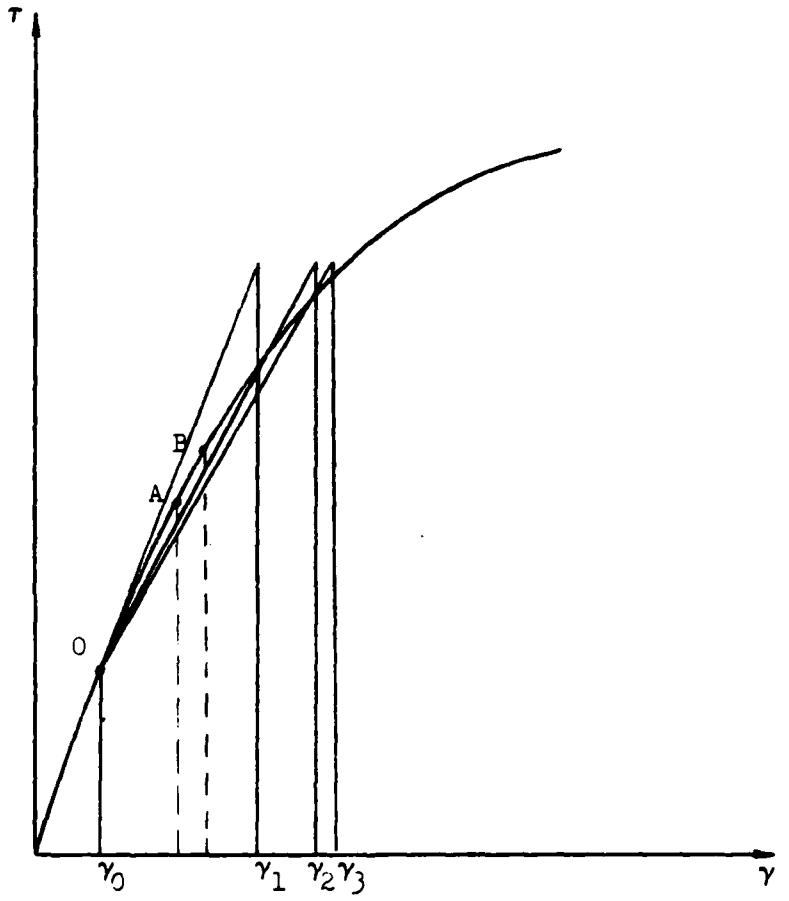

Fig. 2.3 Graphical Illustration of
One-Dimensional Nonlinear Response

strain, γ_2, is calculated based on the modulus at A. Again, the modulus corresponding to the average of γ_2 and γ_0 (point B) is determined and the load reapplied, giving rise to γ_3. For this simple case the procedure is repeated for the given load increment until,

$$(\gamma_{n+1} - \gamma_n)/\gamma_n < 0.001 \qquad (2.36)$$

For graphite/epoxy and glass/epoxy, the materials used in this study, nonlinearity is most pronounced in the shear direction (relative to the material axes) while in the normal and transverse directions the stress-strain response is nearly linear (See appendix B for experimental stress-strain curves). While it might be reasonable to assume the normal and transverse responses to be linear, such an assumption is not made in this study. Any nonlinearity that exists in any of the material property curves will be accounted for. An assumption that is made, however, is that nowhere in the off-axis specimen will the strains be of a large enough negative value to justify using true compression curves as indicated in Table 2.1. Instead, the curves obtained for tension will be used. This assumption was found to be valid when the specimen was analyzed.

In the procedure just described, the lamina biaxial strains (ε_1 and ε_2) are modified before being used to determine the elastic constants from the cubic spline stress-strain curves. This modification is required to

allow for the simultaneous existence of longitudinal and transverse stresses in the lamina whereas in the experimental data only one component of stress is present. Consider the differential element of unidirectional material shown in Fig. 2.4 (from Ref. (12)), subject to biaxial stresses σ_1 and σ_2. Recalling that we have assumed an increment of strain is proportional to an increment of stress we can write,

$$d\varepsilon_1 = d\sigma_1/E_1 - \nu_{12}d\sigma_2/E_1 = d\sigma_1/E_1(1-\nu_{12}(d\sigma_2/d\sigma_1)) \qquad (2.37)$$

$$d\varepsilon_2 = d\sigma_2/E_2 - \nu_{21}d\sigma_1/E_2 = d\sigma_2/E_2(1-\nu_{21}(d\sigma_1/d\sigma_2)) \qquad (2.38)$$

Eqs. (2.37) and (2.38) reveal that it would be erroneous to use $d\varepsilon_1$ or $d\varepsilon_2$, corresponding to the biaxial stress state $d\sigma_1$, $d\sigma_2$, associated with an off-axis specimen, to determine E_1 or E_2 from stress strain curves obtained under simple loading conditions. For example, $d\varepsilon_2$ of equation (2.38) corresponds to the curve ON (Fig. 2.4) on the plane OEHG while the simple stress strain curve OM lies on the plane OEDC. Since stress-strain data similar to ON is not available, we have assumed that simple equivalent strain increments can be computed from the following expressions:

$$d\varepsilon_1\Big|_{eq} = d\sigma_1/E_1 = d\varepsilon_1/(1-\nu_{12}(d\sigma_2/d\sigma_1)) \qquad (2.39)$$

$$d\varepsilon_2\Big|_{eq} = d\sigma_2/E_2 = d\varepsilon_2/(1-\nu_{21}(d\sigma_1/d\sigma_2)) \qquad (2.40)$$

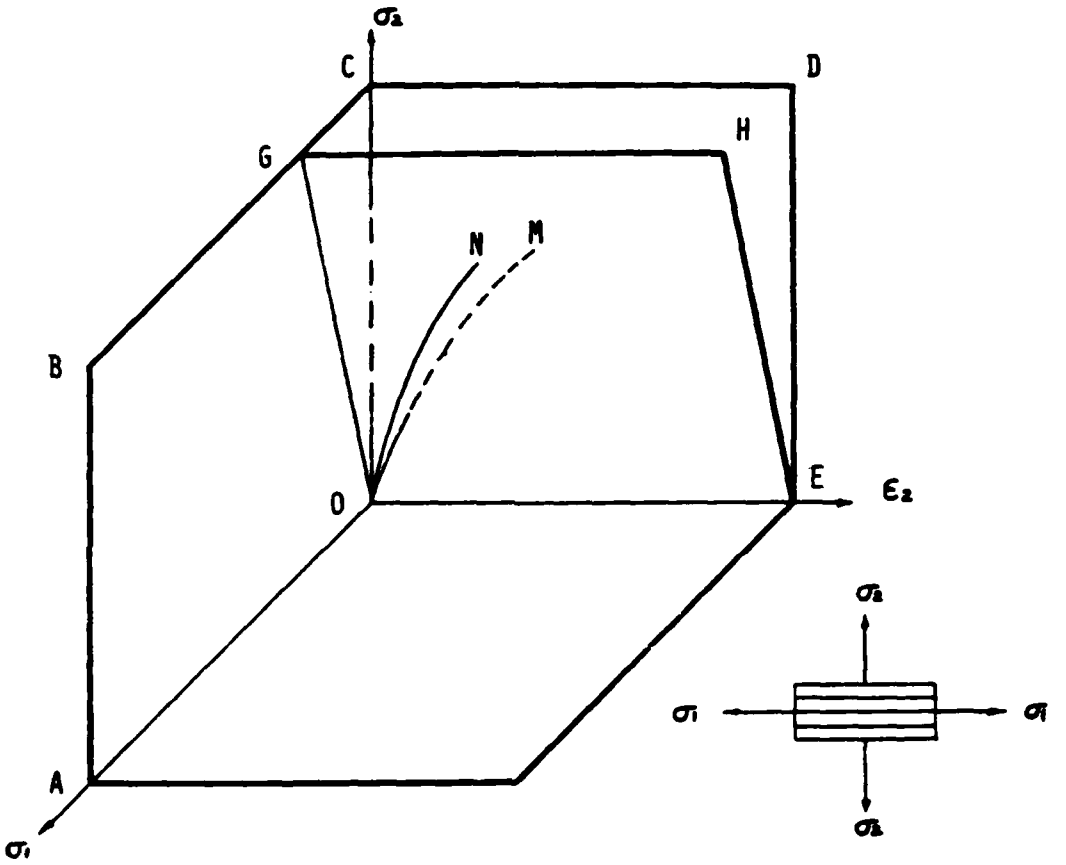

Fig. 2.4 Strain (ϵ_2) Under Biaxial Stress Field (σ_1,σ_2)

The error that would result from using $d\varepsilon_i$ instead of $d\varepsilon_i\big|_{eq}$, can be written from Eqs. (2.39) and (2.40) as,

$$(d\varepsilon_1\big|_{eq} - d\varepsilon_1)/d\varepsilon_1\big|_{eq} = \nu_{12}(d\sigma_2/d\sigma_1) \qquad (2.41)$$

$$(d\varepsilon_2\big|_{eq} - d\varepsilon_2)/d\varepsilon_2\big|_{eq} = \nu_{21}(d\sigma_1/d\sigma_2) \qquad (2.42)$$

From Eq. (2.4) we can write, for the off-axis specimen,

$$d\sigma_1 = m^2 d\sigma_x \qquad (2.43)$$

$$d\sigma_2 = n^2 d\sigma_x \qquad (2.44)$$

which upon substituting into Eqs. (2.41) and (2.42) gives,

$$\nu_{12}(d\sigma_2/d\sigma_1) = \nu_{12}(\tan^2\theta) \qquad (2.45)$$

$$\nu_{21}(d\sigma_1/d\sigma_2) = \nu_{21}(\cot^2\theta) \qquad (2.46)$$

To get a feel for the errors that would result in neglecting this correction let us look at the errors that would arise in a 14° off-axis specimen. For the material properties used in this study we get,

$$\nu_{12}(\tan^2\theta) = 0.0174 = 1.74\ \% \text{ error}$$

$$\nu_{21}(\cot^2\theta) = 0.3514 = 35.14\ \% \text{ error}$$

2.5. Failure Criteria

The incremental loading technique described in the preceding section is a finite process, culminating in the failure of the lamina. To determine the conditions which

result in failure, various criteria have been proposed. These criteria assume linear material behavior to failure. As mentioned earlier, however, this is not an accurate assumption for graphite/epoxy. Consequently a failure criteria has been developed by Sandhu (11 & 12) which can account for nonlinear material behavior.

Following the development found in Ref. (12), a scalar function, f, defining the failure condition of materials exhibiting nonlinear behavior can be written as,

$$f(\varepsilon,\sigma,K) = 1 \qquad (2.47)$$

where ε and σ are the stress and strain states and K represents the material characteristics.

The explicit form of Eq. (2.43) proposed in Ref. (12) uses the scalar strain energy to determine the effect of both stress and strain states on the material behavior. The fact that this criteria is a function of both stress and strain states, helps to account for the nonlinear shear strains that can occur in graphite/epoxy prior to failure.

Assuming strain energies are independent parameters, the failure criterion for orthotropic materials may be expressed for the plane stress condition as,

$$(K_1/\bar{K}_1)^m + (K_2/\bar{K}_2)^m + (K_6/\bar{K}_6)^m = 1 \qquad (2.48)$$

where,

$$K_i = \int_{\varepsilon_i} \sigma_i d\varepsilon_i \qquad (i = 1,2,6) \qquad (2.49)$$

and, using the results of tests under simple load conditions,

$$\bar{K}_i = \int_{\varepsilon_{iu}} \sigma_i d\varepsilon_i \qquad (i = 1,2,6) \qquad (2.50)$$

where ε_i are the current strain components, ε_{iu} are the ultimate normal and shear strains from the simple loading tests and m is a parameter defining the shape of the failure surface in the strain energy space. The m parameter is to be chosen so that experimental-analytical correlation is best.

An analytical comparison of various failure criteria, including the present one, is shown in Fig. 2.5 for boron/epoxy (from Ref. (12)). The criteria is shown for three values of m, namely m = 1/2, 1, and 2. One can see that, in the σ_1,σ_2 plane, the failure envelope is a smooth continuous curve for m = 1. For m > 1 the curve approaches a discontinuity as is found in the maximum stress failure criteria. It may be true that some value of m < 1 would result in a more accurate failure criteria than m = 1, but since there is no biaxial strain energy failure data available to fix m to a specific value it will be taken to be unity as was done by Sandhu in Ref. (12). This reduces the criteria to a simple linear relationship of strain energy ratios.

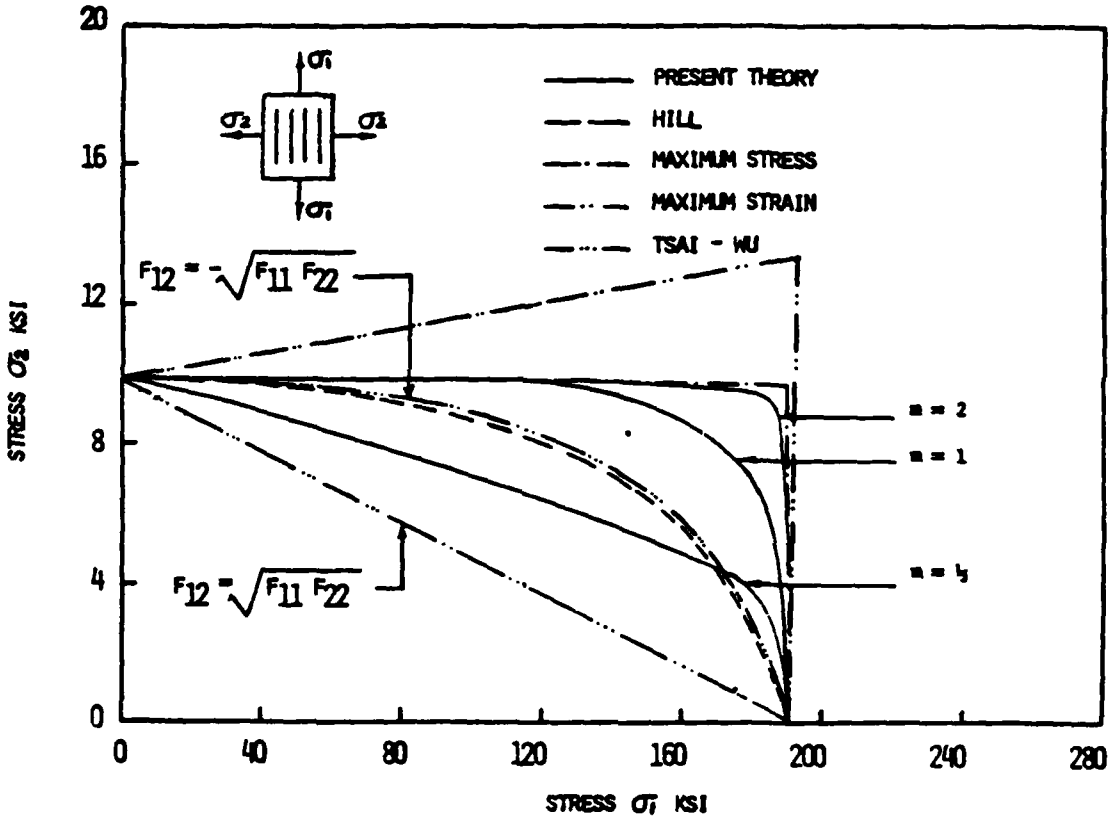

Fig 2.5 Comparison of Various Strength Theories

CHAPTER 3

ANALYSIS

3.1. Introduction

The analysis of the off-axis specimen was carried out in two parts. A parametric study was carried out to determine the amount of tab clamping and point of rotation of the clamped area that yielded the most uniform state of stress in the specimen test section. Then, a nonlinear finite element analysis was carried out to assess the effect of material nonlinearity on stress field uniformity. First, however, a discussion of the specimen geometry and finite element modeling is in order.

3.2. Specimen Geometry

The specimen geometry under consideration is shown in Fig. 3.1. The coupon is fabricated from 16-ply

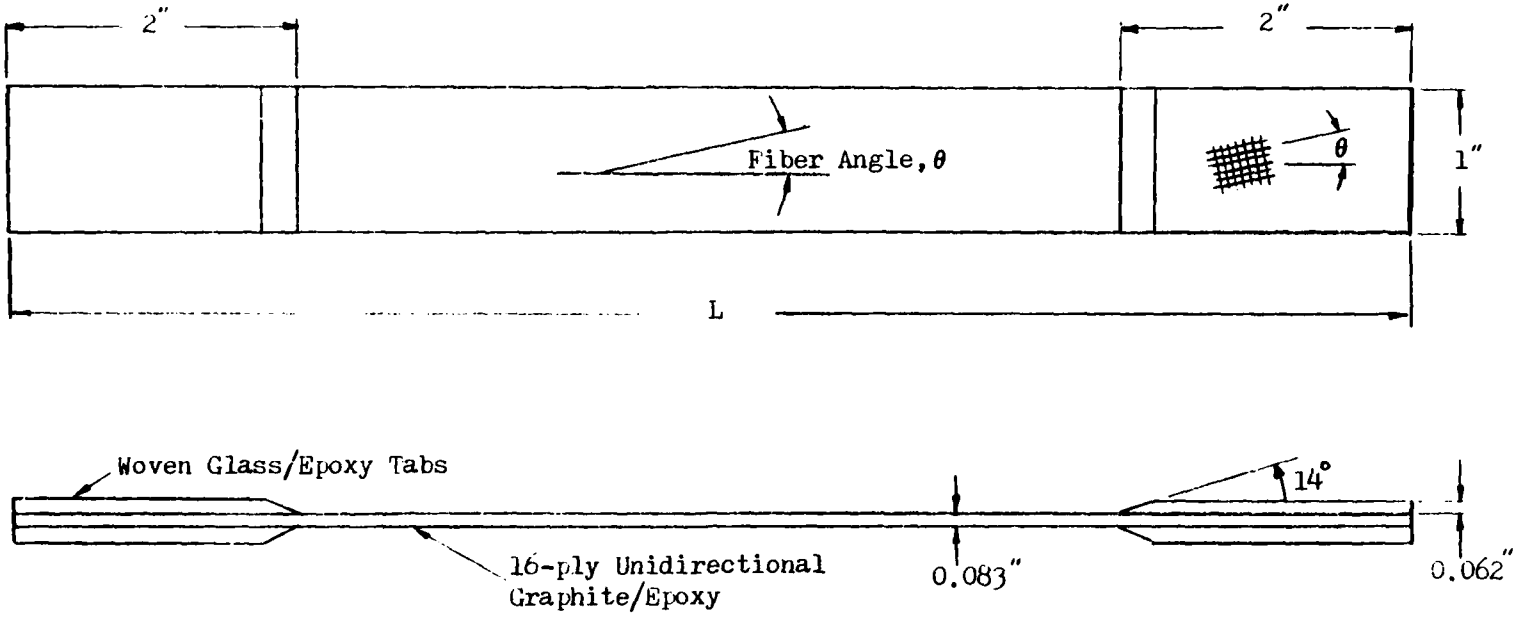

For: $\theta = 10^{\circ}$, L = 12"

$\theta = 14^{\circ}$, L = 10"

Fig. 3.1 Specimen Geometry

graphite/epoxy and is tabbed with bi-directional glass/epoxy tabs (See appendix C for experimental material properties). Note that the tab fibers are aligned parallel and perpendicular to the coupon fibers as suggested in Refs. 8 and 11.

Only two off-axis angles, namely 10° and 14°, were analyzed. The study was limited to only two angles to conserve computer resources and still allow for a comparison of the optimized boundary conditions at different angles.

The first reason for choosing these particular angles is that they bound the peak values of the shear coupling ratio, η_{xy}. From Eq. (2.11), shown here again for clarity,

$$\bar{S}_{11}\bar{S}'_{16} - \bar{S}_{16}\bar{S}'_{11} = 0 \qquad (2.11)$$

we find, upon solving for θ, that for the experimental material properties under consideration, η_{xy} attains its maximum value at an off-axis angle of 12.47° (Note that Eq. (2.11) was solved numerically using a simple secant iterative algorithm). Furthermore, looking at Fig. 3.2 one can see that a definite peak occurs in the shear coupling ratio at this angle. Thus, by optimizing the specimen at these two angles, close bounding to a worst case condition for shear coupling was obtained.

A second reason for choosing these angles is that the shear contribution to failure is maximized in this range of

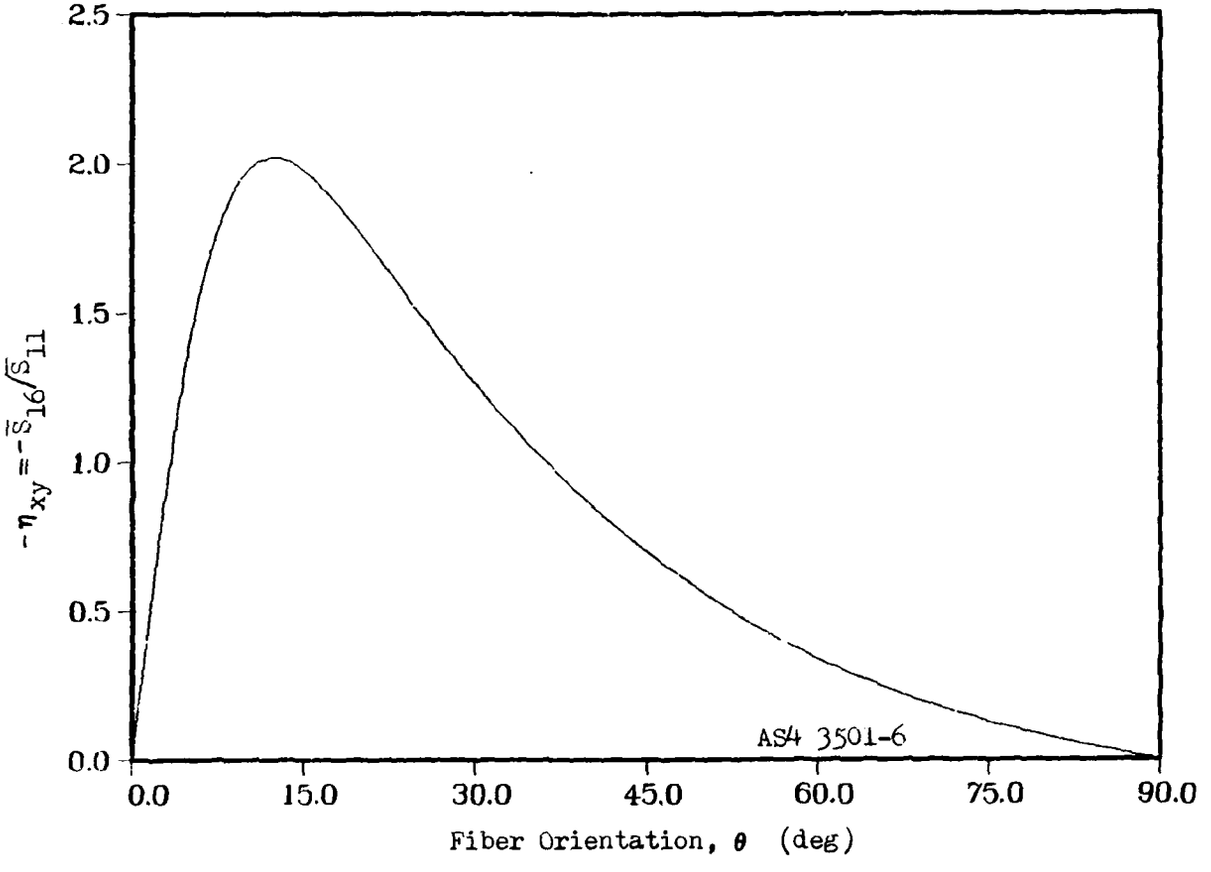

Fig. 3.2 Shear Coupling Ratio, η_{xy}

off-axis angles. Equation (2.18),

$$\tan \theta' = \sqrt{Y/X} \qquad (2.18)$$

yields a value for θ' of 8.5°, using experimentally determined values of Y and X in tension. Adjusting this value for material nonlinearity by the same amount indicated by Ref. (11) (See the end of section 2.2), θ' becomes 10.1°, which falls into the 10° to 14° range.

Note in Fig. 3.1 that the specimen length, L, is different for each off-axis angle. The length is determined from the requirement that a fiber passing through the center of the specimen, begin and end approximately one inch from each tab. This feature is important since past experience indicates that fracture will occur along a fiber/matrix interface. The length requirement insures that such a fracture can occur without constraint from the tabs.

A specimen width of one inch was chosen for two reasons. The first is that one inch is a standard width for composite tensile tests. The second reason is that it reduces the length to width ratio to 6 and 8 for 10° and 14°, respectively. By designing a specimen with such a small length to width ratio, it is possible to observe whether or not the need for large length to width ratios can be eliminated by proper application of the load.

The remaining features of the specimen geometry are essentially standard and self-explanatory. One final note,

however, is that the tab taper angle was adjusted to 14° for no other reason than to allow for convenient finite element dimensioning. Typical values for the taper angle are 15° and 20°.

3.3. Finite Element Modeling

A good finite element model of any structure should accurately predict the displacement field of the actual physical structure under consideration, when a load is applied to it. To obtain such a model, the analyst must accurately model the size, the shape, and the loading (or displacement) boundary conditions of the actual structure. Furthermore, he must provide for adequate refinement of the element mesh in areas where gradients in the displacement field are known or expected to be high. In describing the finite element modeling carried out in the present study, each of the characteristics just mentioned will be discussed.

Sizing and shaping of the finite element model in the width direction was obviously trivial, given the simple rectangular planform of the off-axis specimen. Sizing in the thickness direction was carried out by specifying the average thickness of each layer of material in a given element, i.e., t_i of Eq. (2.26). In the portion of the specimen where there is only graphite/epoxy through the

thickness, an element had one layer with a thickness of 0.083 in. In the tabbed portion of the specimen where there is both graphite/epoxy and glass/epoxy through the thickness, but no clamp, an element had one layer of graphite/epoxy, with a thickness of 0.083 in., and one layer of glass/epoxy with a thickness of 0.094 in. In the tapered portion of the tab, the thickness of the glass/epoxy layer was reduced in a stepwise manner from 0.094 in. to 0.000 in. In the clamped portion of the tab, a third layer of steel, 1.5 in. thick, was added to each element. One may have noticed that the thickness of the glass/epoxy has just been given as 0.094 in. when in Fig. 3.1 it is given as 0.124 in. This is due to a slight modification of the specimen that was required during experimentation. This modification will be discussed in chapter 4. In an effort to keep the experimental and analytical specimens as similiar as possible, this modification was accounted for in the finite element model.

The experimental test fixture used in this study to test off-axis specimens, applies the load with rigid jaws that are free to rotate about a pin and bearing embedded in the jaw. This, in effect, forces all points in the clamped area of the tab to rotate concentrically about the pin. By adjusting the location of the specimen relative to the jaws, the position of the pin, relative to the clamped area, can be adjusted. A detailed description of the test

fixture will be presented in chapter 4.

To model this type of rigid rotating boundary condition, a third layer of steel is added in the clamped area, as mentioned above. The effect, of this essentially rigid layer, is to constrain the clamped portion of the tab to remain rectangular and rotate about the pin, as is true for the actual test fixture. Thus, to apply a load, only the displacements at the two nodes corresponding to the pin locations (one at each end of the specimen) need to be specified. At one end of the specimen, the displacements at the node corresponding to the pin location, are fixed at zero ($u = v = 0$) At the opposite end of the specimen a finite displacement is applied, at the node corresponding to the other pin location, in the X direction while the Y displacement is fixed at zero ($u \neq 0$, $v = 0$). Fig. 3.3 shows graphically how the boundary conditions are applied.

The work of Ref (16) clearly shows that large gradients can exist in the stress field of the off-axis specimen, immediately adjacent to the tabs. Though the purpose of this study is to apply the load in such a manner as to eliminate these gradients, provisions are made to accommodate a worst case condition where such gradients do exist. As can be seen in Fig. 3.3, the mesh is highly refined near the edge of the tabs. The mesh is also refined in the tapered portion of the tab so that a smooth transition from glass/epoxy and graphite/epoxy to just

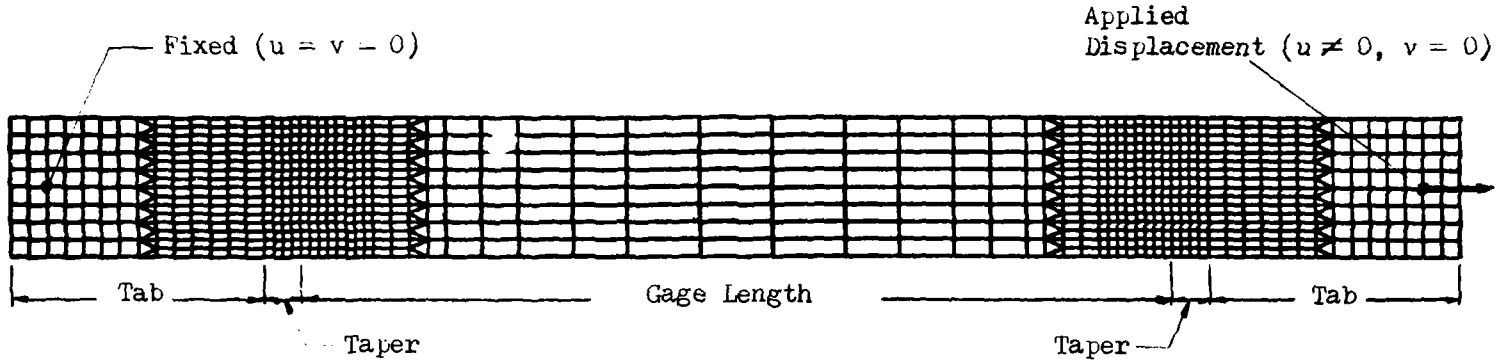

Fig. 3.3 Fine Mesh Finite Element Model
with Typical Applied Displacements

graphite/epoxy is obtained.

To insure that the final finite element model design would yield results that had converged to a solution, a convergence study was carried out with the 14° specimen in arriving at the final model. The three models used are shown in Fig. 3.4. As a measure of convergence, axial stress along the centerline of the models is plotted in Fig. 3.5. One can see that the final model has converged to a solution since at all points along the curve, the difference between the medium and fine models is less that 5.0 %. It should be noted that the quadrilateral elements shown in all of the finite element models are subdivided into four constant strain triangles. The triangles are formed by adding a node at the center of each quadrilateral. The interior node is subsequently removed by static condensation.

3.4. Parametric Analysis

A parametric study was carried out using the finite element technique of section 2.3 to determine the amount of tab clamping and point of rotation of the clamped area which produce the most uniform state of stress in the gage length (area between the tabs) of the off-axis specimen.

The clamped area was assumed to extend across the entire width of the tab for a distance D_c, measured from

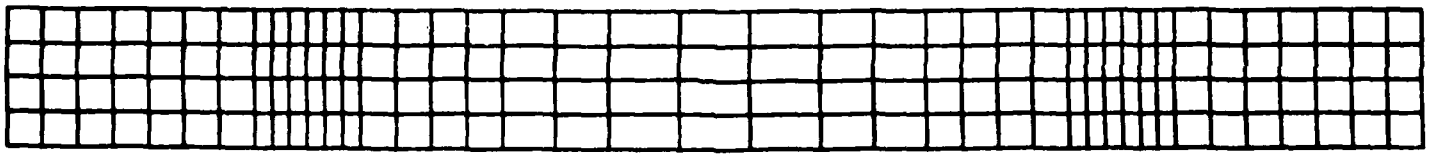

Coarse Mesh

374 nodes
656 elements

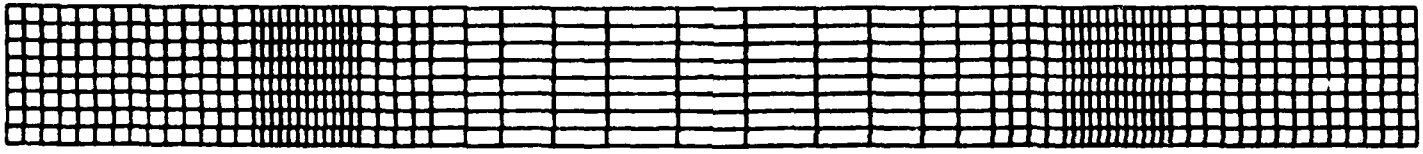

Medium Mesh

1216 nodes
2272 elements

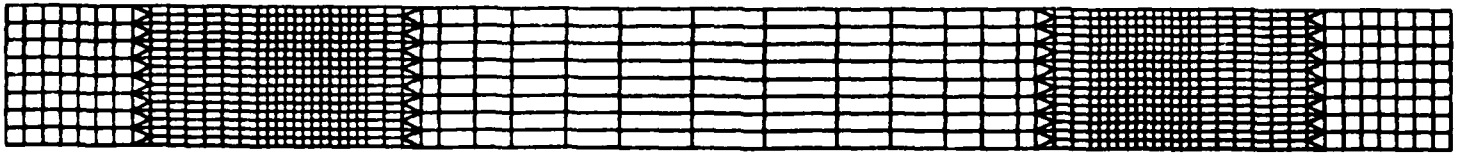

Fine Mesh

1840 nodes
3520 elements

Fig. 3.4 Finite Element Models used for Convergence

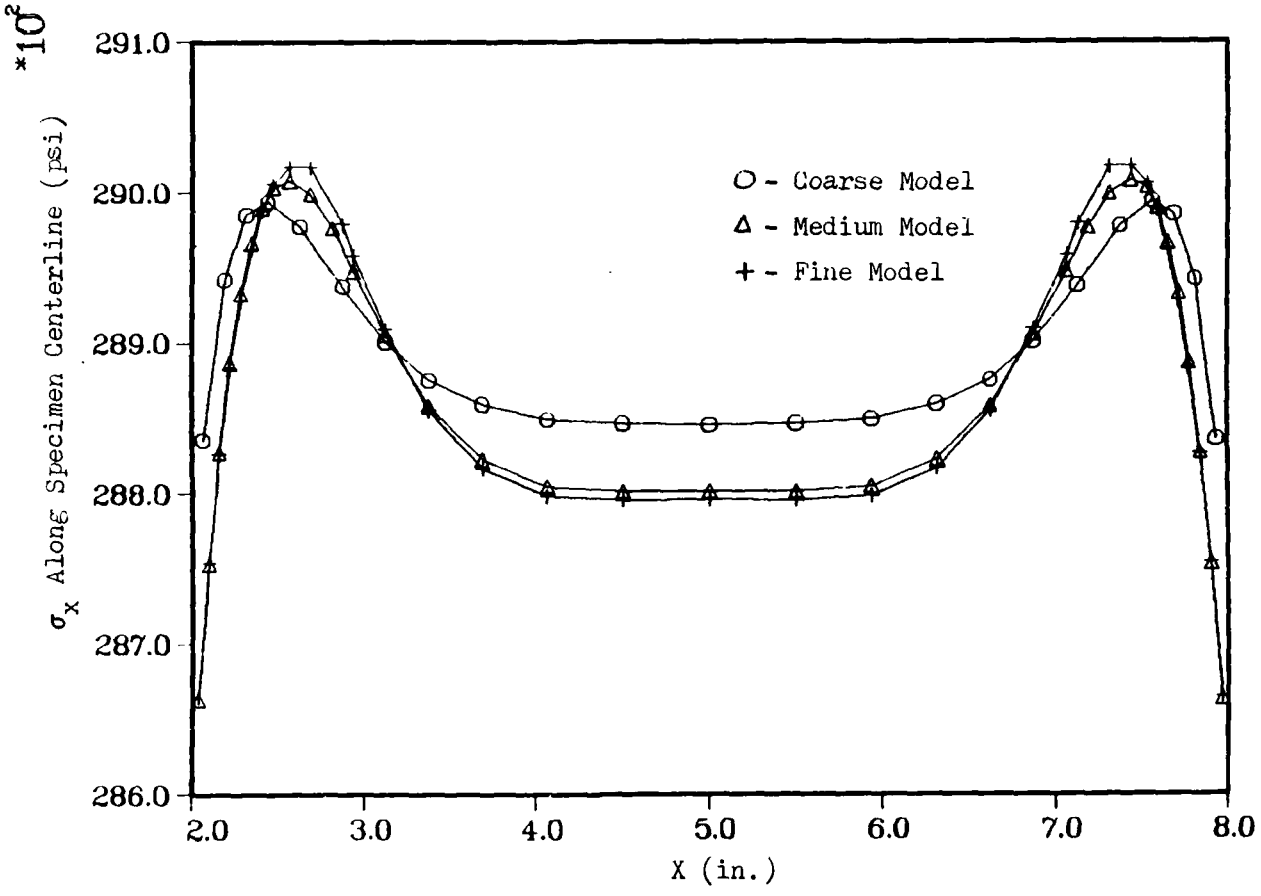

Fig. 3.5 Plot of Axial Stress Along Specimen Centerline to Show Convergence

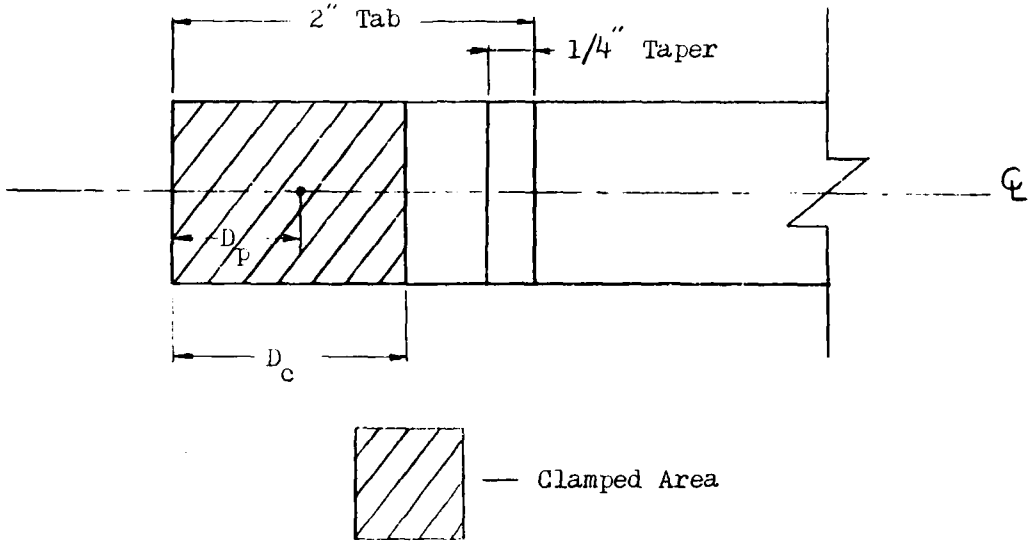

Fig. 3.6 Plan View of End of Specimen

the end of the specimen, as shown in Fig. 3.6.

The pin (or point of rotation of the clamped area) was assumed to be located along the centerline of the clamped area, a distance D_p from the end of the specimen. Note that the pin can only be located at the boundaries of, or within, the clamped area. This is due to the physical limitations of the experimental test fixture.

For the parametric analysis, the clamping distance, D_c, was allowed to vary from 1 in. to 1 3/4 in. For a given value of D_c, D_p was allowed to vary from 0 to D_c. Or,

$$1" \leq D_c \leq 1\ 3/4"$$

$$0" \leq D_p \leq D_c$$

where D_c and D_p varied in 1/8 in. increments since in the finite element model the clamp must terminate at an element edge and the pin must be located at a node.

D_c was limited to a minimum of 1 in. due to the physical limitations of the fixture and specimen. It was felt that clamping less than 1 in., would very probably result in the specimen pulling out of the clamps during testing.

As a measure of stress field uniformity, the difference between the maximum and minimum axial stress occuring anywhere in the gage length, $\Delta\sigma_x$, was plotted versus pin position for a given amount of clamping. The ideal amount of clamping and position of the pin correspond

to the values of D_c and D_p for which $\Delta\sigma_x$ is a minimum. The curves for the 10° specimen are presented in Fig. 3.7. Those for the 14° specimen are presented in Fig. 3.8. Note that the results for each pin position were normalized to a center section axial stress of 30,000 psi to show relative differences in $\Delta\sigma_x$.

One might ask whether forcing $\Delta\sigma_x$ to go to zero will also cause the other components of stress (σ_y and τ_{xy}) to also go to zero. If $\Delta\sigma_x$ is zero in the gage length then σ_x will be a constant in the gage length. From the x direction plane stress equation of equilibrium,

$$\partial\sigma_x/\partial x + \partial\tau_{xy}/\partial y = 0 \qquad (3.1)$$

we can see that if σ_x is a constant, τ_{xy} can only change in the x direction. This forces τ_{xy} to be zero due to the stress free edges. From the y direction equation of equilibrium,

$$\partial\sigma_y/\partial y + \partial\tau_{xy}/\partial x = 0 \qquad (3.2)$$

one can see that if τ_{xy} is zero, σ_y must also be zero due to the stress free edges. Thus, by driving $\Delta\sigma_x$ to zero, σ_y and τ_{xy} are also driven to zero.

One can see that for each amount of clamping there is a minimum value of $\Delta\sigma_x$. Figure 3.9 shows this minimum value of $\Delta\sigma_x$ plotted versus amount of clamping (D_c), for the 10° and 14° models, respectively.

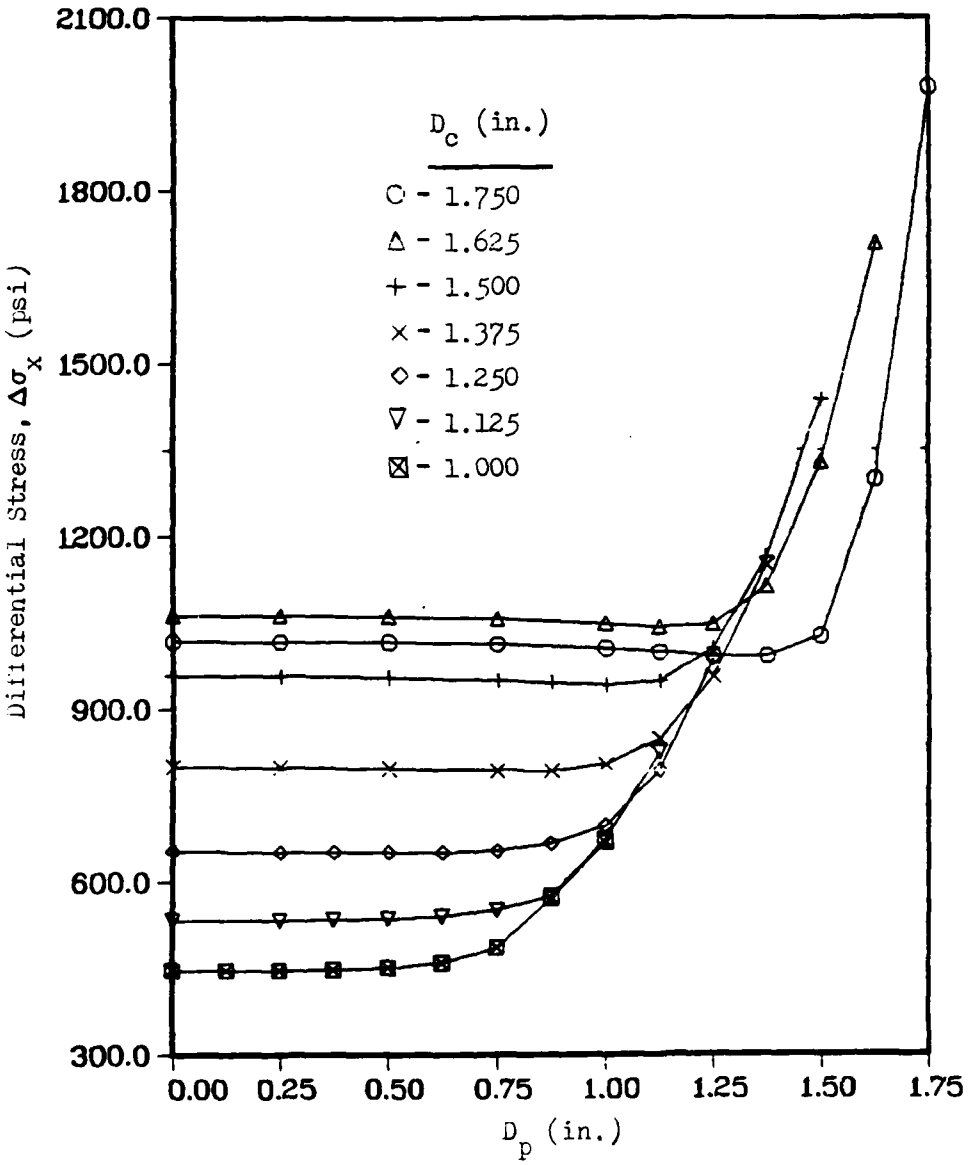

Fig. 3.7 Differential Stress, $\Delta\sigma_x$, versus Pin Position, D_p, for the 10° Off-Axis Specimen

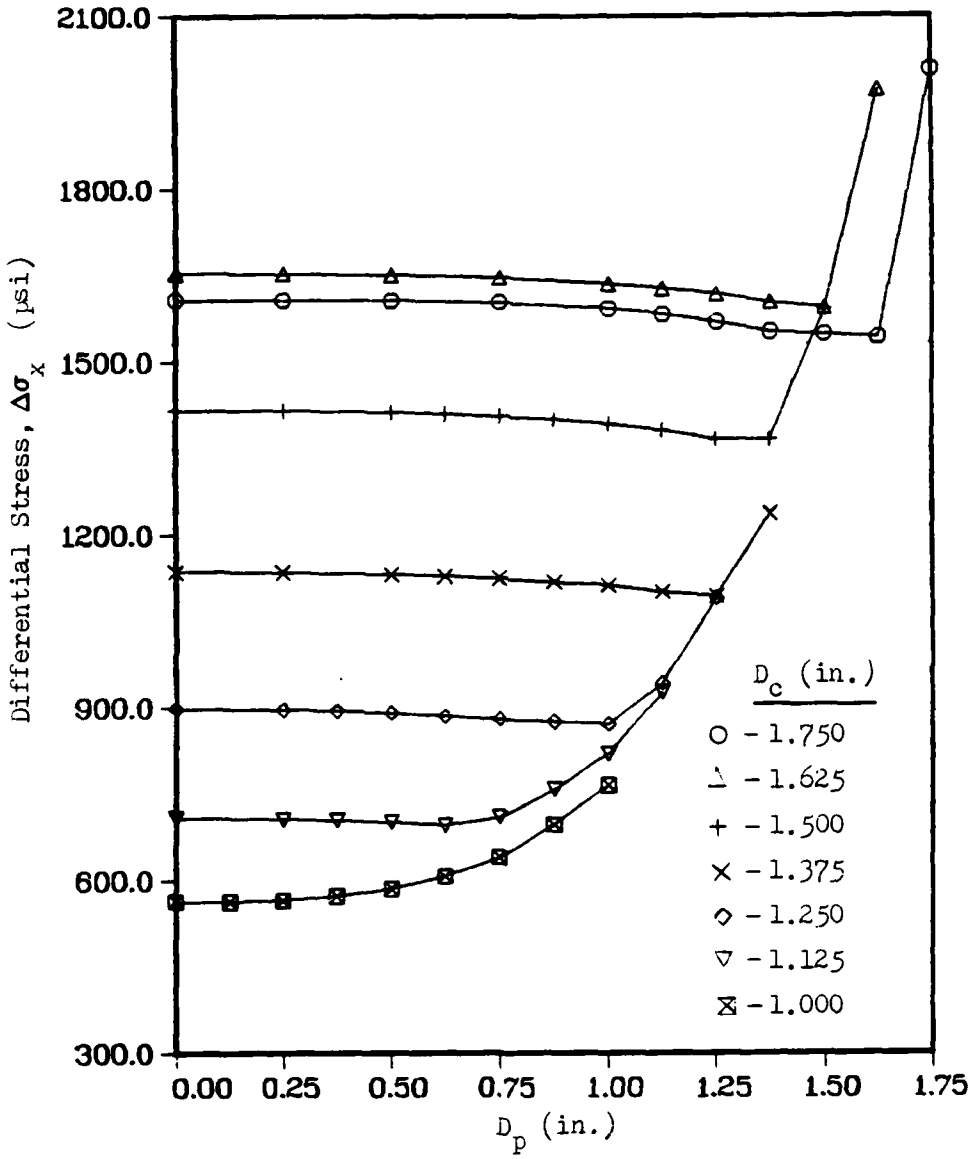

Fig. 3.8 Differential Stress, $\Delta\sigma_x$, versus Pin Position, D_p, for the 14° Off-Axis Specimen

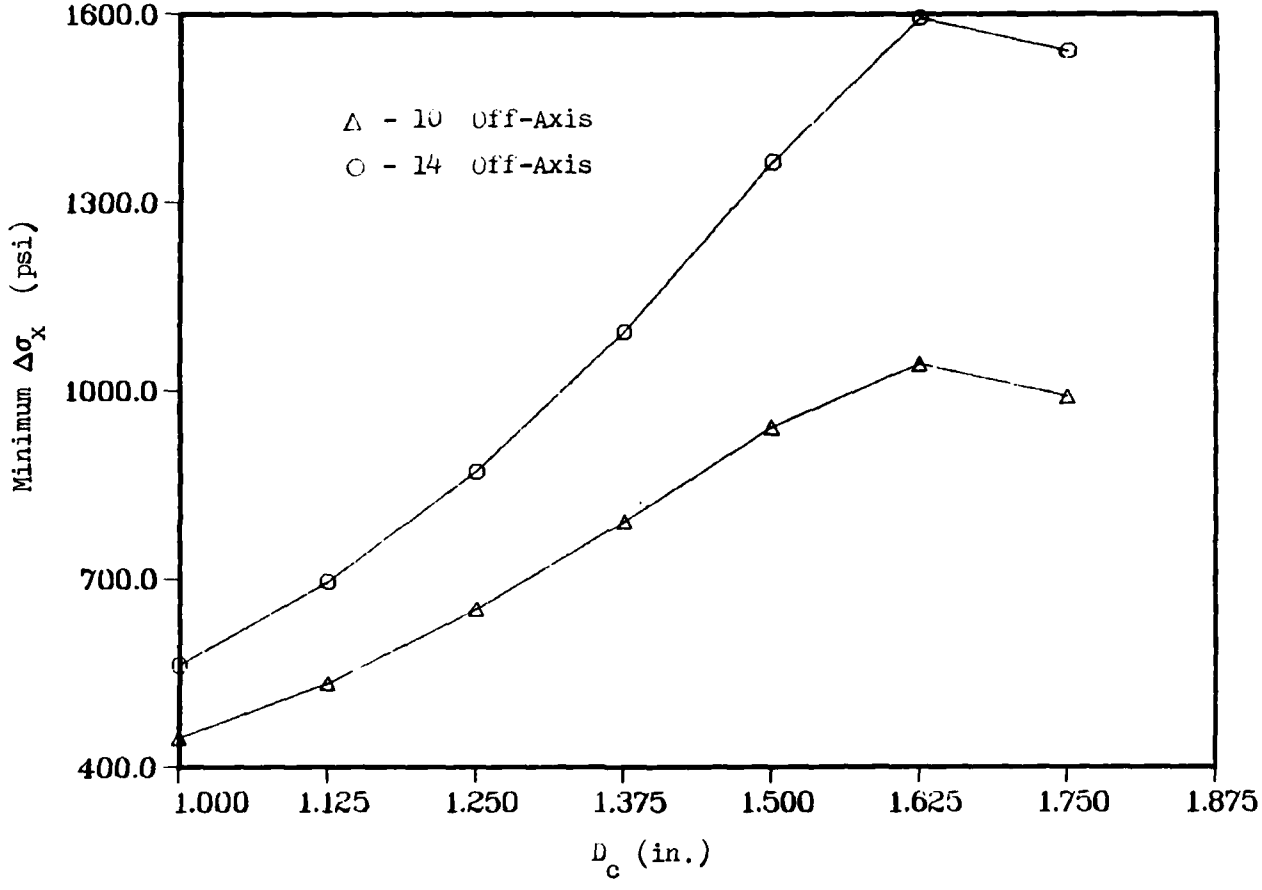

Fig. 3.9 Minimum Differential Stress, $\Delta\sigma_x$ for Given Amount of Clamping

3.5. Non-Linear Analysis

To assess the effect of material nonlinearity on the off-axis specimen stress field, the specimen was analyzed a second time using the nonlinear finite element technique presented in section 2.4. For this analysis, only the ideal boundary condition for each off-axis angle, determined in the preceding section, were considered.

From the linear parametric study just discussed, one can see that the ideal amount of clamping for both off-axis angles was 1 in. The ideal pin positions, however, were not the same. For the 10° case, the ideal pin location was at $D_p = 1/4$ whereas for the 14° case the ideal pin position was at $D_p = 0$.

Note that the ideal boundary conditions were determined using a parametric analysis that assumed linear material properties. The author recognizes that due to the nonlinear behavior of the graphite/epoxy off-axis specimen, this assumption may result in a certain amount of error in determining ideal values of D_c and D_p. The work of Ref. (11) indicates that the uniformity of the stress field is degraded by material nonlinearity. That study also indicates, however, that the optimized boundary conditions arrived at assuming material linearity are a good approximation to the more accurate boundary conditions that are obtained if the nonlinear technique is used for the

parametric analysis. Considering that the ratio of computer cpu seconds for a nonlinear run to cpu seconds for a linear run is approximately 150 (3000 sec vs. 20 sec), the error appears to be tolerable.

One may have noticed, from the convergence study, that the medium model is nearly as accurate as the fine model for the non-ideal case of full tab clamping (D_c = 1 3/4") used in the convergence study. Since for the nonlinear analysis the boundary conditions are more ideal, the stress field is more uniform and hence the fine model is not required to give a good overall picture of the specimen behavior. Therefore, the medium model was used in the nonlinear analysis of the specimen. This resulted in approximately a 40% savings in cpu time. It is estimated that a nonlinear run using the fine model would have taken 5000 cpu sec (computer used was a Cyber 170/845).

The above results will be discussed in depth in chapter 5.

CHAPTER 4

EXPERIMENTATION

4.1. Introduction

Two sets of experiments were carried out in the present study. The first set of experiments were simple tension tests to obtain the basic tensile material properties of the materials used to fabricate the off-axis specimens. The second set of experiments were off-axis tension tests using a new fixture which could apply the load with the ideal boundary conditions determined in chapter 3.

4.2. Specimen Fabrication

The material system used in this study was AS4 3501-6 graphite/epoxy. The material was supplied by Hercules Incorporated in the form of 12-in. wide prepreg tape. The

prepreg material was used to fabricate one 16-ply panel, 30 x 30 in., and one 8-ply panel, 12 x 12 in. The 16-ply panel had a $(0)_{16}$ lay-up while the 8-ply panel had a $(\pm 45)_{2S}$ layup. Both panels were cured according to manufacture's specifications. After curing, both panels were subjected to C-scan and X-ray inspection for flaws, before being cut into specimens. The inspection did not reveal significant defects.

A single panel of 1/16 in. thick G-10 glass/epoxy (0/90 woven) was also obtained from a local plastics dealer for tabbing of the basic material properties specimens and the off-axis specimens.

Specimens for basic material properties were fabricated from the above panels for tension tests to determine values of E_1, E_2, G_{12}, and ν_{12}. Five specimens were fabricated for each fiber direction. Refer to Table 4.1 for the tests used to determine the various material properties. Note that the commonly used $\pm 45^\circ$ laminate was used for determining τ_{12} vs. γ_{12}. The specimen dimensions are shown in Fig. 4.1 except for the 0° graphite/epoxy specimens which had a reduced width of 1/2 in. This reduction was required because the 1 in. wide 0° specimens could not be loaded to failure with the test machine used.

Specimens for off-axis tests were fabricated from the $(0)_{16}$ graphite/epoxy panel. Five specimens were fabricated for each off-axis angle. The specimen dimensions are shown

Curve	Experiment
σ_1 vs. ε_1	0° tension
σ_2 vs. ε_2	90° tension
τ_{12} vs. γ_{12}	$\pm 45^\circ$ tension
ν_{12} vs. ε_1	0° tension

Table 4.1 Stress-Strain Curves and Corresponding Experimental Tests

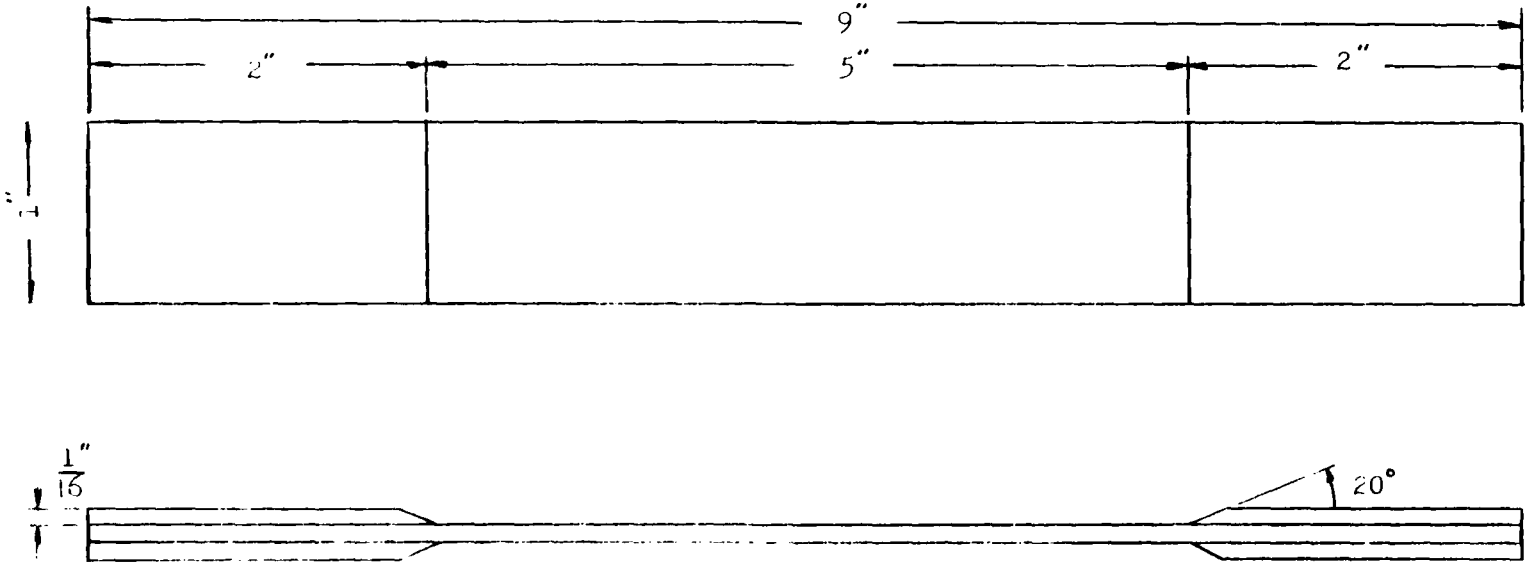

Fig. 4.1 0°, 90°, and ±45° Tension Test Specimens

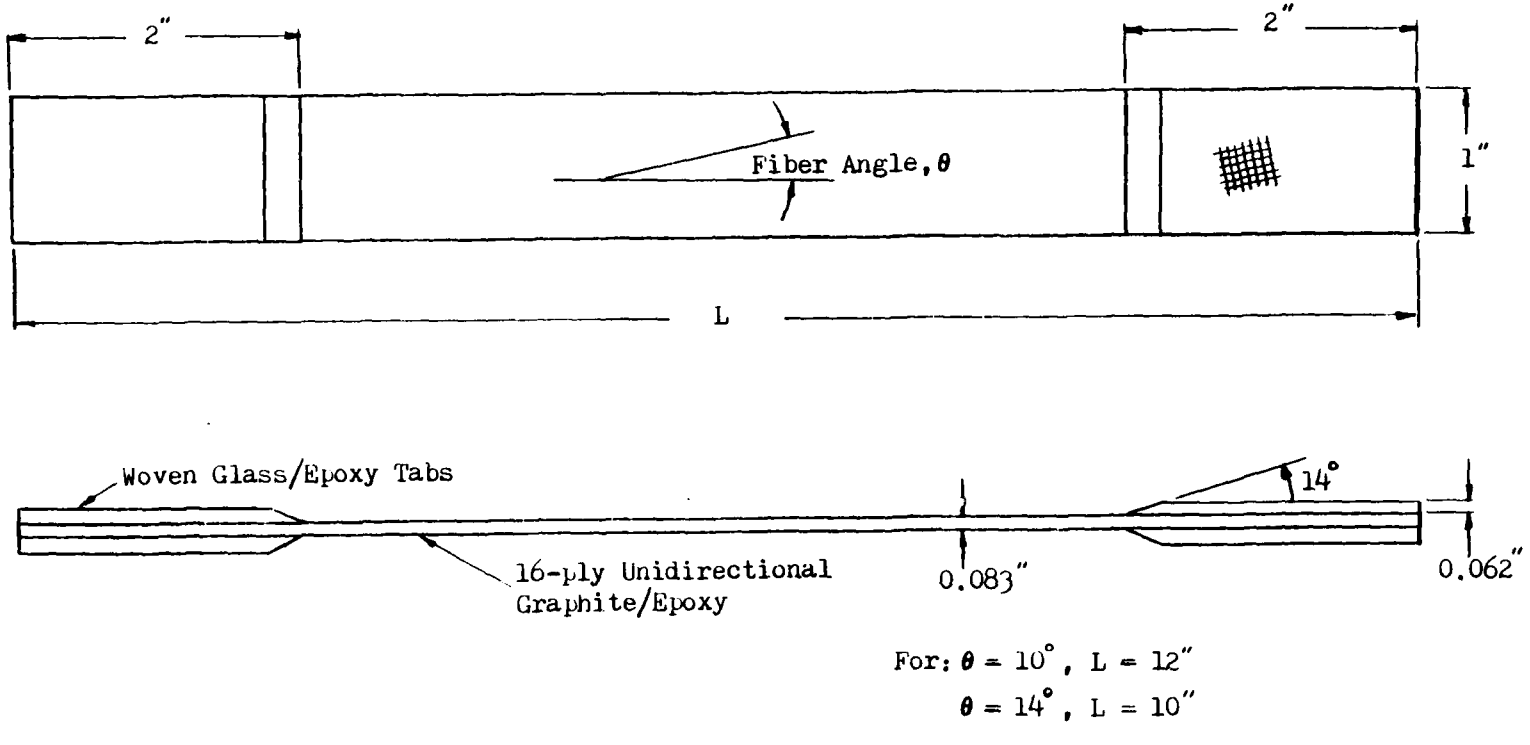

Fig. 4.2 Off-Axis Tension Specimens

in Fig. 4.2. Note that the 0° fibers in the tabs are oriented parallel to the fibers in the graphite/epoxy. As was done for the finite element model in section 3.2.

4.3. Basic Material Property Tests

All specimens were instrumented with two 3-element strain gage rosettes, one on each face, at the center of the test section of the specimen. An Instron Test Machine, Floor Model TT-1115, was used to test all specimens at ambient environments. The maximum load for this machine is 20,000 lbs. The crosshead speed was 0.05 in. per minute.

For each test, strain was read from all six strain gage elements and load was read from the Instron Test Machine load cell at up to four times a second using an analog to digital converter and a computer. The gage readings from the two faces were averaged to reduce the effect of any bending or torsion that might have been present during testing. Strain gage element numbering and orientation is shown in Fig. 4.3.

To obtain a desired stress-strain curve, the needed data was read, manipulated, and plotted. To determine, for instance, σ_1 vs. ε_1, the axial stress (σ_1) was plotted versus the average of the strains from the #1 gages (ε_1) from a 0° tension test. All five experimental σ_1 vs. ε_1 curves were then placed on one plot and an average curve

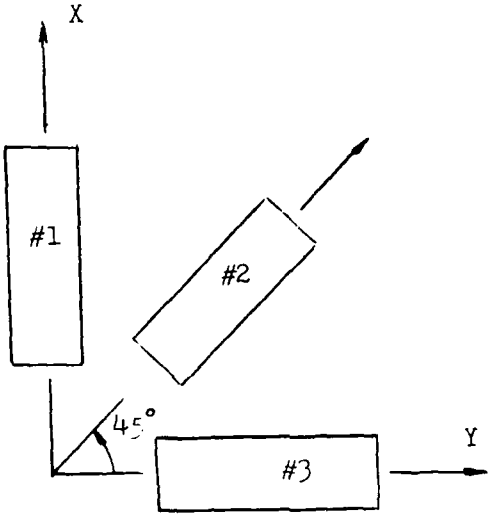

Fig. 4.3 Rosette Strain Gage
Numbering and Orientation

was drawn by hand through the five experimental curves. these average curves are shown in appendix B and the average engineering elastic constants and average strengths are tabulated in appendix C. The engineering elastic constants (initial values of E_1, E_2, G_{12}, and ν_{12}) were used in the linear finite element analysis and the average curves were represented by the cubic spline functions in the nonlinear finite element technique described earlier.

4.4. Off-Axis Tension Tests

The off-axis specimens were instrumented and tested in the same manner as the basic property specimens except for the loading fixture used (Fig. 4.4 through 4.8). The fixture is a new design inspired by deficiencies of the fixture used in Ref. (11). The fixture was designed by the engineers of the Structural Concepts Branch, of the Structures and Dynamics Division of the Flight Dynamics Laboratory. The fixture is shown alone in Fig. 4.4. Overall dimensions of the fixture are 9 1/2 x 5 x 3 in. Fig. 4.5 shows the fixture installed in the Instron Test Machine. Notice the partial clamping of the specimen tabs. Fig. 4.6 shows a close-up view of the pin, clamp, and embedded self-aligning bearing. Notice that part of the pin has been machined to a larger diameter to form a collar which enhances rigidity. The pin is also press

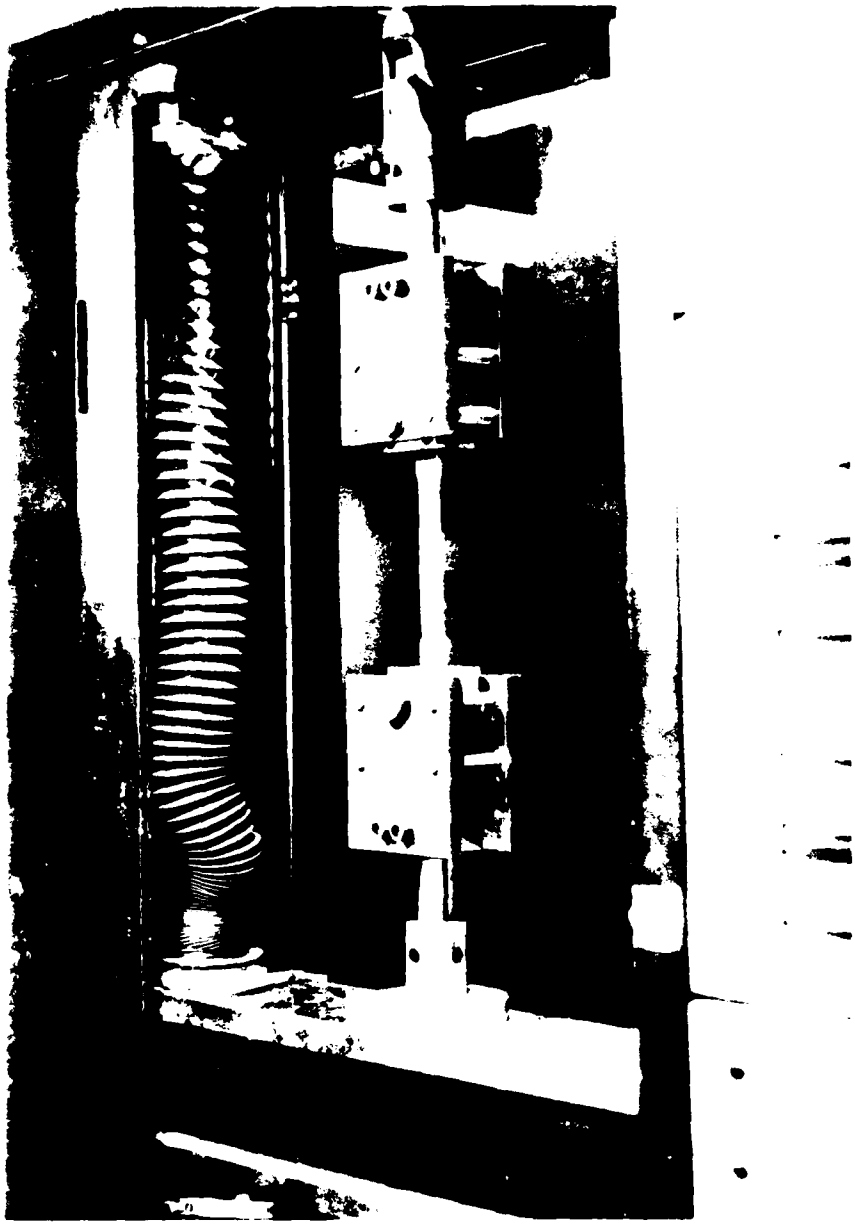

Fig. 4.5 Fixture and Specimen in Instron Machine

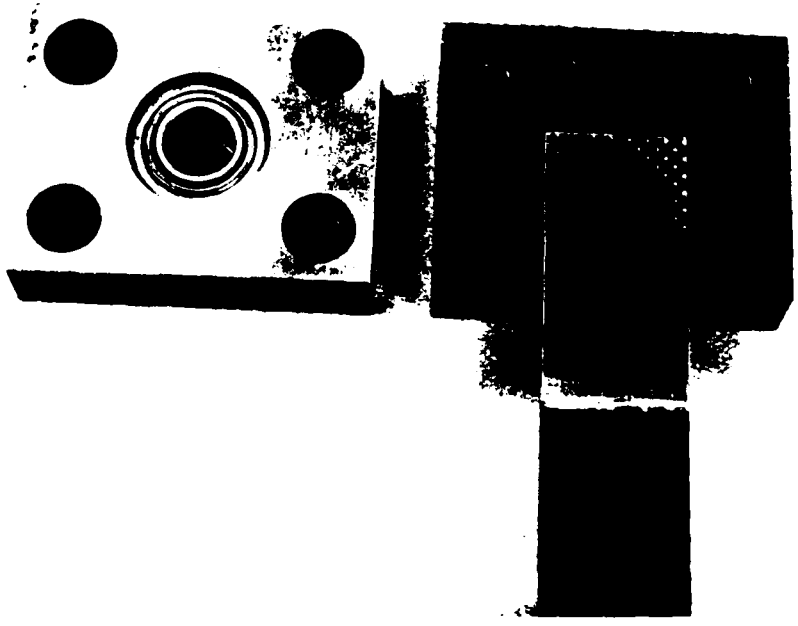

Fig. 4.7 Close Up of Clamp and Specimen

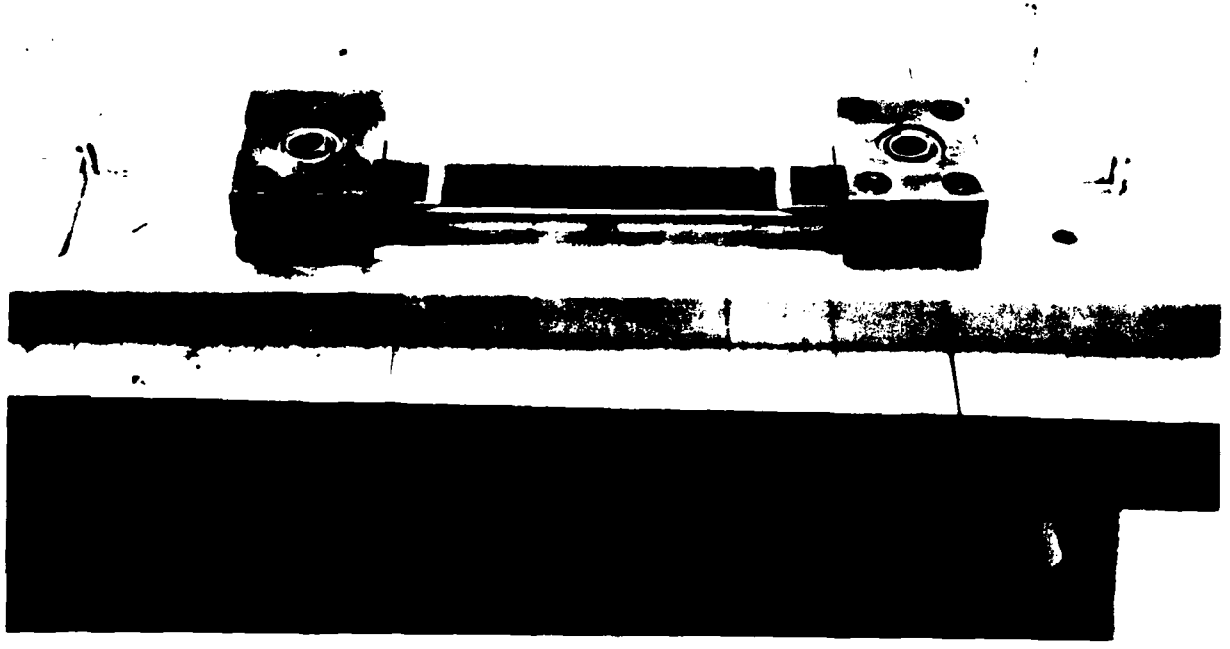

Fig. 4.8 Fixture for Aligning Clamp and Specimen While Being Tightened

fitted into the side plates. Fig. 4.7 shows how the specimen is placed into the clamp. Note the knurled clamping surface of the clamp. Fig. 4.8 shows an alignment fixture used to maintain alignment of the specimen while the clamp bolts are being tightened. The fixture is bolted down so that the specimen and clamp remain fixed while the clamp bolts are being torqued.

Looking at Fig. 4.7, one can see that the jaws used to clamp the specimen tabs are of fixed dimensions. This presents a slight problem when one desires to adjust the amount of the tab that is clamped (D_c) and still allow for variations in the pin position (D_p). Ideally, the fixture would allow for independant variations of D_c and D_p. Since with the present fixture this is not possible, the portion of the tab that was not to be clamped was milled down approximately 0.015 in. This prevented the knurled surface of the jaws from bitting into that portion of the tab. This modification to the specimen is not recommended as a general practice in off-axis specimen design. Rather, the jaws should be modified instead, leaving the simple specimen design intact.

The values of D_c and D_p used in the off-axis test were 1.0 in. and 0.5 in., respectively. The choice of D_c = 1.0 is obvious when one looks at Fig. 3.9. While D_p = 0.5 does not correspond to the absolute minimum value of $\Delta\sigma_x$ for either the 10° or 14° specimens it was used, nevertheless,

for two reasons. The first reason is that it allowed the technicians to apply a uniform clamping pressure very conveniently with a torque wrench. The second reason is that it allowed for all four clamping bolts to carry an equal share of the clamping force. With the specimen moved forward so that $D_p = 0.0$, nearly all of the clamping force is carried by two of the bolts. Concern over the specimen possibly pulling out under these conditions prompted the change to $D_p = 0.5$ in. The difference in $\Delta\sigma_x$ that resulted from using $D_p = 0.5$, rather than the absolute optimum value, was 1.04 % and 3.98 % for the 10° and 14° specimens, respectively.

Various experimental stress-strain curves were obtained from the off-axis tests. These will be presented and compared with the stress-strain plots obtained from the nonlinear analysis, in chapter 5.

A coating of photoelastic plastic, used for evaluating stress uniformity, was applied between the strain gage and the tab on one of the 10° and one of the 14° specimens. The coating was cemented to the specimen surface with a uniformly reflective adhesive. Note that the coating was only applied to one half of one side of the specimen. The coating specifications were,

$$t = 0.010 \pm 0.001 \text{ in.}$$

$$k = .14$$

$$f = 8100$$

where,

t = thickness

k = strain optical coefficient

f = stress optical coefficient

As the coated specimens were loaded, they were illuminated with white light and photographed through a polarizer at discrete load levels. The photograhs will be presented and discussed in chapter 5.

CHAPTER 5

RESULTS AND DISCUSSION

5.1. Introduction

In this section, results from the analytical and experimental efforts will be presented and discussed. In general, the discussion will be carried out in terms of the goals of the study. Again, these are 1) determination of boundary conditions (D_c and D_p) that produce the most uniform state of stress in the specimen gage length and 2) limited verification of the aforementioned failure criteria.

5.2. Results of the Linear Parametric Study

Referring back to Figs. 3.7 through 3.9 one can clearly see from these plots that, as mentioned earlier, $\Delta\sigma_x$ attains a minimum for 1 in. of clamping and the pin

toward the rear of the specimen for both off-axis angles. There is, however, more that can be drawn from these plots.

First is the fact that, regardless of the amount of clamping, the worst possible place to locate the pin is at the inside edge ($D_p = D_c$) of the clamped area. In all cases there is a decrease in $\Delta\sigma_x$ when the pin is moved away from the edge of the clamp. For the the 10^o specimen, when $D_c = D_p = 1.750$, $\Delta\sigma_x$ is 99.7 % greater than the minimum $\Delta\sigma_x$ for that amount of clamping. One can also see that, for all values of D_c for both off-axis angles, once the pin has been moved 1/2 in. away from the clamp edge ($D_p < D_c - 1/2$), there is less than 4 % subsequent variation in $\Delta\sigma_x$. This is especially interesting in light of the suggestion by several researchers (1,6, & 10) that the pin should be located exactly at the inside edge of the clamp.

A possible reason for the relatively large values of $\Delta\sigma_x$ when $D_p = D_c$ is that when the pin is at this location it is coincident with two discontinuities in the specimen, namely, a change in thickness and a change in materials through the thickness. These discontinuities have the effect of restraining nodal displacements in the local area which, in turn, causes an increase in stress field non-uniformity. Since, in all cases, the maximum and minimum axial stresses occured in elements adjacent to the tab, this nonuniformity has a direct influence on $\Delta\sigma_x$. Locating the pin at, or near, these discontinuities places yet

another restraint on the local displacements, adding to the effect of the discontinuities and, thus further perturbing the uniformity of the stress field.

One might ask whether this phenomena accurately represents what occurs in experimentation since, in the test fixture, the displacement is not applied at a discrete point. Rather, it is applied to the entire clamp through the pin and embedded bearing. Recall, however, that in the finite element model, a third layer of steel is added in the clamped region. The effect of this relatively rigid layer is to effectively apply the displacement to the entire clamp, just as is done in the experimental fixture.

The reason that $\Delta\sigma_x$ decreases when the amount of clamping is reduced, appears to be mainly due to an increase in specimen flexibility in the vicinity of the load application. The portion of the tab that remains unclamped serves as a flexible transition between the rigid clamps and the specimen test section. The distorted finite element models shown in Fig. 5.1 and 5.2 show very clearly how this increase in flexibility effects Poisson type contraction near the clamps. In Fig. 5.1 one can see that when $D_c = 1.750$, Poisson contraction is forced to take place in the test section, giving rise to an increase in stress field nonuniformity. For $D_c = 1.0$ (Fig. 5.2), on the other hand, most of the Poisson contraction and hence, stress field non uniformity, takes place in the unclamped

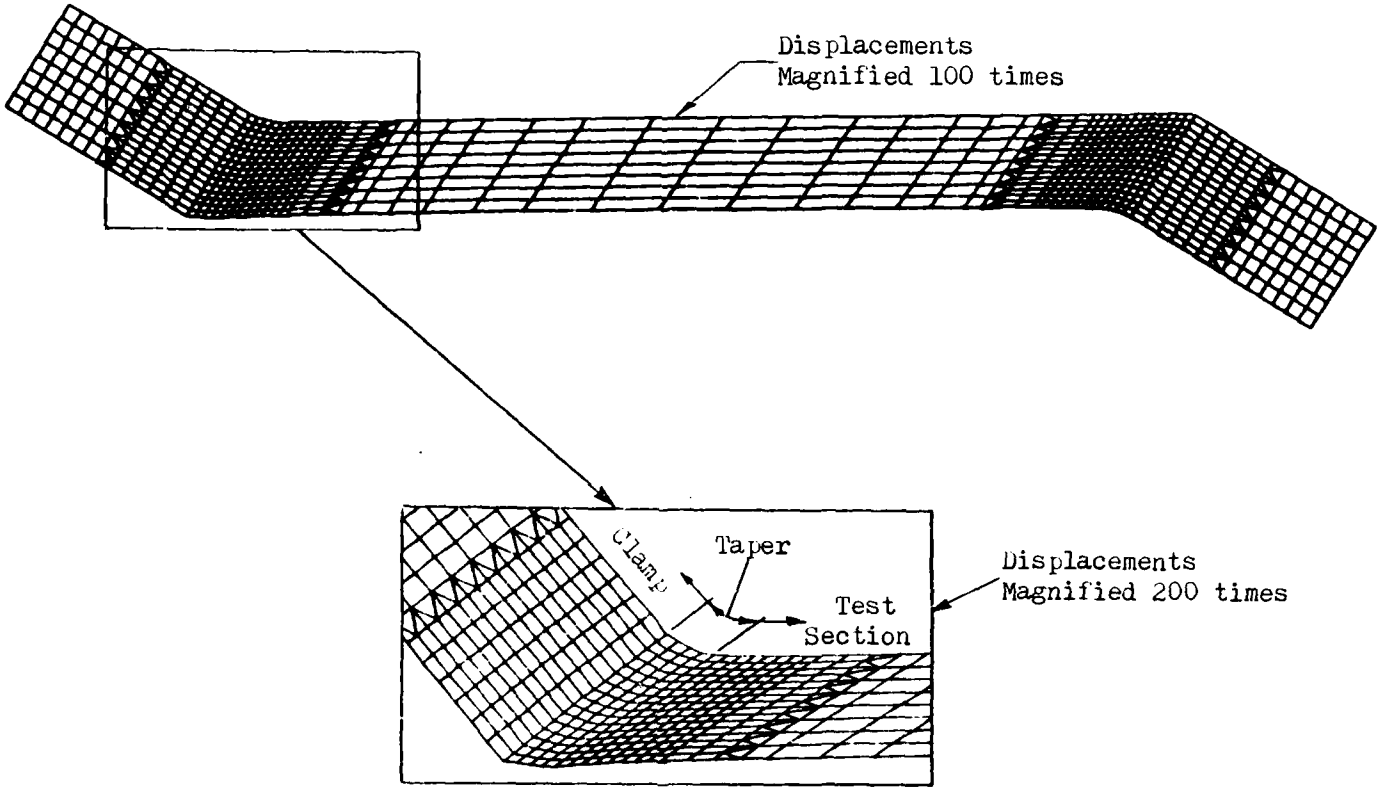

Fig. 5.1 Displaced Finite Element Model with $D_c = D_t = 1.75''$

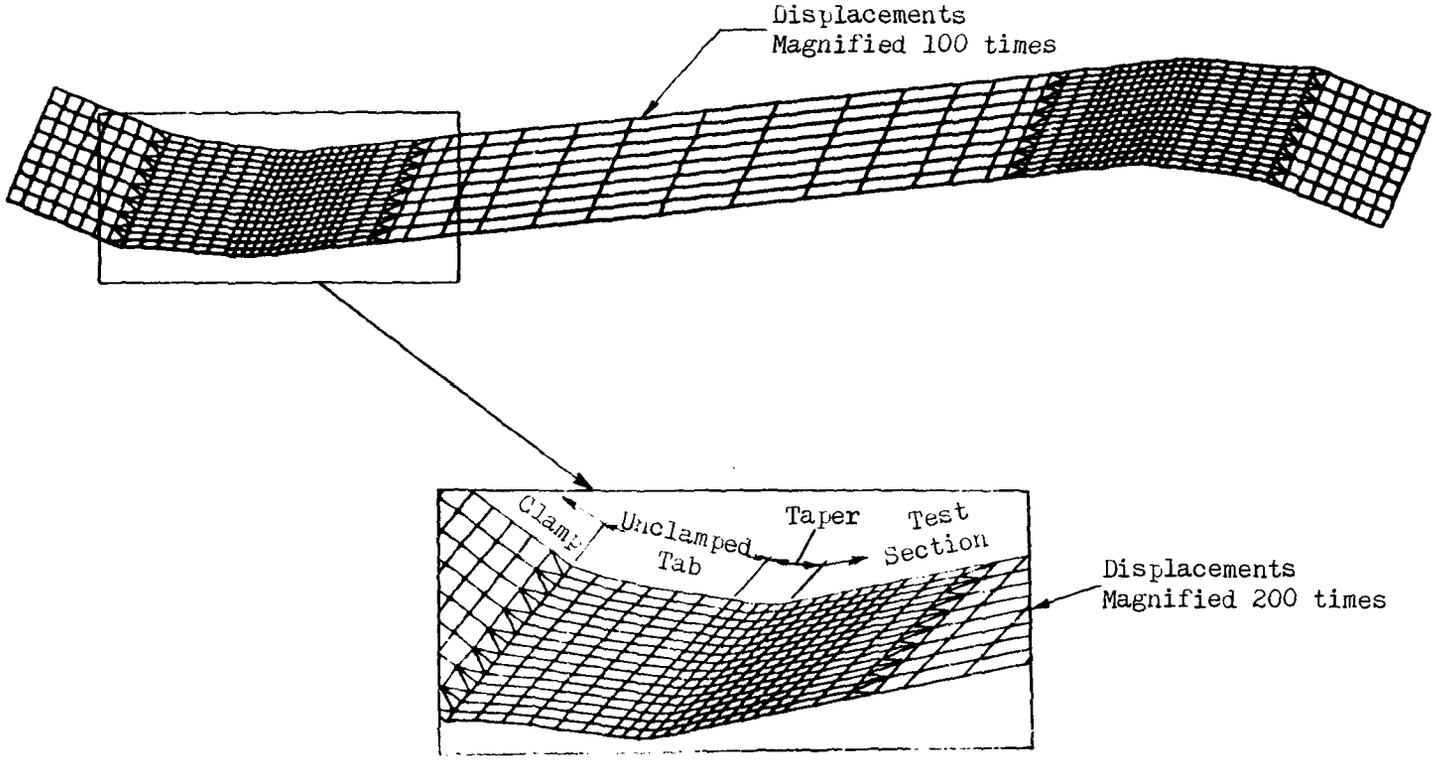

Fig 5.2 Displaced Finite Element Model with $D_c = 1.0''$, $D_p = 0.25''$

portion of the tab, leaving the test section less affected by the rigid clamp. Stress field nonuniformities in the tab are relatively unimportant since, due to the increased strength supplied by the tab, failure is not likely to occur there. Subsequent experimentation with off-axis specimens showed that failure does not occur in the tabbed portion of this specimen design.

Fig. 5.3 shows graphically how stress field uniformity is enhanced by this increase in specimen flexibility. Fig. 5.3a shows contours of σ_x when $D_c = D_p = 1.750$ while Fig. 5.3b shows the contours when $D_c = 1.0$ and $D_p = 0.25$ for the 14° specimen. Visual comparison reveals that the stress field has become more uniform with increased specimen flexibility. Notice the regions of maximum and minimum stress indicated in these figures.

Finally, looking again at Figs. 3.7 and 3.8, one can see that sensitivity of $\Delta\sigma_x$ to variations in D_p is greater for the 10° specimen. On the other hand, looking at Fig. 3.9. one can see that the sensitivity of $\Delta\sigma_x$ to variations in D_c is greater for the 14° specimen.

5.3. Qualitative Assessment of Stress Uniformity

Qualitative information concerning the uniformity of the stress field in the gage length of the off-axis specimens was obtained from two sources. The first source,

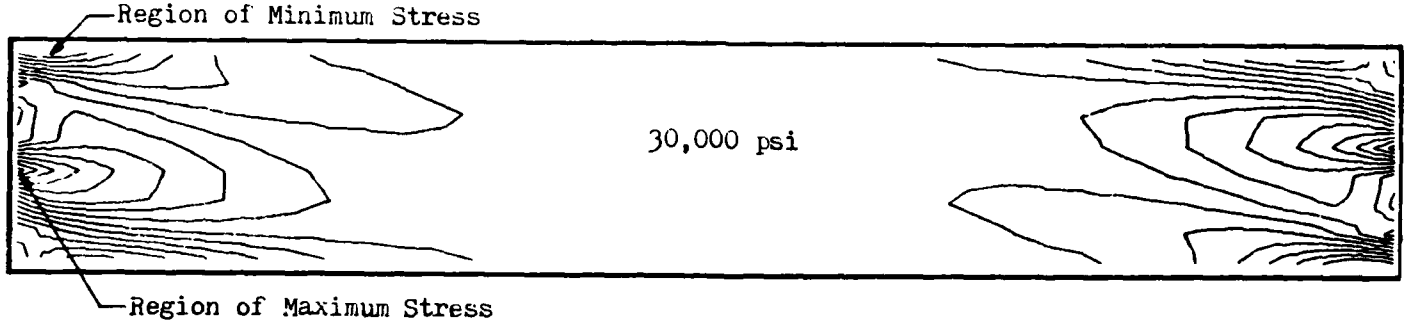

a) $D_c = D_p = 1.75''$, $\theta = 14°$

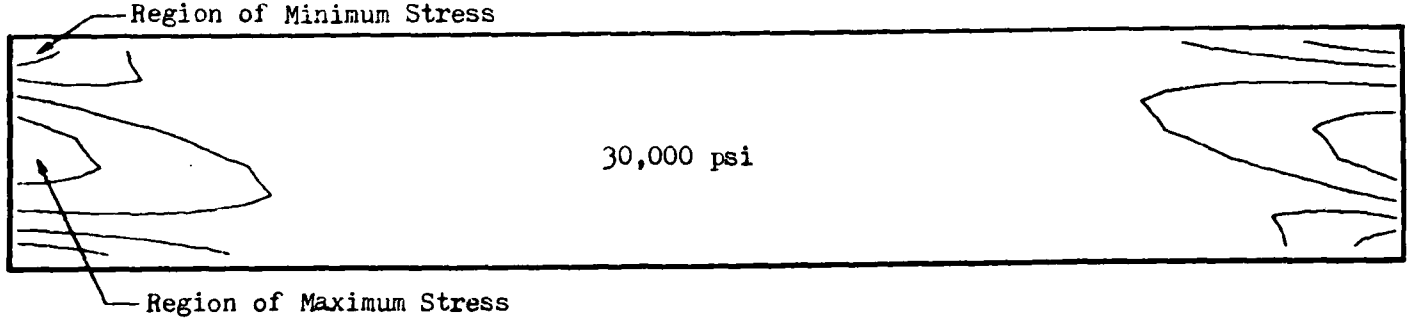

b) $D_c = 1.00''$, $D_p = 0.25''$, $\theta = 14°$

Fig. 5.3 Axial Stress, σ_x, Contours. Contour Increment = 100 psi

was photographs of specimens coated with a photoelastic plastic material. The second source is the fractured specimens.

From the theory of photoelastic analysis, it can be shown that when a photoelastic material is illuminated with white-light, the shade (or combination of colors) at any point in the material will be, for a two dimensional model, a unique function of $\sigma_1 - \sigma_2$ (the difference in the principal stresses). If a coating of photoelastic material is applied to an actual structure, made uniformly reflective by use of a reflective paint or cement, the colors will be proportional to $\sigma_1 - \sigma_2$ in the structure as well (Ref. 17).

Since, in the present study, the state of stress in the gage length is essentially two dimensional, such a method of analysis allows one to make qualitative judgements as to the uniformity of the off-axis specimen stress field. If the experimental stress field is in fact uniform, then the color of the photoelastic coating should be uniform.

The photographs of the 14° specimens are shown in Fig. 5.4 and those for the 10° specimens are shown in Fig. 5.5. The load levels at which the photographs were taken, accompanies each picture. The photoelastic material covers the entire width of the specimen between one of the tabs and the strain gage. In each picture, the tab is at

the top and the strain gage is at the bottom (see Fig. 5.4a).

One can see that in all of the photographs the stress field is essentially uniform between the tab and the strain gage. There are however some color variations that require explanation. The first is the oval shaped discontinuity in the color field in the lower part of the coated area in all of the 10° specimen pictures. Upon inspection of the specimen, this variation was found to be due to poor bonding between the plastic and the reflective adhesive. The second is the color variation present near the bottom of the coated area in all of the 14° specimen pictures. Upon close inspection of the lower boundary of the photoelastic coating, it could be seen, and is somewhat visible in the pictures, that a large amount of adhesive had squeezed out from under the photoelastic coating such that the entire free edge of the photoelastic plastic was embedded in the adhesive. This appears to have distorted the stress field in that area of the photoelastic plastic. Finally, one can see that there are bands of color appearing parallel to the fibers for both specimens. The exact cause for this variation is difficult to determine. However, it appears to be a manifestation of the high stresses occuring in the load carrying fibers. Apparently the bands corresponding to fibers that are closer to the surface than neighboring fibers and, thus, have a greater

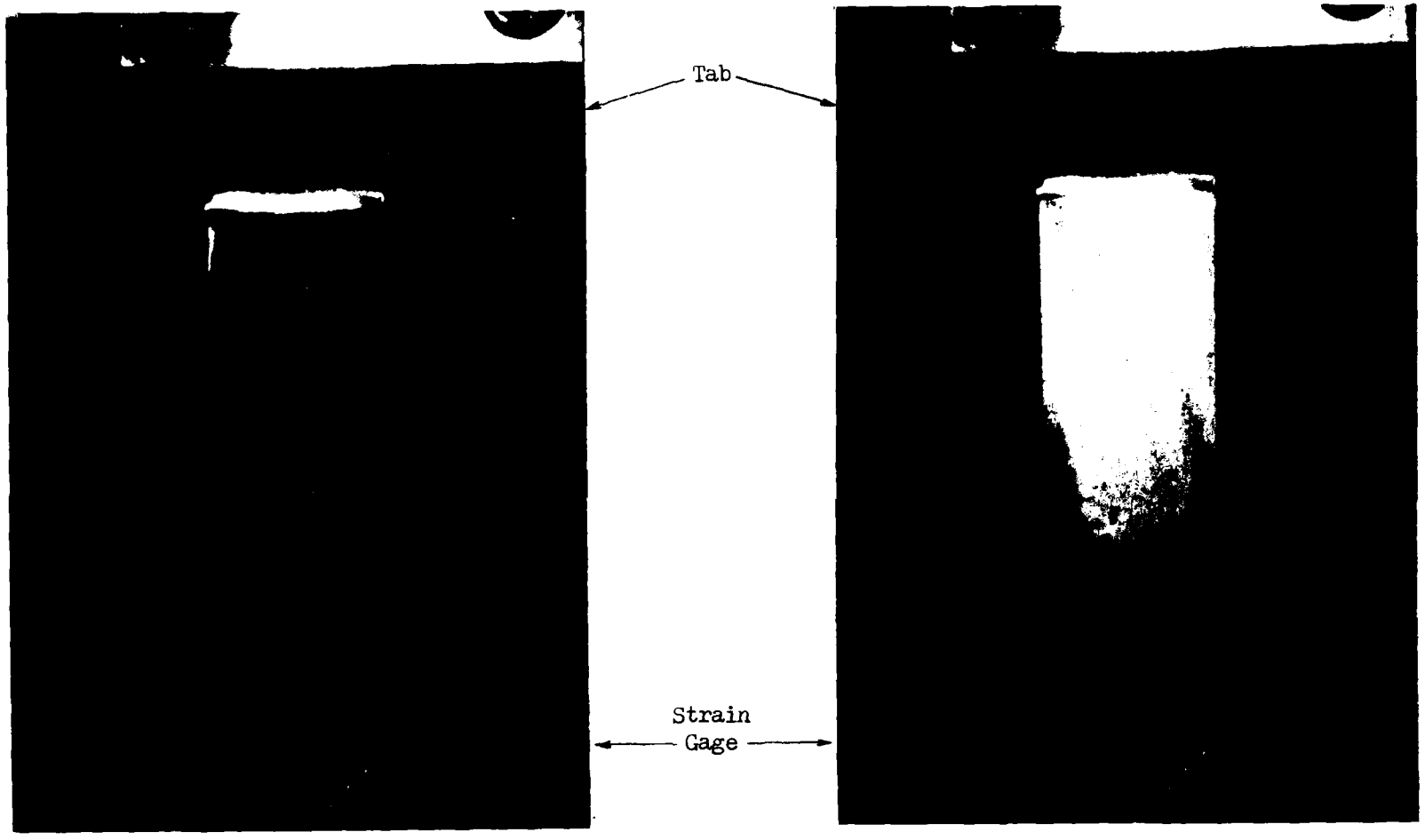

a) 500 lb

b) 1500 lb

Fig. 5.4 14° Specimens Coated with Photoelastic at Various Loads

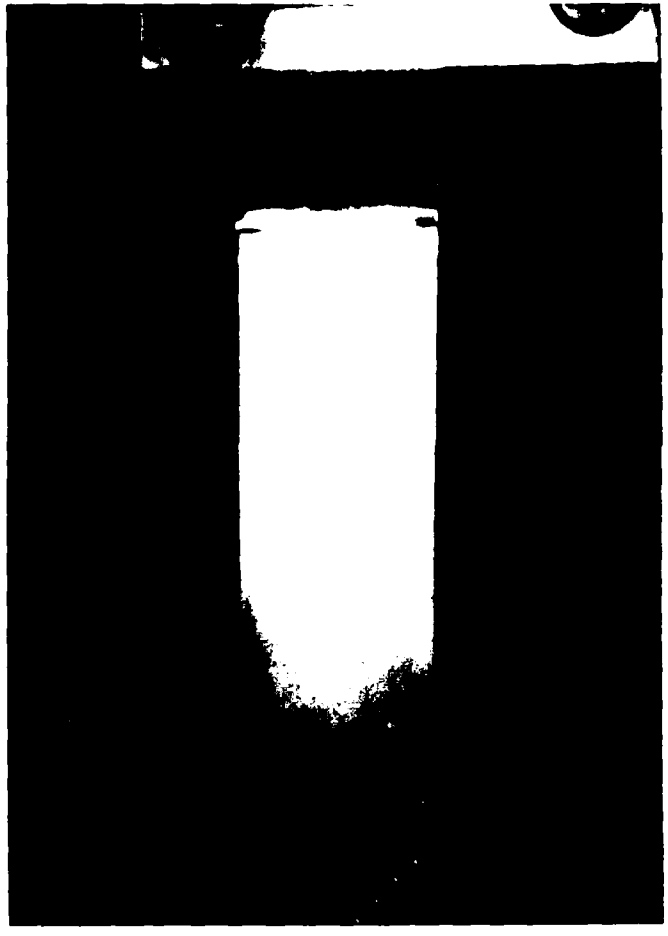

c) 2500 lb

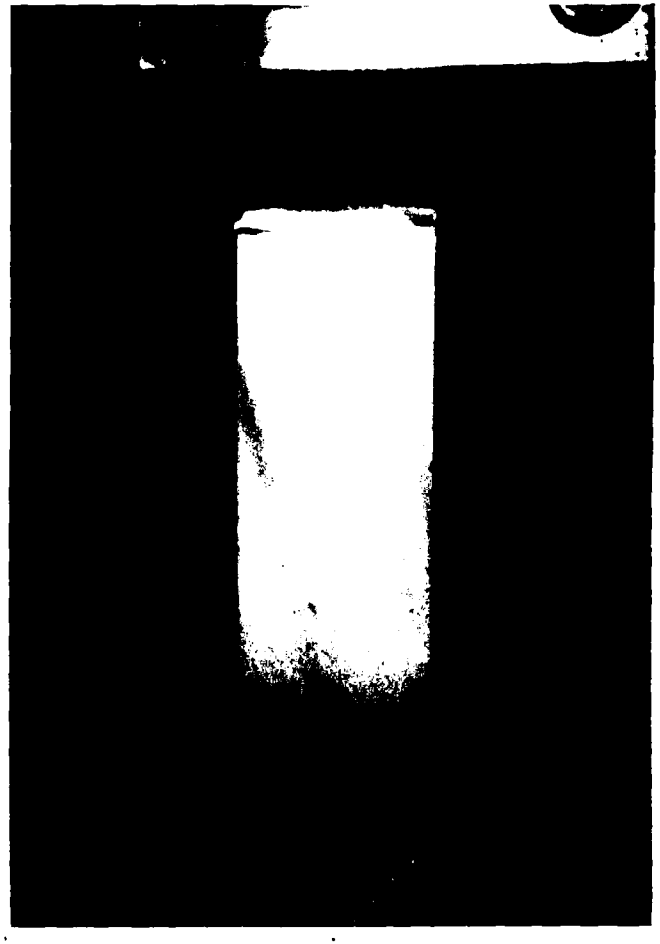

d) 3000 lb

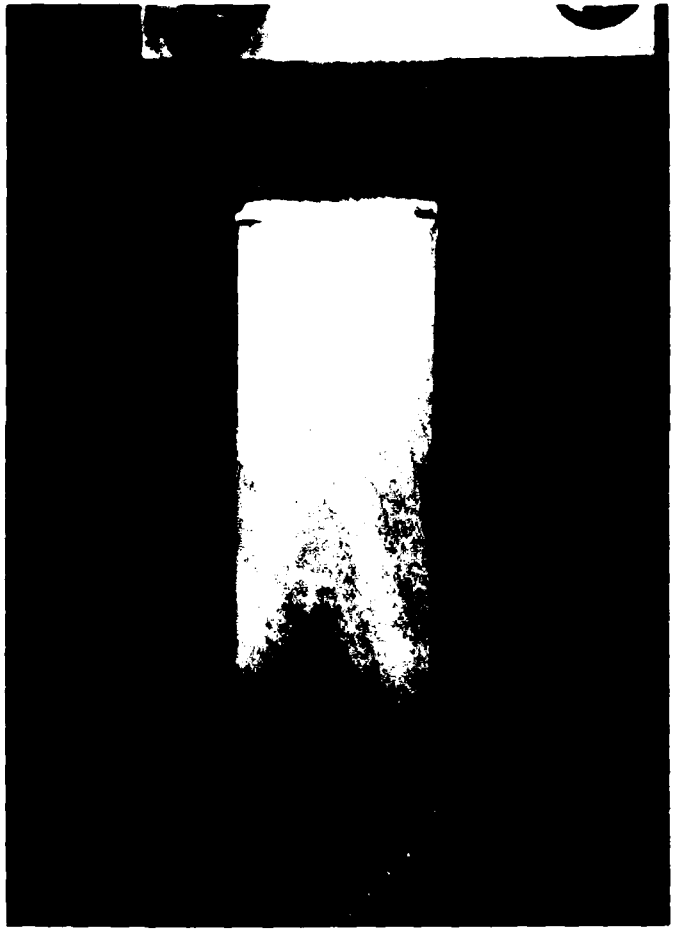

e) 3500 lb

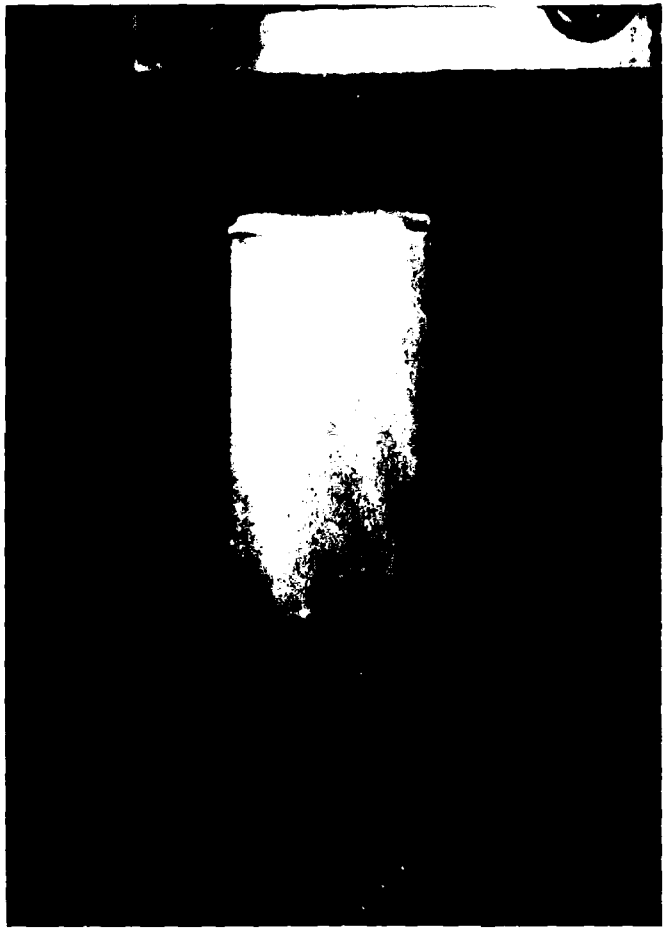

f) 3700 lb

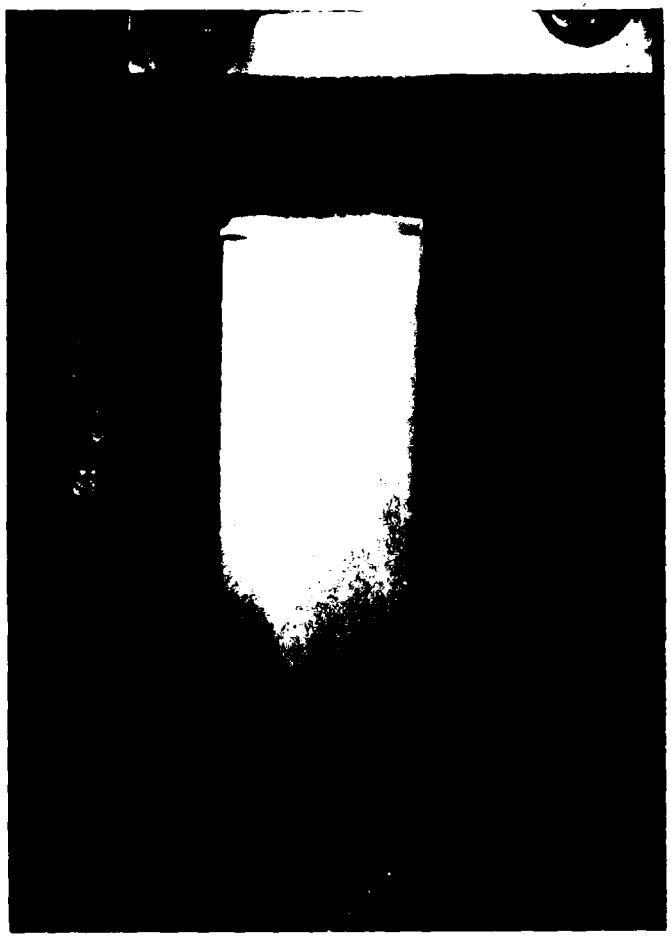

g) 3800 lb

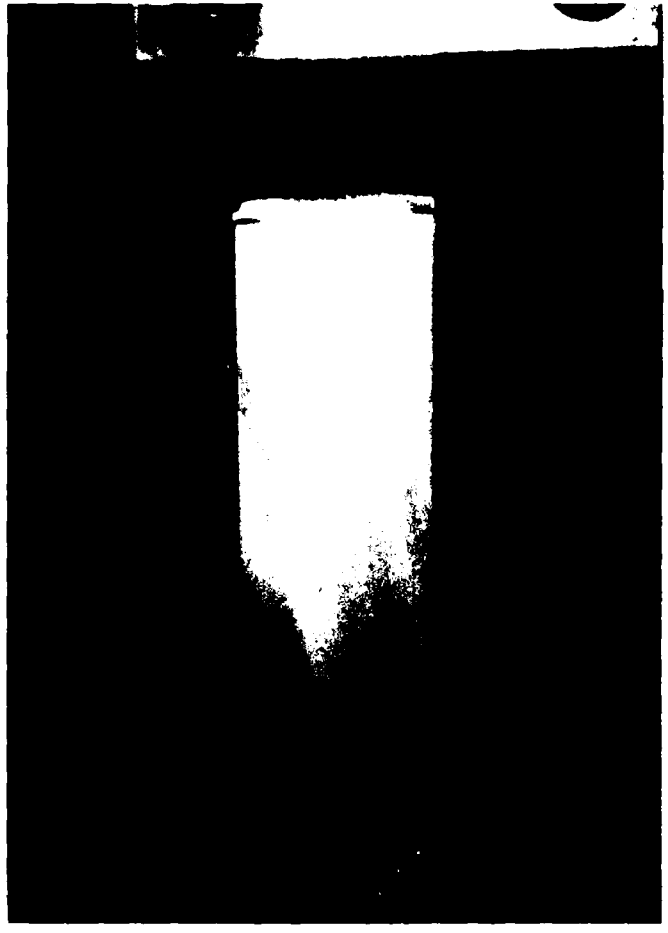

h) 4000 lb

i) Failure

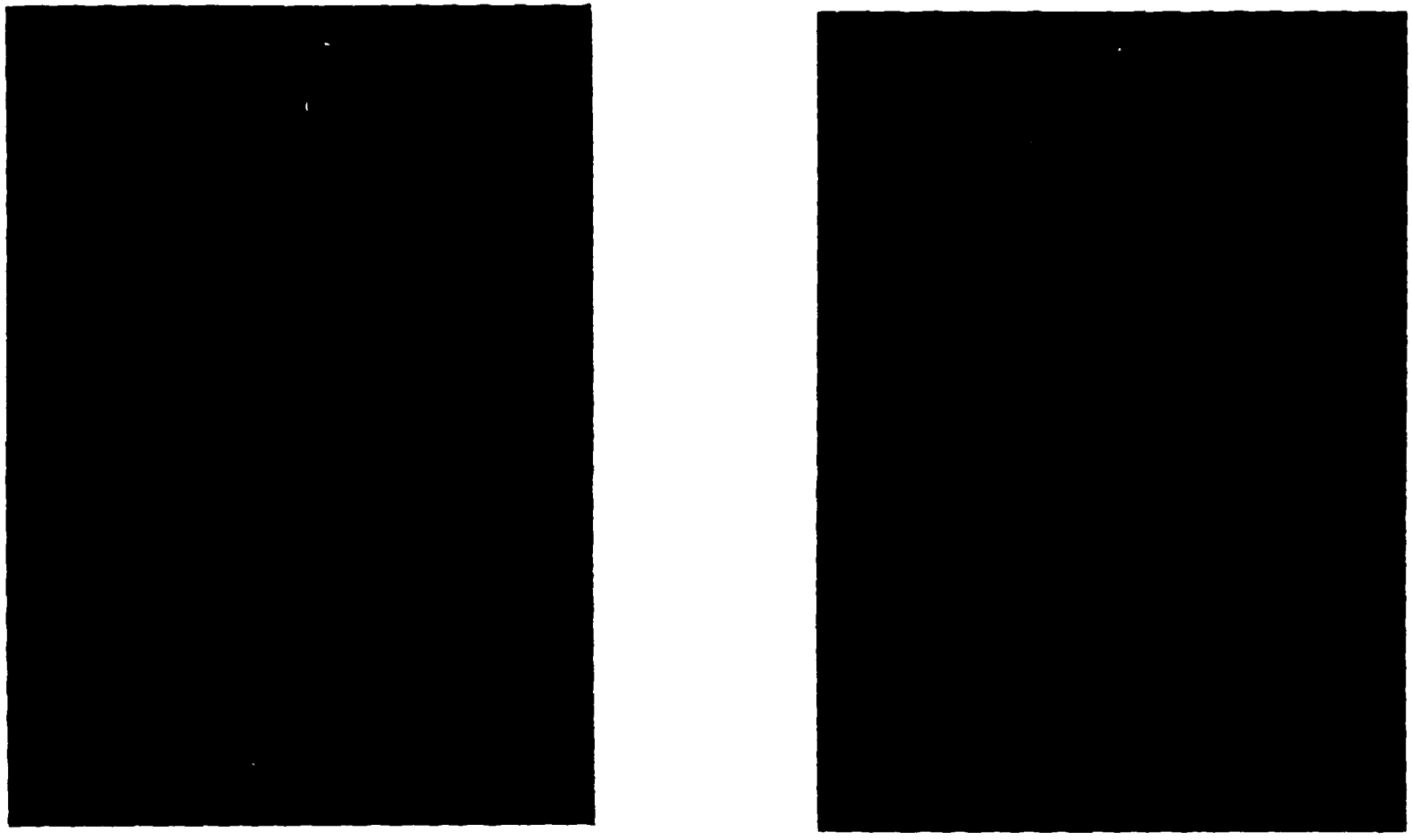

a) 500 lb

b) 1500 lb

Fig. 5.5 10 Specimens Coated with Photoelastic Plastic at Various Loads

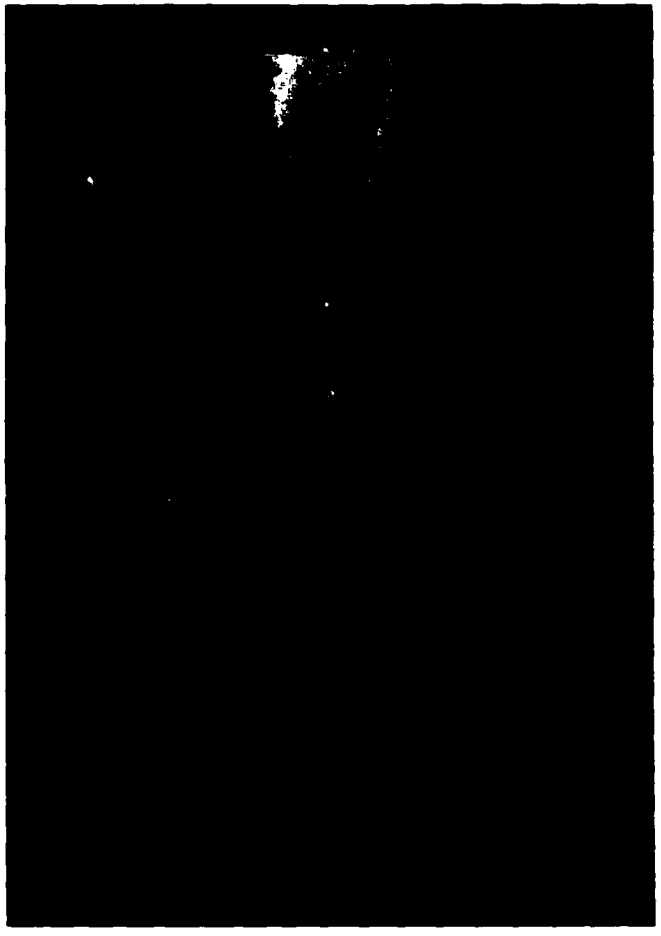

c) 2500 lb

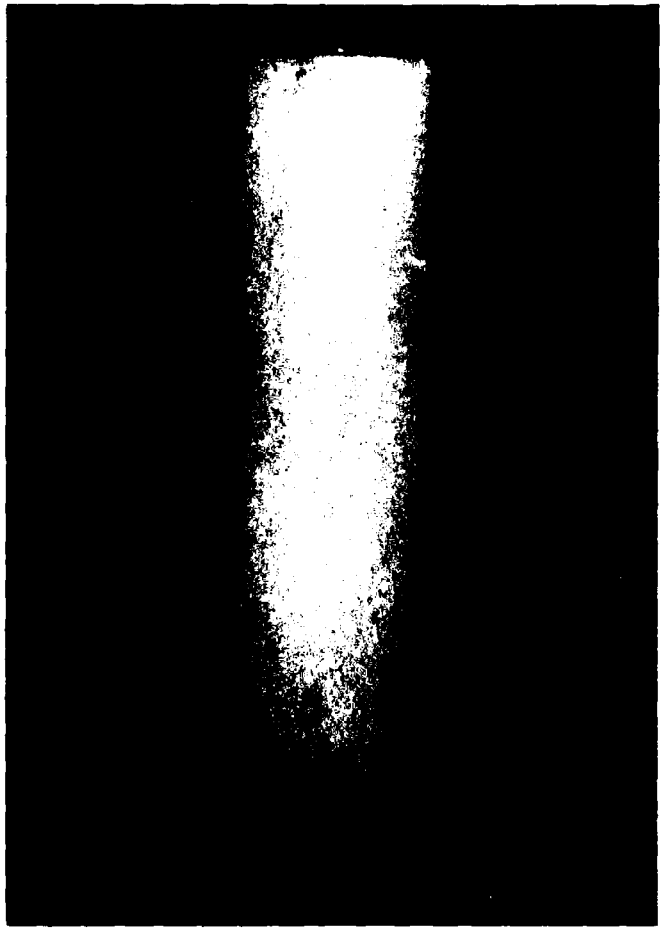

d) 3000 lb

e) 3500 lb

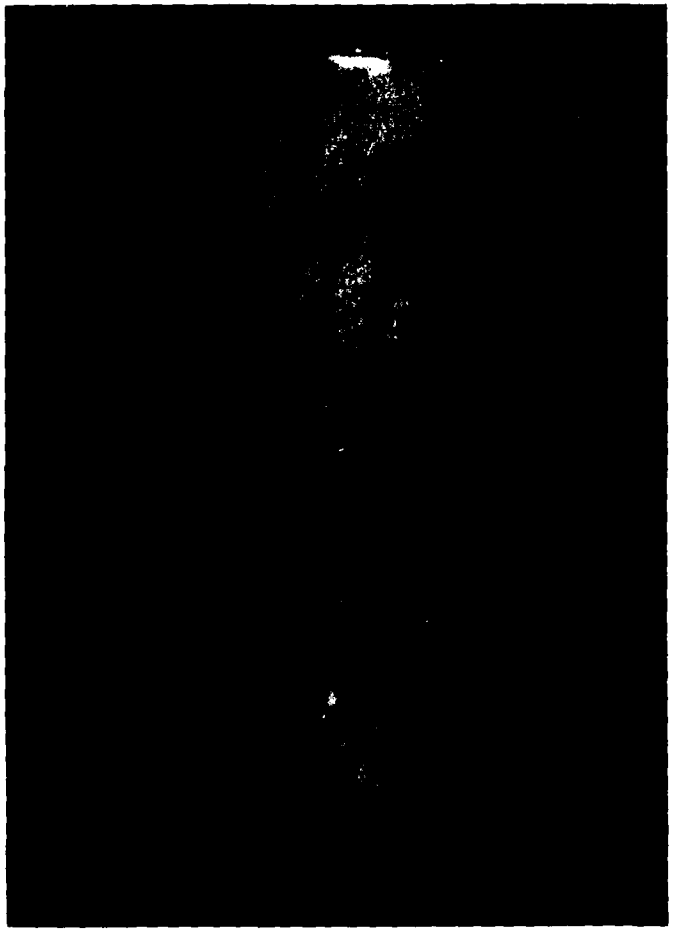

f) 4000 lb

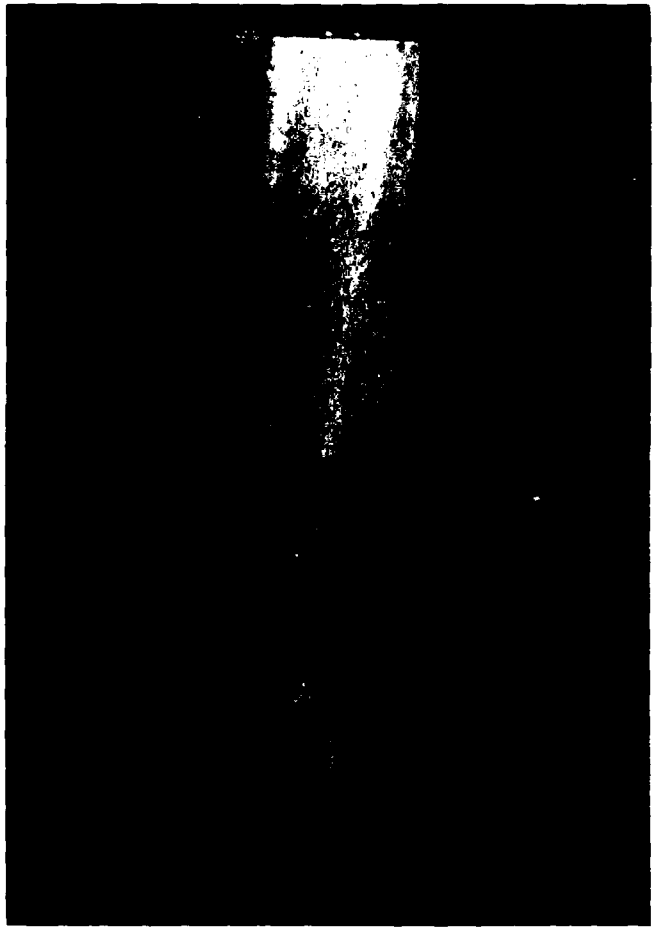

g) 4500 lb

h) 4700 lb

i) 4900 lb

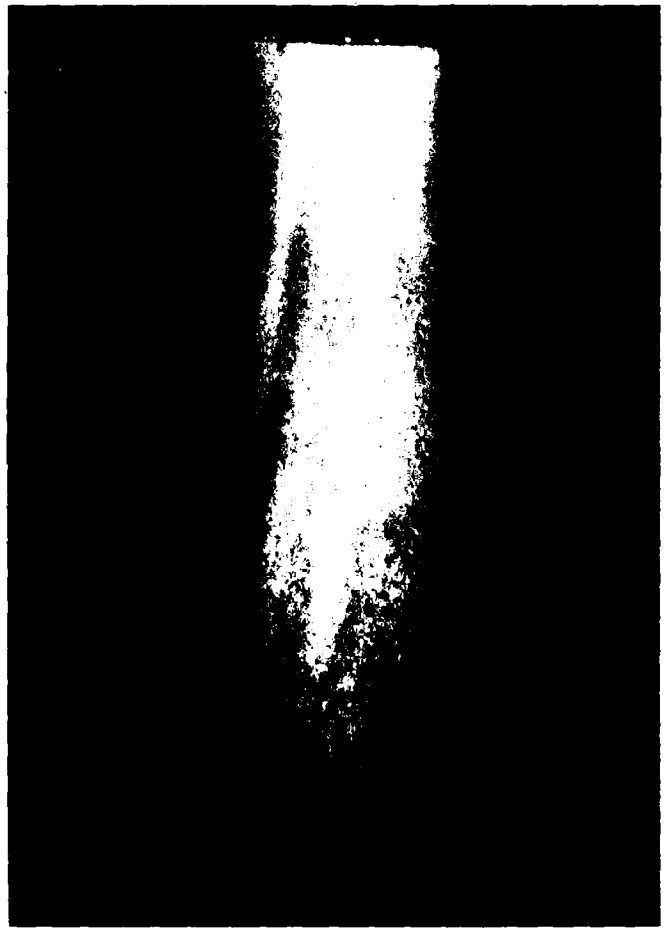

j) 5100 lb

AD-A164 321 IMPROVEMENT OF END BOUNDARY CONDITIONS FOR OFF-AXIS 2/2
TENSION SPECIMEN USE(U) AIR FORCE INST OF TECH
WRIGHT-PATTERSON AFB OH SCHOOL OF ENGI... S M CRON
UNCLASSIFIED DEC 85 AFIT/GAE/AA/85D-3 F/G 20/11 NL

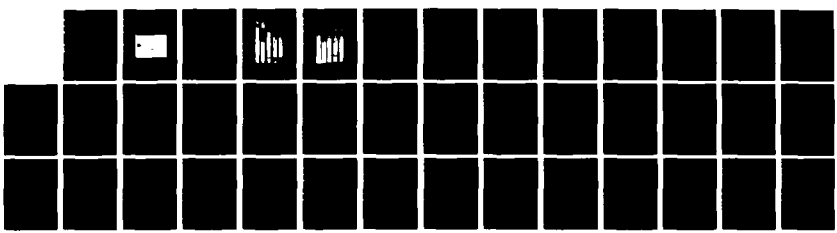

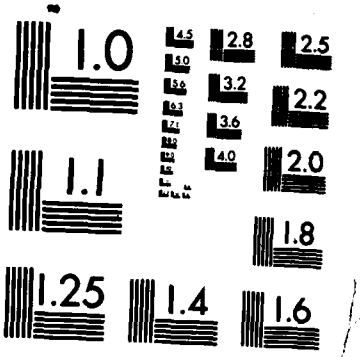

MICROCOPY RESOLUTION TEST CHART
NATIONAL BUREAU OF STANDARDS-1963-A

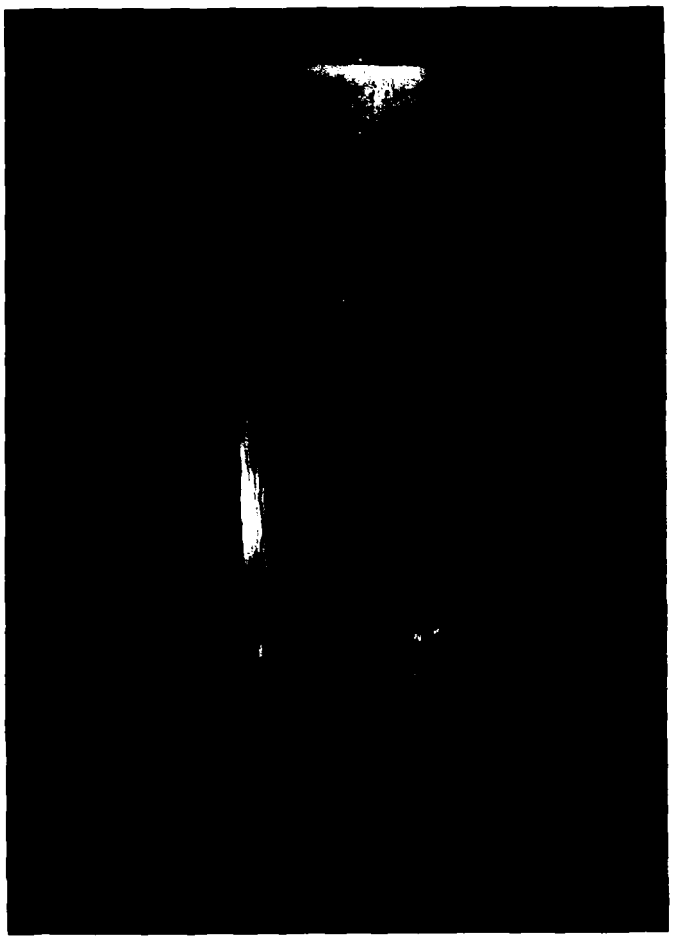

k) Failure

influence on the color field. Notice that the bands correspond to the dominant color from the next load level (compare Fig. 5.5e with 5.5f). This indicates that the stresses in the bands are higher than in the surrounding area. Also note that the bands occur at different places for the two specimens, indicating that the variations are likely a function of material variation rather than a function of specimen geometry.

The important observation to be made from these pictures is that near the source of the stress field nonuniformity, the end clamps and tabs, there is no apparent region of stress concentration or variation for either the 10° or 14° specimens. As one looks at the color field immediately adjacent to the tab, one sees the same colors that appear 1 in. or 2 in. away from tab.

The photographs of the fractured specimens are shown in Figs. 5.6 and 5.7. One can see from these pictures that for all but one of the 10° specimens, failure occured entirely in the test section of the specimen. Furthermore, for eight of the ten specimens, the failure surface was at least 3/8 in. away from the tabs. This is an indication that the stress field was of a uniform enough nature to prevent failure from initiating from a particular point of stress concentration near the tabs.

At this point it is important to observe that the finite element technique used has thus far proved quite

Fig. 5.6 Failed 10° Off-Axis Specimens

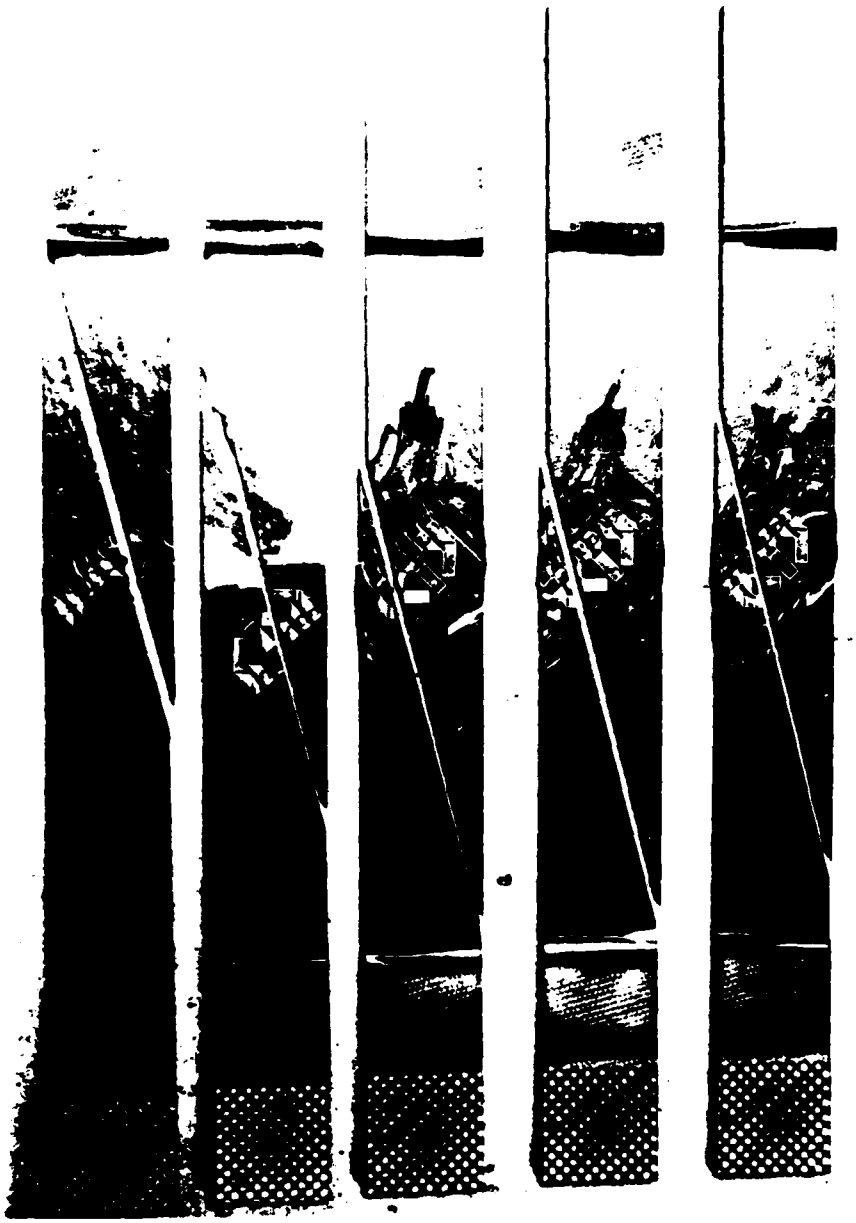

Fig. 5.7 Failed 14° Off-Axis Specimens

accurate in predicting the behavior of the off-axis tension specimen. It has been used to determine ideal values of D_c and D_p which have, in fact, resulted in a nearly uniform test section stress field. This uniformity has manifested itself quite clearly through the uniform colors of the photoelastic coating and consistent test section failures. With this in mind let us now look at the results of the nonlinear analysis of the off-axis specimen.

5.4. Results of the Nonlinear Analysis

The bulk of the nonlinear results were obtained for comparison with experimental data and will be discussed as such in subsequent sections. It is appropriate, however, to observe the effect of material nonlinearity on stress uniformity at this point since it cannot be directly measured experimentally. Fig. 5.8 shows how $\Delta\sigma_x$ varied from initial loading to failure. In this plot $\Delta\sigma_x$ is plotted as a percentage of midsection axial stress, σ_x, so that the effect of nonlinearity can be more readily observed. One can see that, as indicated in Ref. (11), the uniformity of the stress field is degraded slightly by the material nonlinearity. For the 10° specimen there is a 0.32 % increase from initial load to failure, while for the 14° specimen there is a 0.76 % increase. These small increases in $\Delta\sigma_x$, relative to the midsection axial stress,

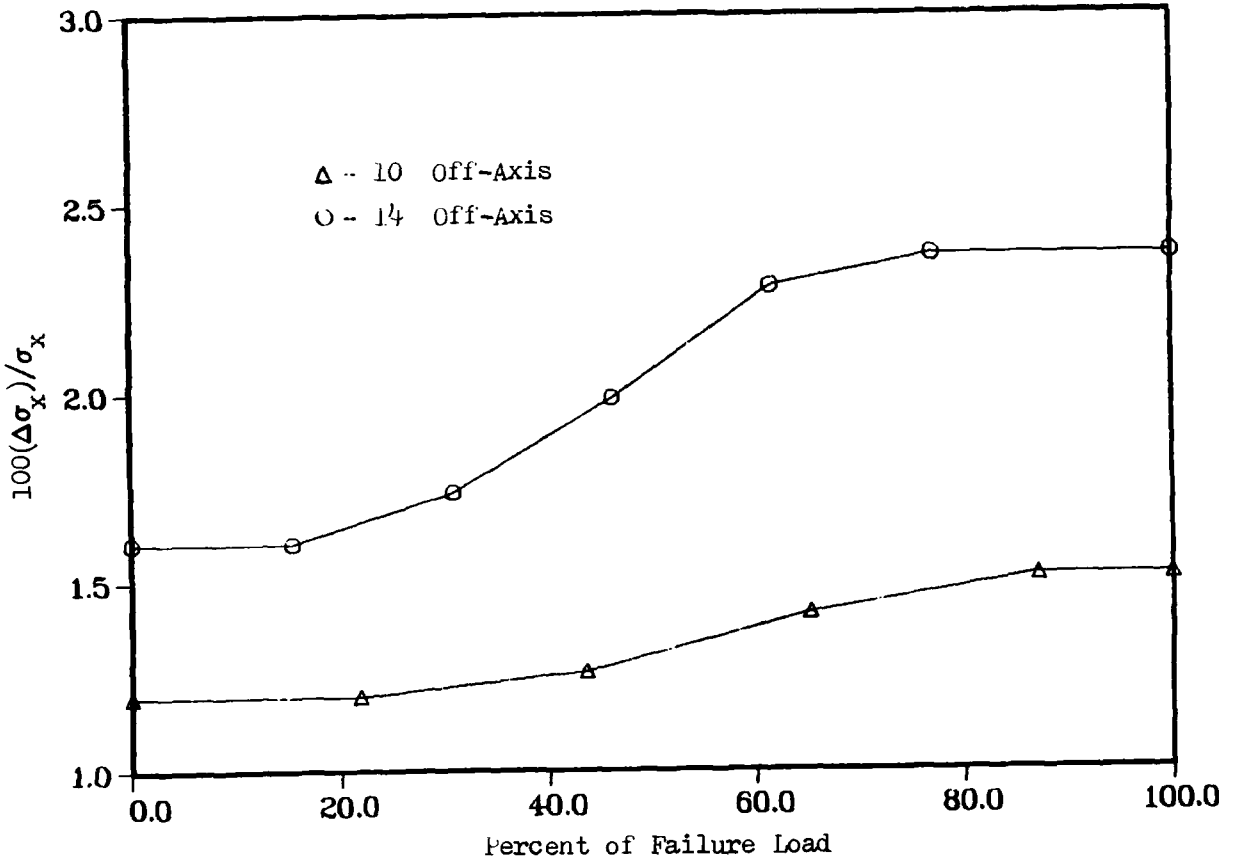

Fig. 5.8 Variation in $\Delta\sigma_x$ as Load is Applied

indicate that the assumption of material linearity for the design of the off-axis specimen resulted in little, if any, error in determining D_c and D_p.

5.5. Comparison of Analytical and Experimental Stress-Strain Responses

Figs. 5.9 and 5.10 show the experimental and analytical stress-strain curves for the 10° and 14° specimens, respectivley. The experimental curves represent an average of 5 tests. One can see that from initial loading up to approximately 60 % of the analytical failure load, correlation is quite good for both off-axis angles. For the remainder of the loading, however, the correlation is degraded. Exact errors in failure stresses and strains will be compared in the next section in terms of the failure criteria. For now, a reason for the overall lack of correlation is sought.

Looking at Figs 5.9 and 5.10 one can see that the axial stress at which the 10° responses begin to diverge is around 44,000 psi while for the 14° responses divergence begins at around 32,000 psi. Referring back to eq. 2.4, we can determine the shear stresses in the fiber direction, corresponding to these axial stresses.

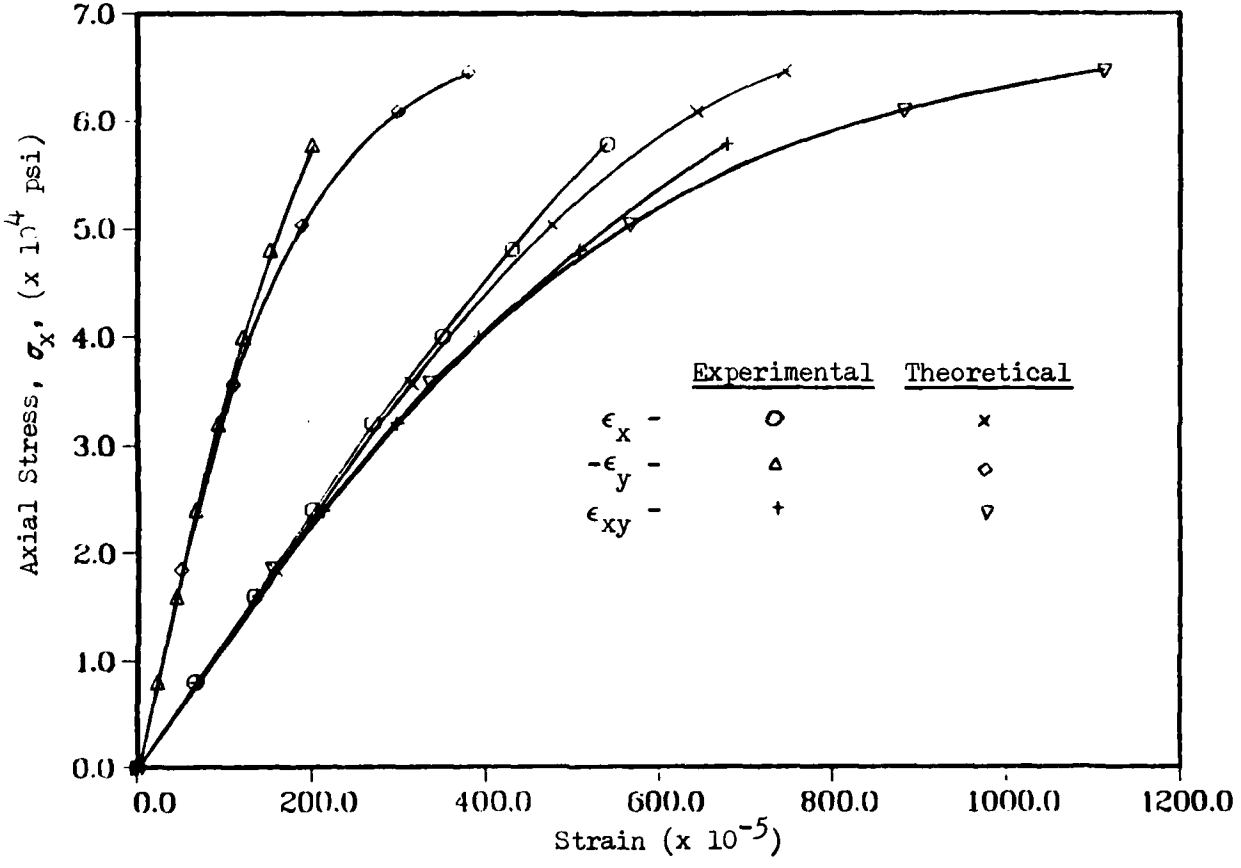

Fig. 5.9 Experimental-Analytical Stress-Strain Curves for 10° Off-Axis

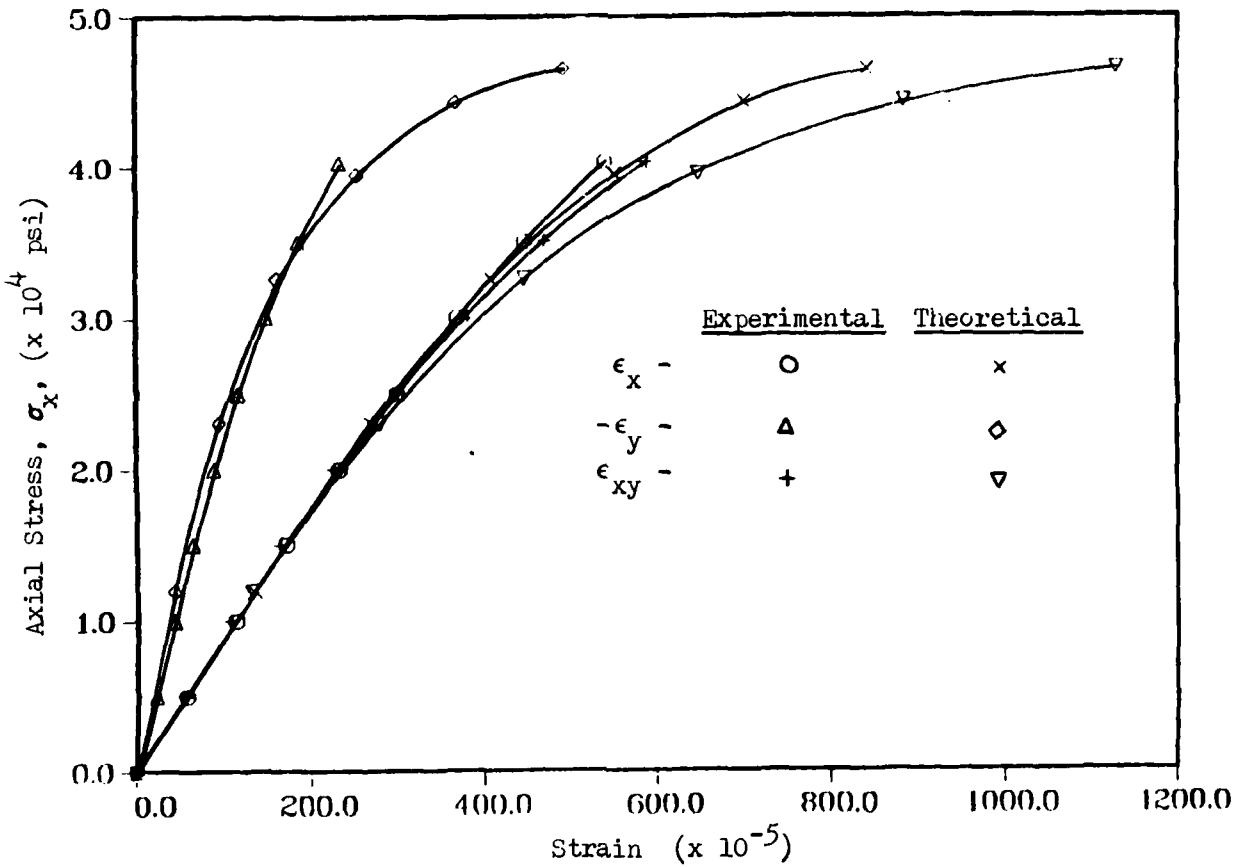

Fig. 5.10 Experimental-Analytical Stress-Strain Curves for 14° Off-Axis

For the 10° response,

$$\tau_{12} = 44{,}000 \times \cos(10^{\circ}) \times \sin(10^{\circ}) = 7524.4 \text{ psi}$$

For the 14° response,

$$\tau_{12} = 32{,}000 \times \cos(14^{\circ}) \times \sin(14^{\circ}) = 7511.5 \text{ psi}$$

Thus we can see that the initial divergence corresponds to a fiber direction shear stress of, nominally, 7500 psi. Now referring back to appendix B, to the experimental shear stress strain curve for graphite/epoxy, we can see that a shear stress of 7500 psi corresponds, approximately, to the point where the one dimensional shear stress-strain curve becomes highly nonlinear. Since the one-dimensional normal and transverse stress-strain curves are essentially linear at all stress levels, and since the correlation in the linear range is quite good, it follows that the shear stress-strain curve, which is input to the nonlinear finite element program, is cause for at least part of the lack of correlation subsequent to the two axial stresses given above.

Recalling that the input shear stress-strain curve was obtained experimentally from a laminate ($(\pm 45)_{2S}$) it seems that it would be safe to say that, for this case, the shear stress-strain response of a graphite/epoxy laminate is not the same as that of unidirectional graphite/epoxy in the nonlinear regime. One can see that it is at the point where the $(\pm 45)_{2S}$ laminate shear stress-strain curve begins to exhibit appreciable nonlinearity, that the responses

diverge.

This argument is further born out in Fig 5.11 where experimental shear stress-strain curves are shown for 10° and 14° off-axis and $(\pm 45)_{2S}$ laminate along with analytical off-axis curves. One can readily see that despite the apparent uniformity of the off-axis specimen stress field, the experimental shear response of the off-axis specimen does not continue as far into the nonlinear regime as does the $(\pm 45)_{2S}$ laminate. Furthermore, beyond approximately 3000 psi the shear modulus of the off-axis curve is above that of the $(\pm 45)_{2S}$ laminate. In short, outside of the linear regime, the shear response of the unidirectional off-axis specimen differs somewhat from that of the $(\pm 45)_{2S}$ laminate. Notice also that the analytical off-axis shear stress-strain curves are almost exactly the same as the experimental $(\pm 45)_{2S}$ curve. This is an indication that the finite element technique was operating properly given the stress strain-curves input to it.

It should be pointed out that if, in the nonlinear regime, the shear stress-strain response of the $(\pm 45)_{2s}$ laminate is, in fact, different from that of the off-axis specimen, the divergence we have observed is really of no surprise. In choosing to analyze the 10° and 14° specimens, we have chosen off-axis angles where the specimen behaviors are essentially controlled by their shear characteristics. Thus, to the extent that the shear

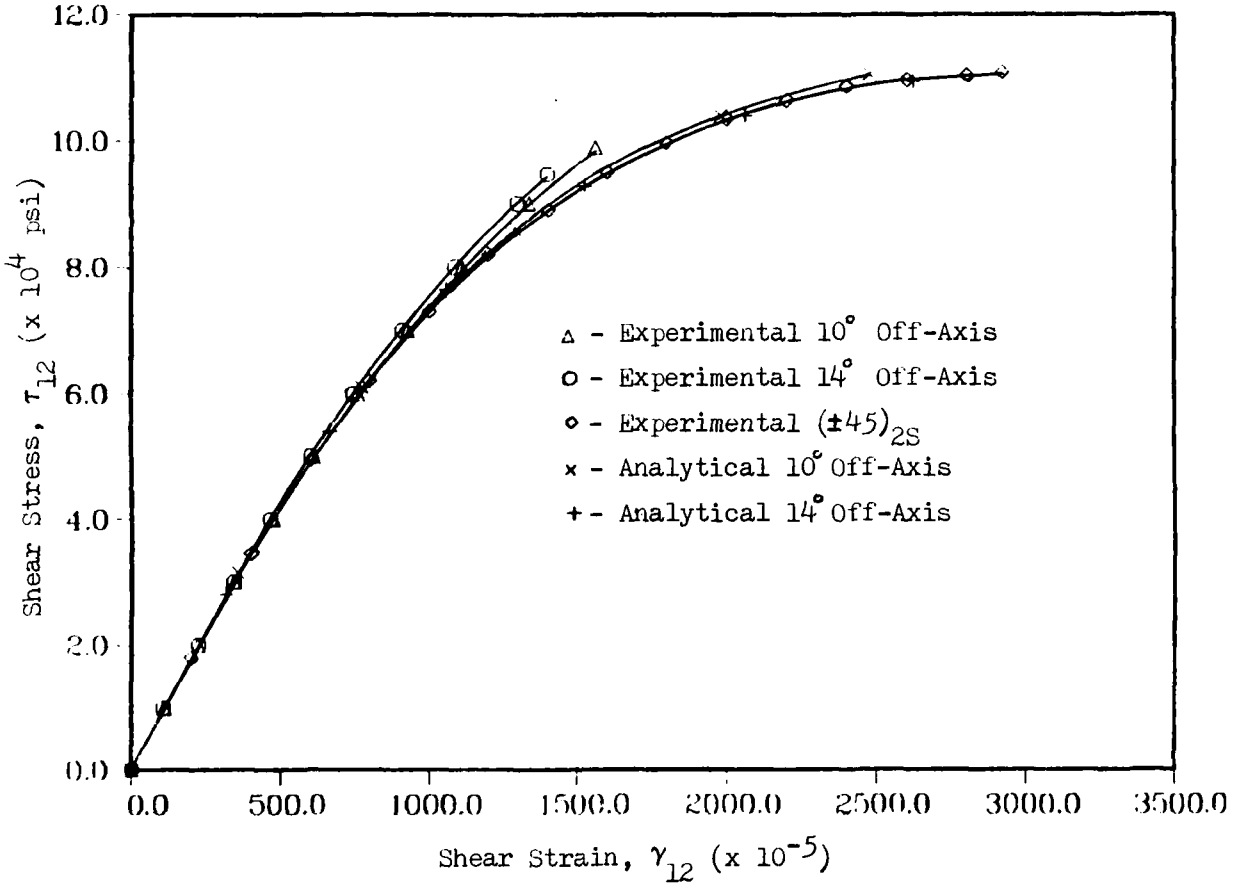

Fig. 5.11 Analytical-Experimental Shear Stress-Strain Curves

stress-strain curve input to the finite element program is inaccurate in the nonlinear regime, the predicted response will likewise be inaccurate.

To this point, we have observed that the finite element technique itself is not responsible for the lack of correlation between the analytical and experimental responses. We have seen, however, that the shear stress-strain response of the $(\pm 45)_{2s}$ laminate misrepresents the off-axis shear response and consequently causes some of the lack of correlation. The extent of the error caused by this misrepresentation and the error caused by the failure criteria will now be discussed.

5.6. Comparison of Analytical and Experimental Failure Data

One can see from Figs. 5.9 and 5.10 that if the failure criteria had predicted failure at, or at least closer to, the failure loads of the experimental specimens, the errors in the ultimate strain states predicted by analysis would have been fairly small. Table 5.1 shows the errors in the strain states corresponding to the experimental failure loads. These relatively small errors indicate that using the $(\pm 45)_{2S}$ shear stress-strain curve is not the primary reason for the overall lack of correlation. Rather, it is the failure criteria that is

	ε_x ($\times 10^{-6}$)			ε_y ($\times 10^{-6}$)			ε_{xy} ($\times 10^{-6}$)		
Angle	exp	theo	%error	exp	theo	%error	exp	theo	%error
10°	5400	5852	7.7	2000	2543	21.4	6800	7531	9.7
14°	5408	5753	6.0	2336	2679	12.8	5900	6765	12.8

Table 5.1 Analytical and Experimental Strains at the Experimental Failure Loads

causing it.

Let us look, then, to see how an earlier (lower stress level) prediction of failure might have been affected with the given criteria.

Recalling the discussion of section 2.5, the m parameter of the failure criteria was taken to be unity. It was not clear, however, whether this was in fact the best choice for accurately predicting failure of the material used in this study. To observe what value of m might have been a better choice, let us plot the function,

$$(K_1/\bar{K}_1)^m + (K_2/\bar{K}_2)^m + (K_6/\bar{K}_6)^m = 1 \qquad (5.1)$$

for the first element that failed (see Fig. 5.12 for location of the element), for m = 1, m = 3/4, and m = 1/2. These plots for the 10° and 14° specimens are shown in Figs. 5.13 and 5.14, respectively. Vertical lines are drawn at the experimental and analytical failure stress levels. One can see that for m = 1/2, a definite improvement in correlation would have resulted. For the 10° specimen the error in failure load would be reduced to 0.0 % and for the 10° specimen the error would be reduced to 4.3 %. This adjustment of m is not meant to be conclusive, but to show a trend in the effect m has on the predicted failure load.

Let us now look at a second parameter of the failure criteria that may influence the predicted failure load.

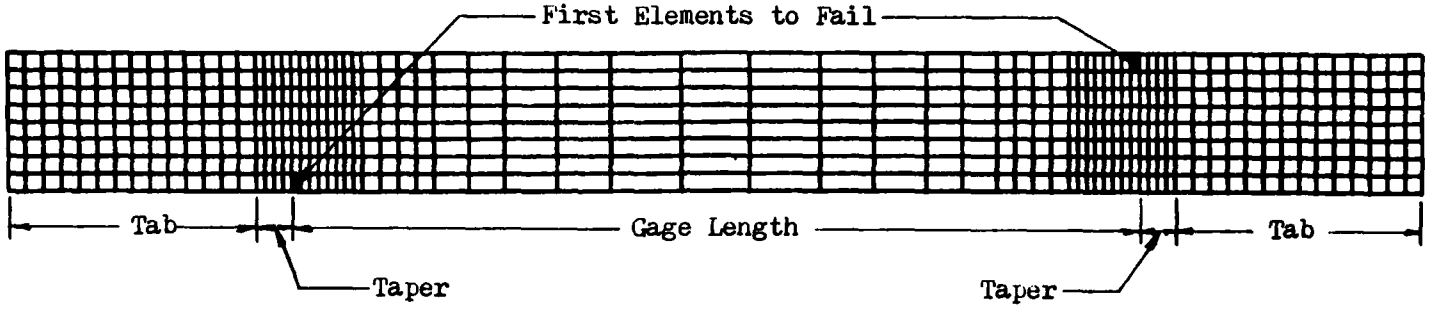

Note: Both elements shown fail simultaneously since the off-axis specimen is antisymmetric about the midpoint

Fig. 5.12 Location of First Elements Predicted to Fail

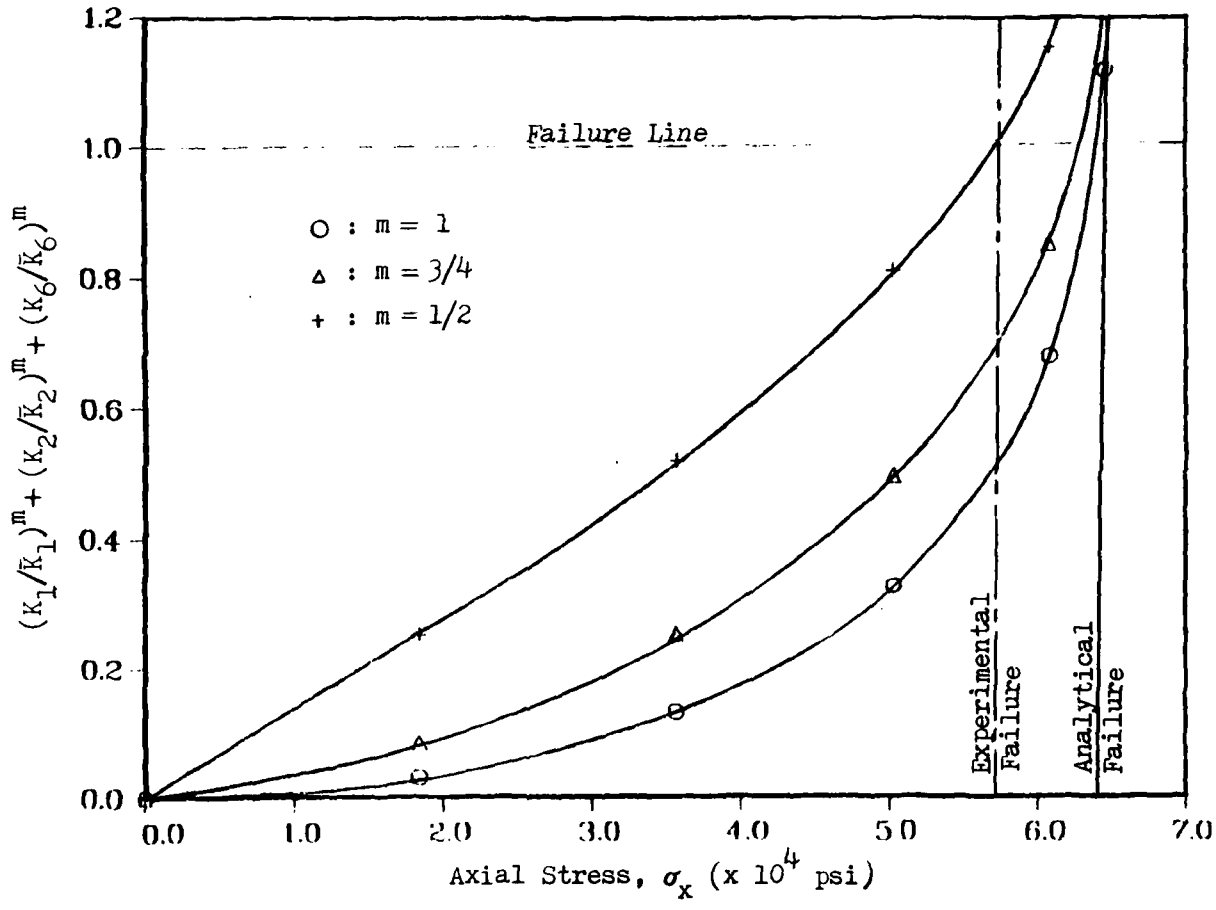

Fig. 5.13 Effect of Variation of m Parameter on Failure Criteria For 10° Off-Axis Specimen

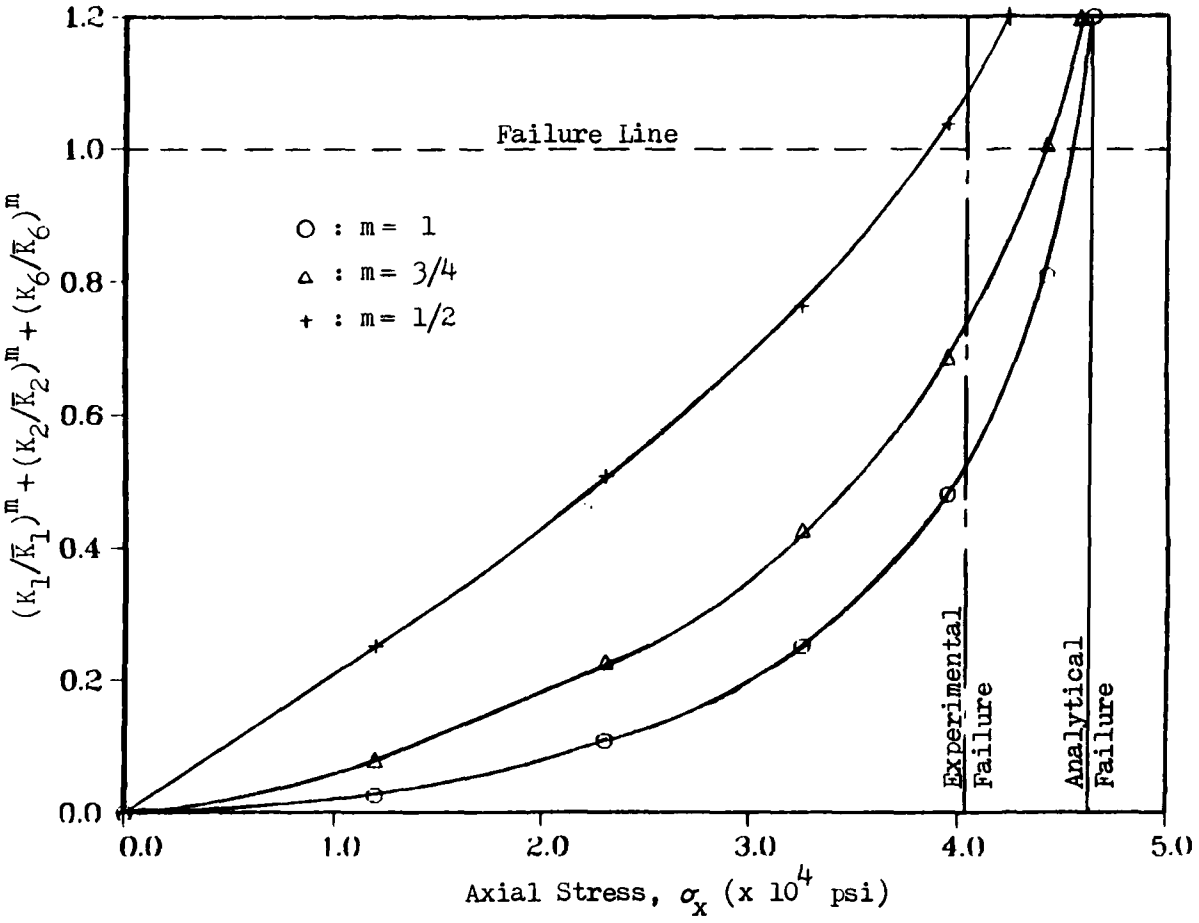

Fig. 5.14 Effect of Variation of m Parameter on Failure Criteria for 14° Off-Axis Specimens

Recalling that the failure of the 10° and 14° specimens is primarily in shear, the first two ratios of eq. 5.1 are small relative to the third, thus the value of $\bar{K}_6$ (the area under the one dimensional shear stress-strain curve), has a very strong influence on the failure criteria. Referring to Fig. 5.11, one can see that the areas under the shear stress-strain curves for the experimental off-axis specimens (89.09 psi and 74.82 psi for 10° and 14°, respectively) are much less than the area under the shear stress-strain curve for the $(\pm 45)_{2S}$ laminate (230.77 psi). Since there is some doubt as to whether the $(\pm 45)_{2S}$ shear stress-strain curve is representive of the unidirectional material, let us again plot eq. 5.1 for, $m = 1$ and $\bar{K}_6$ equal to the area under the experimental off-axis shear stress-strain curve. These plots are shown in Figs. 5.15 and 5.16. Note that the actual shear stress-strain curve used by the finite element program is still that from the $(\pm 45)_{2S}$ laminate. Only the value of $\bar{K}_6$ has been changed. One can see that using the areas under the off-axis shear stress-strain curves, the failure load would be underestimated in both cases. Note however that the predicted failure load has moved in the direction of the experimental failure load. Again, using the off-axis values of $\bar{K}_6$ is not a conclusive solution to the problem, but it does indicate a possible method of improving the results.

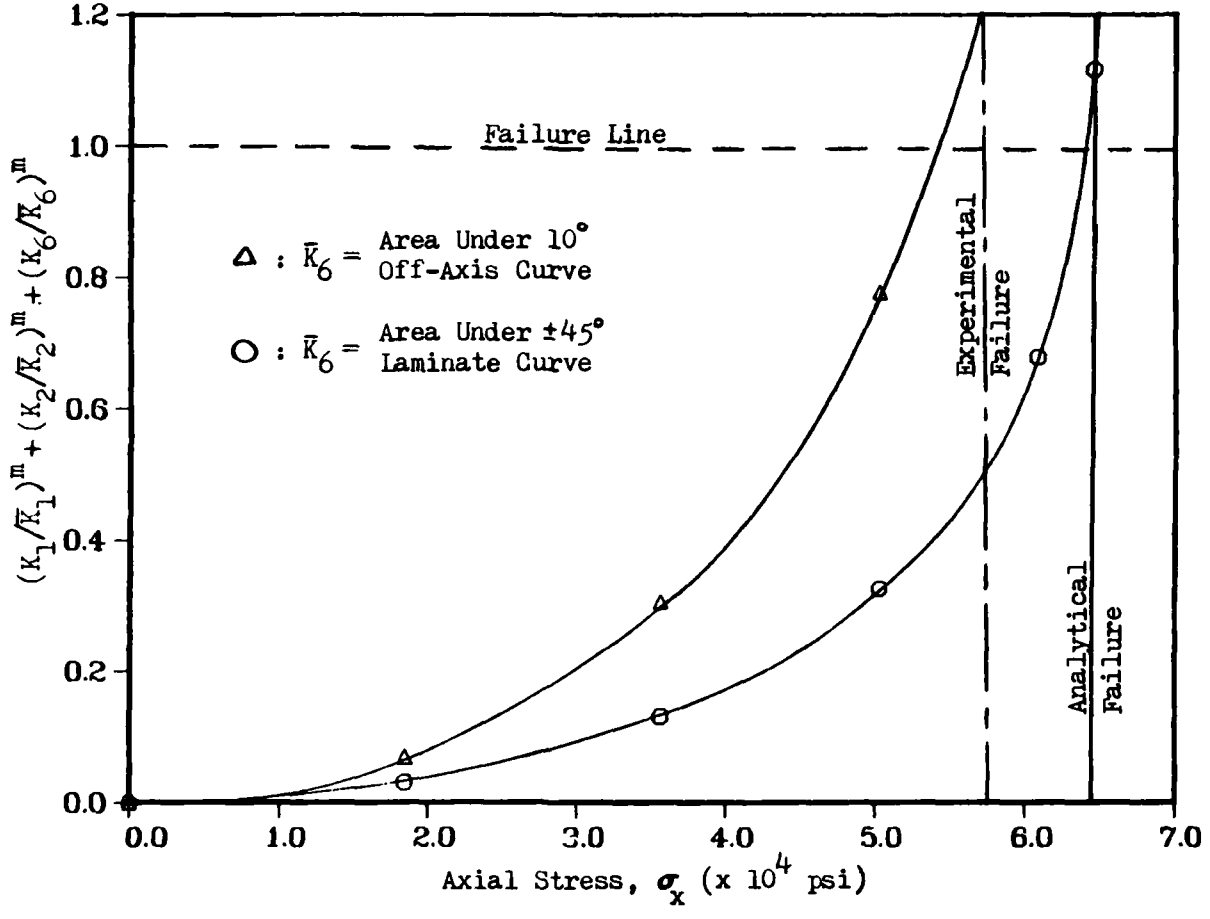

Fig. 5.15 Effect of Variation of $\bar{K}_6$ on Failure Criteria for 10° Off-Axis Specimen

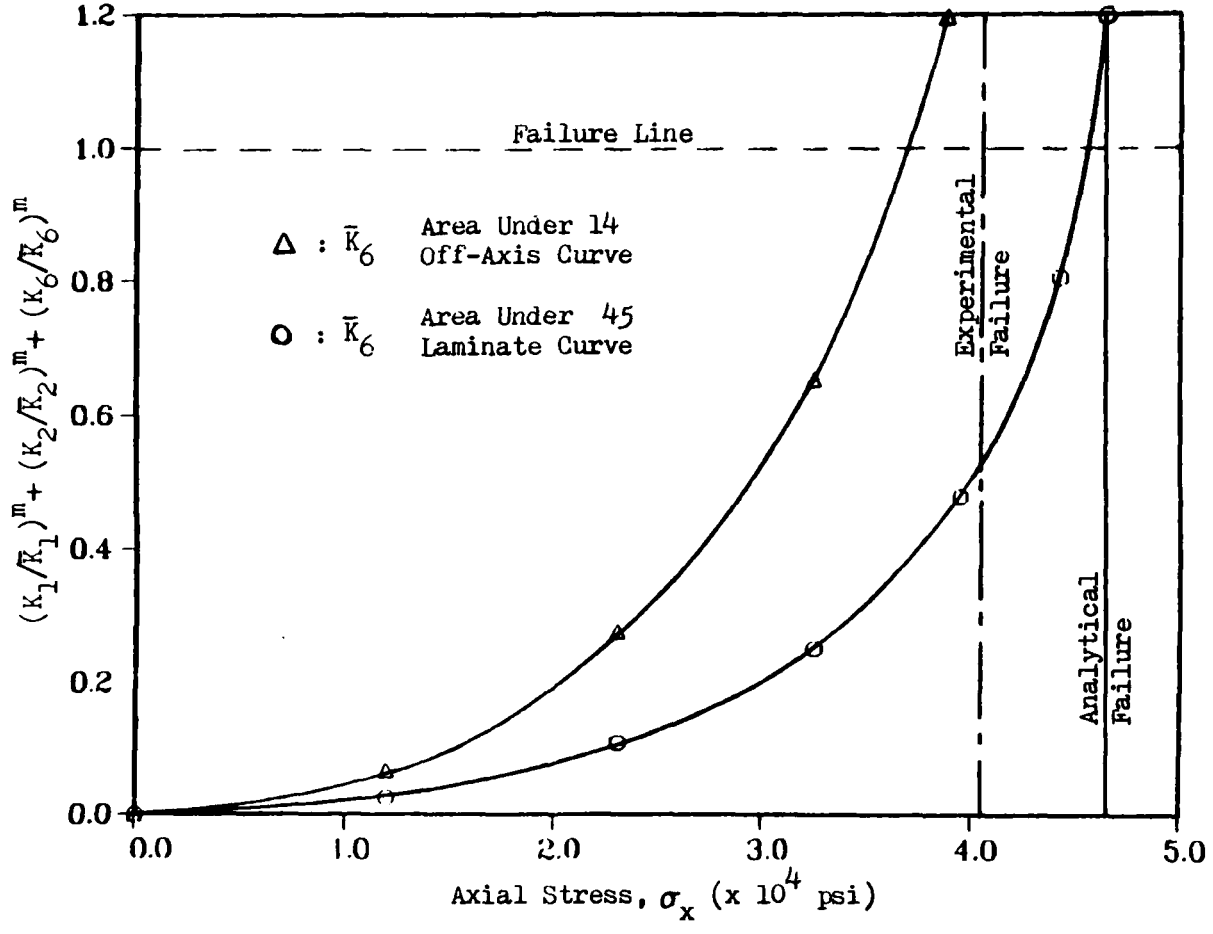

Fig. 5.16 Effect of Variation of $\bar{K}_6$ on Failure Criteria for 14° Off-Axis Specimen

CHAPTER 6

CONCLUSIONS

It is possible to separate the conclusions drawn from this study into two areas. The first being related to the determination of values of D_c and D_p which produce the most uniform state of stress in an off-axis specimen.

The conclusions drawn from this first area are the following:

1) The length to width ratios necessary for accurate testing of off-axis specimens can be greatly reduced.

2) Clamping only a portion of the tab area can reduce the differential stress in the gage length.

3) Selectively locating the pin can also reduce the differential stress in the gage length.

4) A combination of ideal clamping and pin location can minimize the differential stress in the gage length to a point where a nearly uniform stress can be produced in an economical standard geometry off-axis specimen.

5) Regardless of the amount of clamping, the pin should be located at least 1/2 in. behind the clamp edge.

6) The new test fixture can be used to experimentally produce the desired uniform state of stress in off-axis specimens using the ideal boundary conditions.

A second area of this study from which conclusions can be drawn is related to the verification of the strain energy failure criteria and nonlinear analysis.

The conclusions drawn from this area are the following:

1) Material linearity can be assumed when designing off-axis composite specimens with a minimal loss in accuracy.

2) Using the $(\pm 45)_{2S}$ laminate shear stress-strain curve in the nonlinear finite element analysis resulted in a small but tolerable error in correlation between experimental and analytical response of the off-axis specimen.

3) The graphite/epoxy off-axis specimen optimized for shear does not yield as much of the shear stress-strain curve as does the $(\pm 45)_{2S}$ laminate.

4) Reducing the exponential m parameter may improve the accuracy of the strain energy failure criteria.

5) Reducing the $\bar{K}_6$ term may also improve the accuracy of the strain energy failure criteria.

Appendix A

Stiffness and Compliance Matrices (Ref. (18))

Compliance Coefficients,

$$S_{11} = 1/E_1$$

$$S_{12} = -\nu_{12}/E_1 = -\nu_{21}/E_2$$

$$S_{22} = 1/E_2$$

$$S_{66} = 1/G_{12}$$

$$S_{16} = S_{26} = 0$$

$$\bar{S}_{11} = S_{11}m^4 + (2S_{12}+S_{66})n^2m^2 + S_{22}n^4$$

$$\bar{S}_{12} = S_{12}(n^4+m^4) + (S_{11}+S_{22}-S_{66})n^2m^2$$

$$\bar{S}_{22} = S_{11}n^4 + (2S_{12}+S_{66})n^2m^2 + S_{22}m^4$$

$$\bar{S}_{16} = (2S_{11}-2S_{12}-S_{66})nm^3 - (2S_{22}-2S_{12}-S_{66})n^3m$$

$$\bar{S}_{26} = (2S_{11}-2S_{12}-S_{66})n^3m - (2s_{22}-2S_{12}-S_{66})nm^3$$

$$\bar{S}_{66} = 2(2S_{11}+2S_{22}-4S_{12}-S_{66})n^2m^2 + S_{66}(n^4+m^4)$$

where,

$$n = \sin\theta \quad \text{and} \quad m = \cos\theta$$

Stiffness Coefficients,

$$Q_{11} = E_1/(1-\nu_{12}\nu_{21})$$

$$Q_{12} = \nu_{21}E_1/(1-\nu_{12}\nu_{21})$$

$$Q_{22} = E_2/(1-\nu_{12}\nu_{21})$$

$$Q_{66} = G_{12}$$

$$Q_{16} = Q_{26} = 0$$

$$\bar{Q}_{11} = Q_{11}m^4 + 2(Q_{12}+2Q_{66})n^2m^2 + Q_{22}n^4$$

$$\bar{Q}_{12} = (Q_{11}+Q_{22}-4Q_{66})n^2m^2 + Q_{12}(n^4+m^4)$$

$$\bar{Q}_{22} = Q_{11}n^4 + 2(Q_{12}+2Q_{66})n^2m^2 + Q_{22}m^4$$

$$\bar{Q}_{16} = (Q_{11}-Q_{12}-2Q_{66})nm^3 + (Q_{12}-Q_{22}+2Q_{66})n^3m$$

$$\bar{Q}_{26} = (Q_{11}-Q_{12}-2Q_{66})n^3m + (Q_{12}-Q_{22}+2Q_{66})nm^3$$

$$\bar{Q}_{66} = (Q_{11}+Q_{22}-2Q_{12}-2Q_{66})n^2m^2 + Q_{66}(n^4+m^4)$$

where,

$$n = \sin\theta \quad \text{and} \quad m = \cos\theta$$

Appendix B

Experimental Stress-Strain Curves

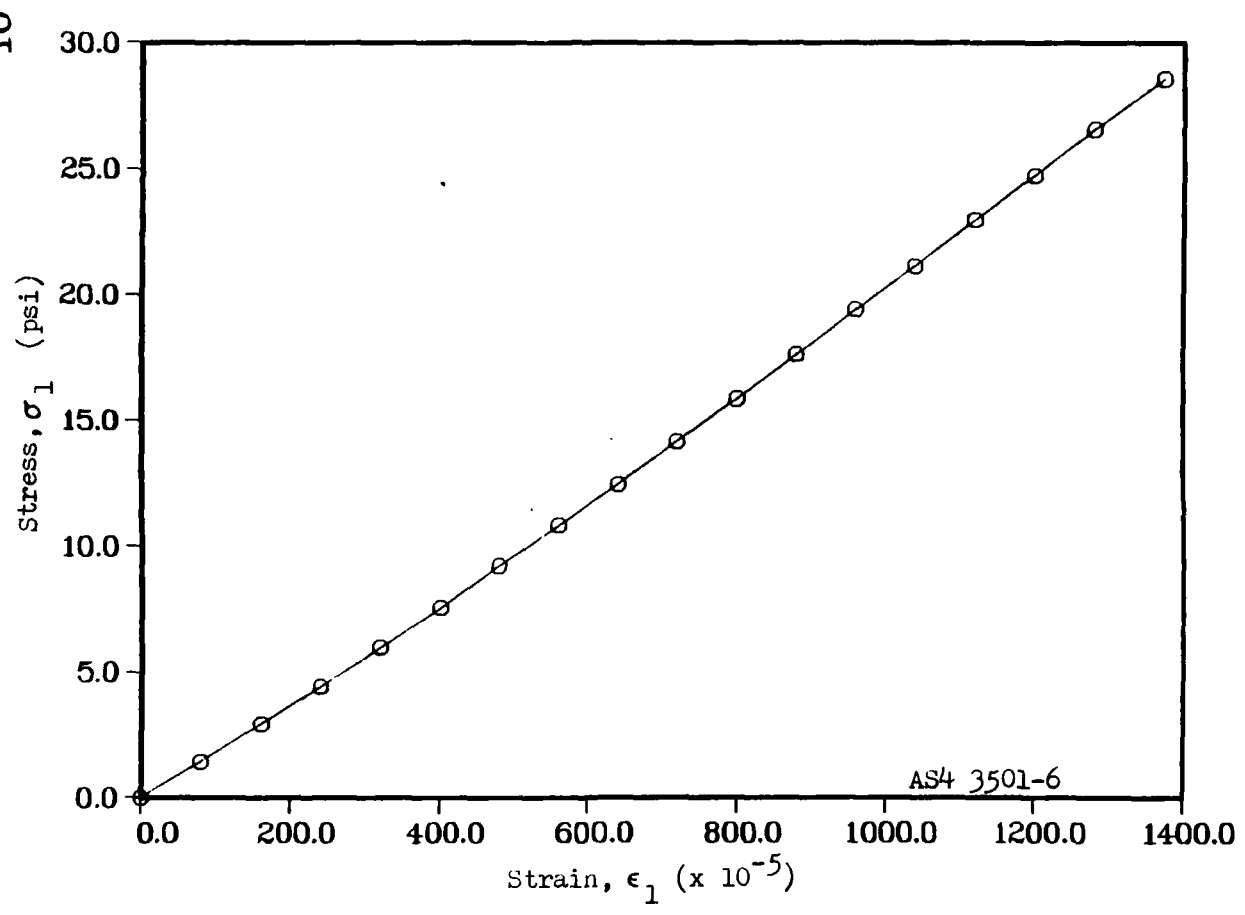

Fig. B.1 Experimental σ_1 vs. ϵ_1 for Graphite/Epoxy

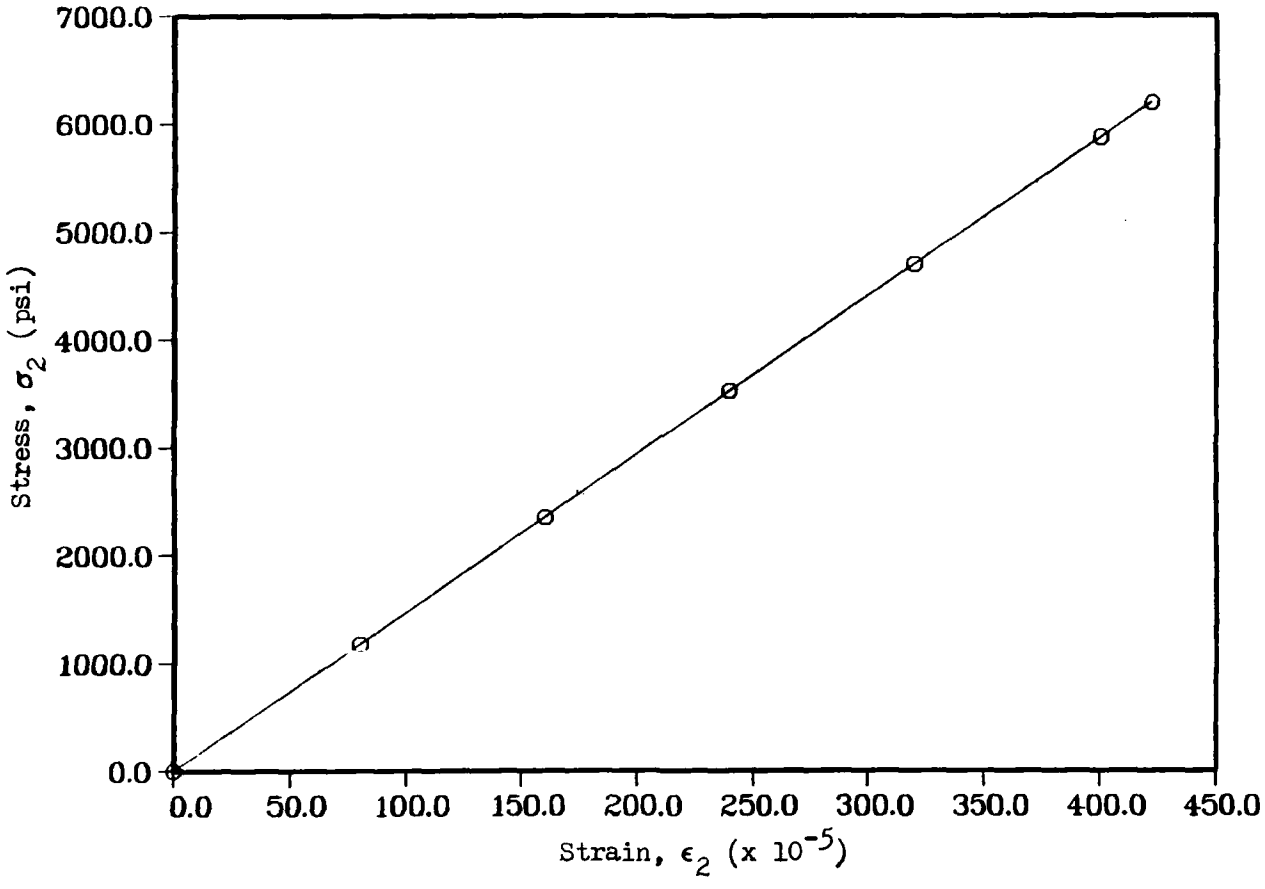

Fig. B.2 Experimental σ_2 vs. ϵ_2 for Graphite/Epoxy

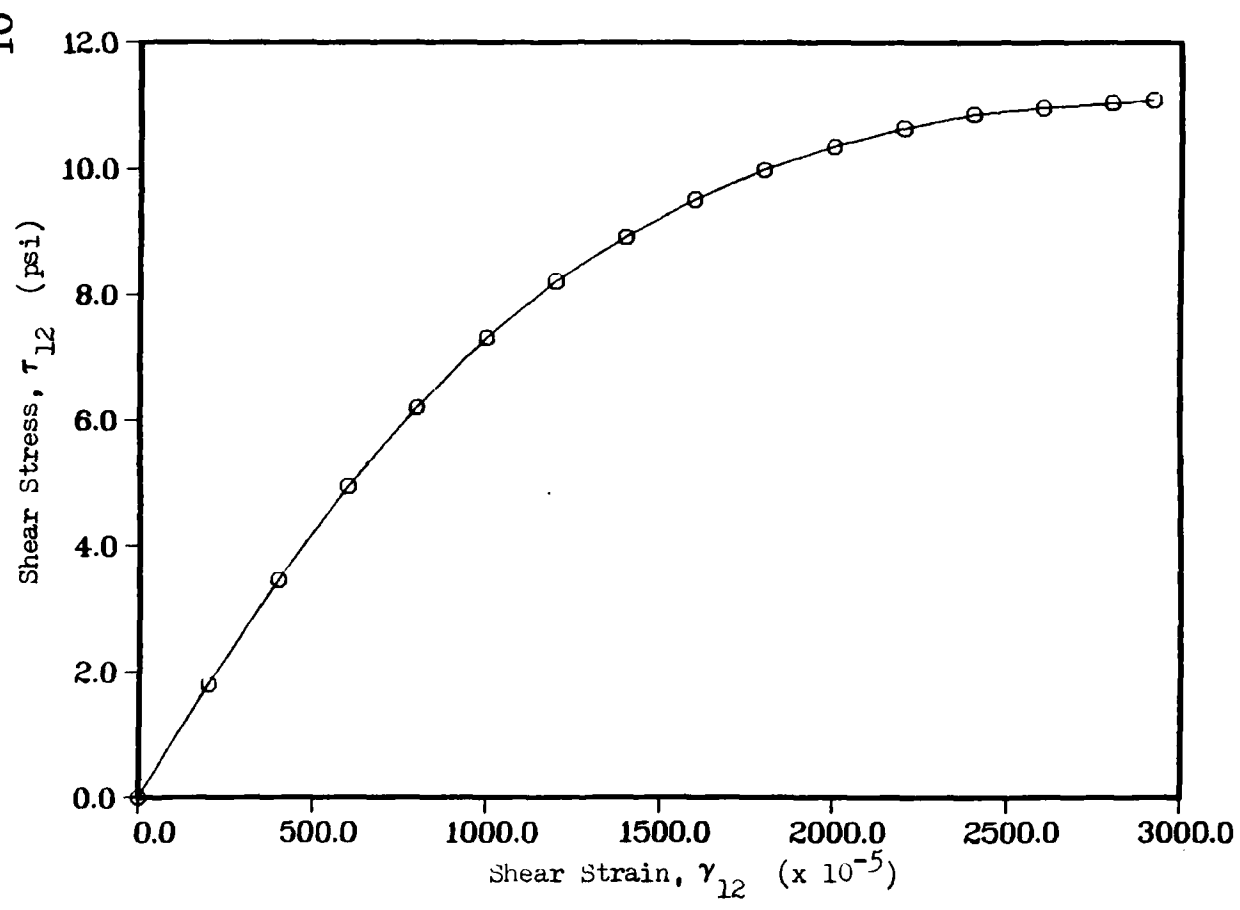

Fig. B.3 Experimental τ_{12} vs. γ_{12} for Graphite/Epoxy

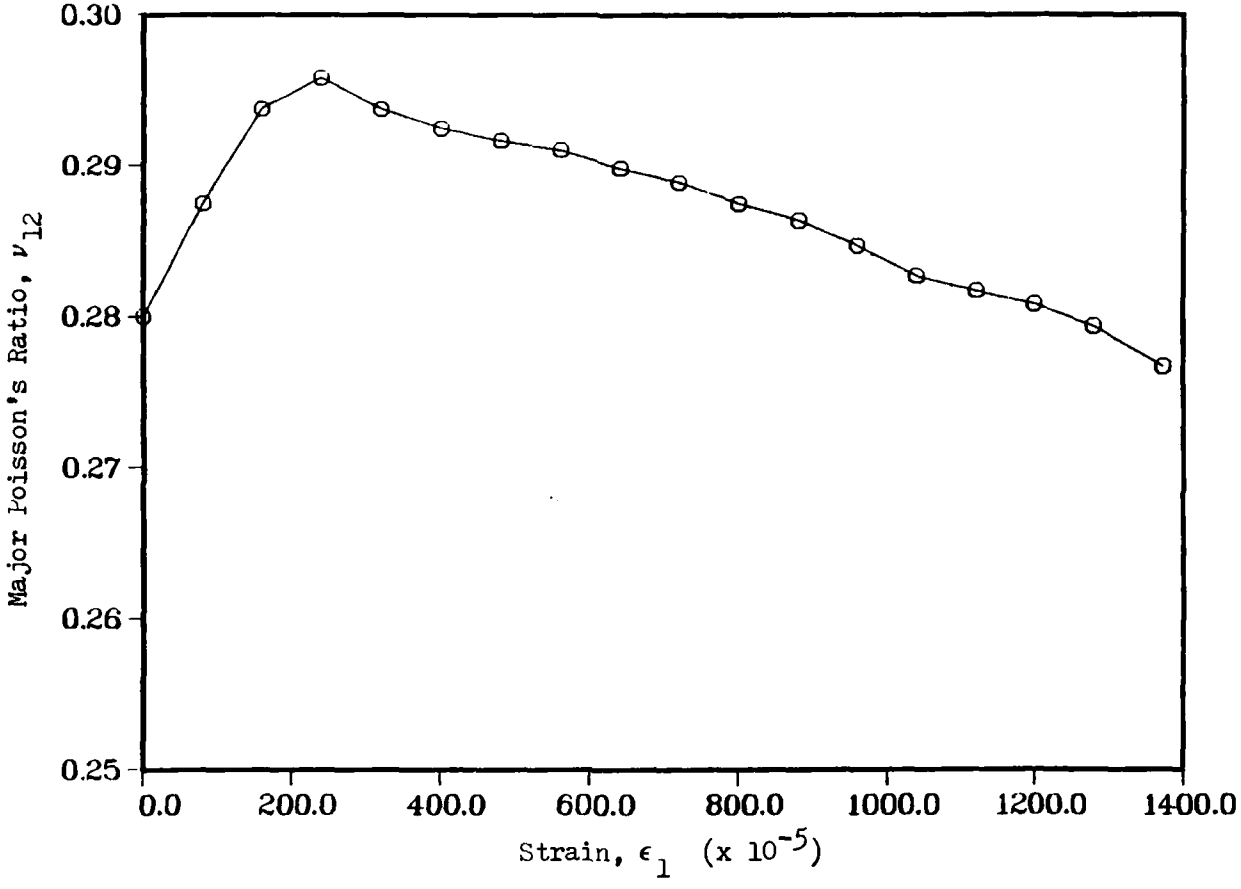

Fig. B.4 Experimental ν_{12} vs. ϵ_1 for Graphite/Epoxy

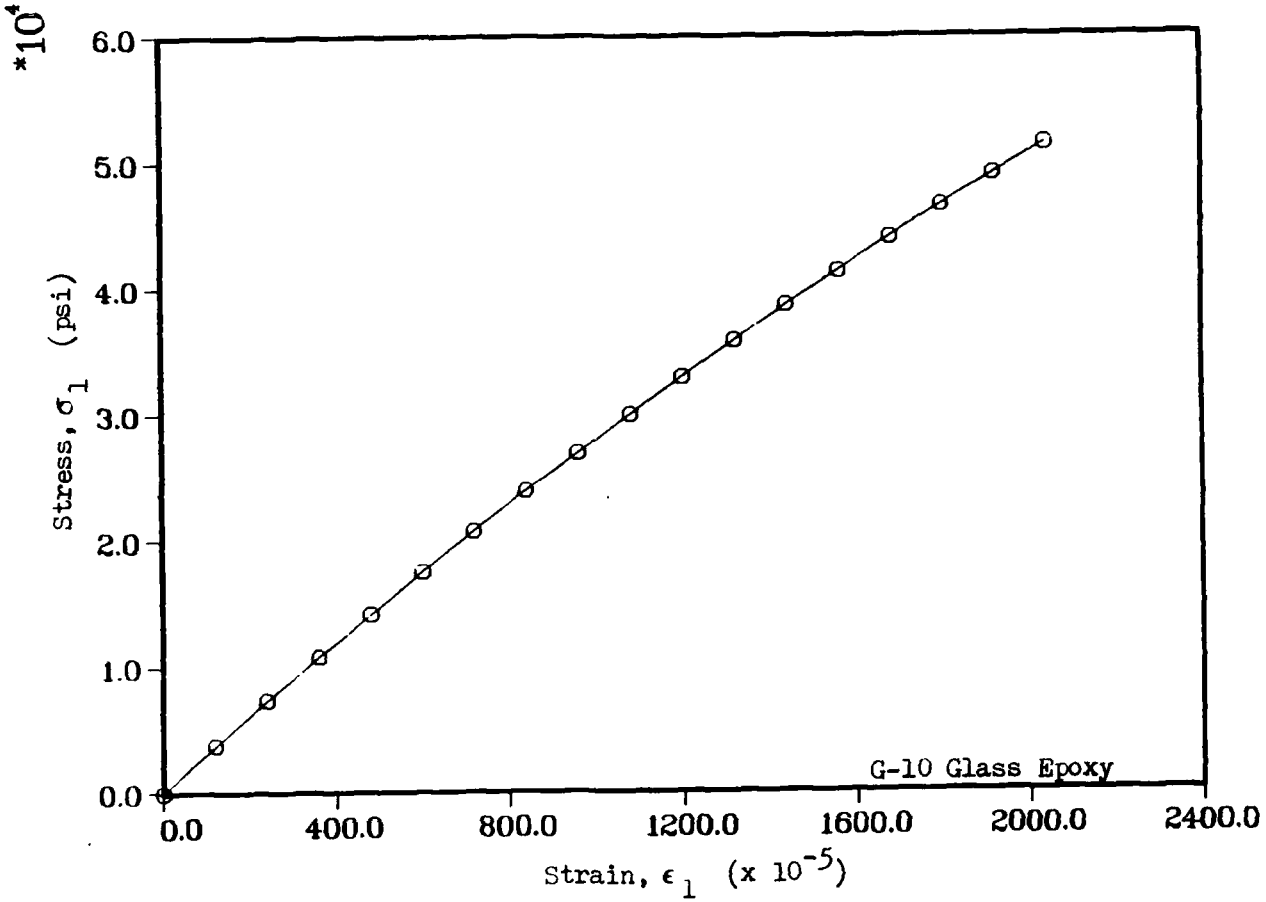

Fig. B.5 Experimental σ_1 vs. ϵ_1 for Glass/Epoxy

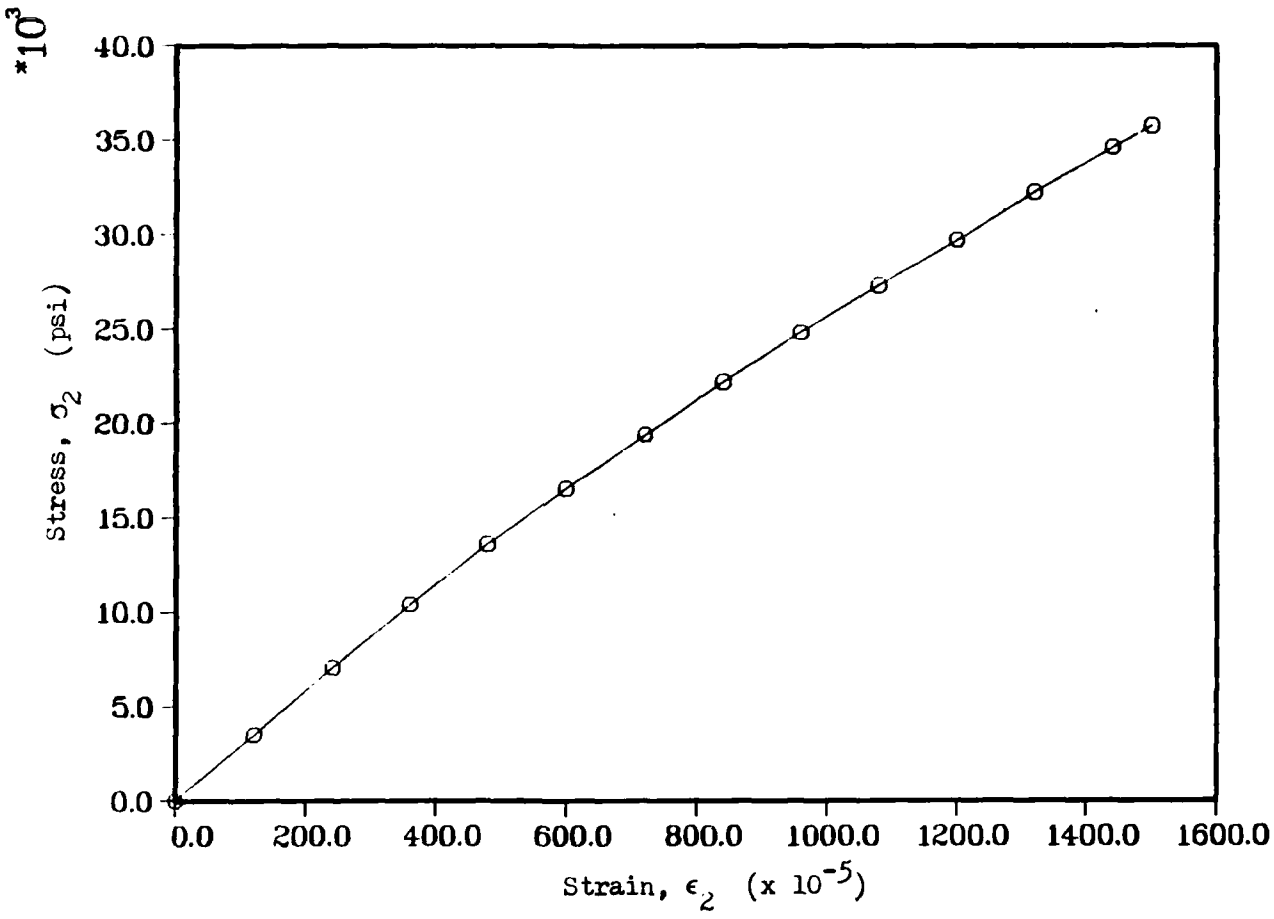

Fig. B.6 Experimental σ_2 vs. ϵ_2 for Glass/Epoxy

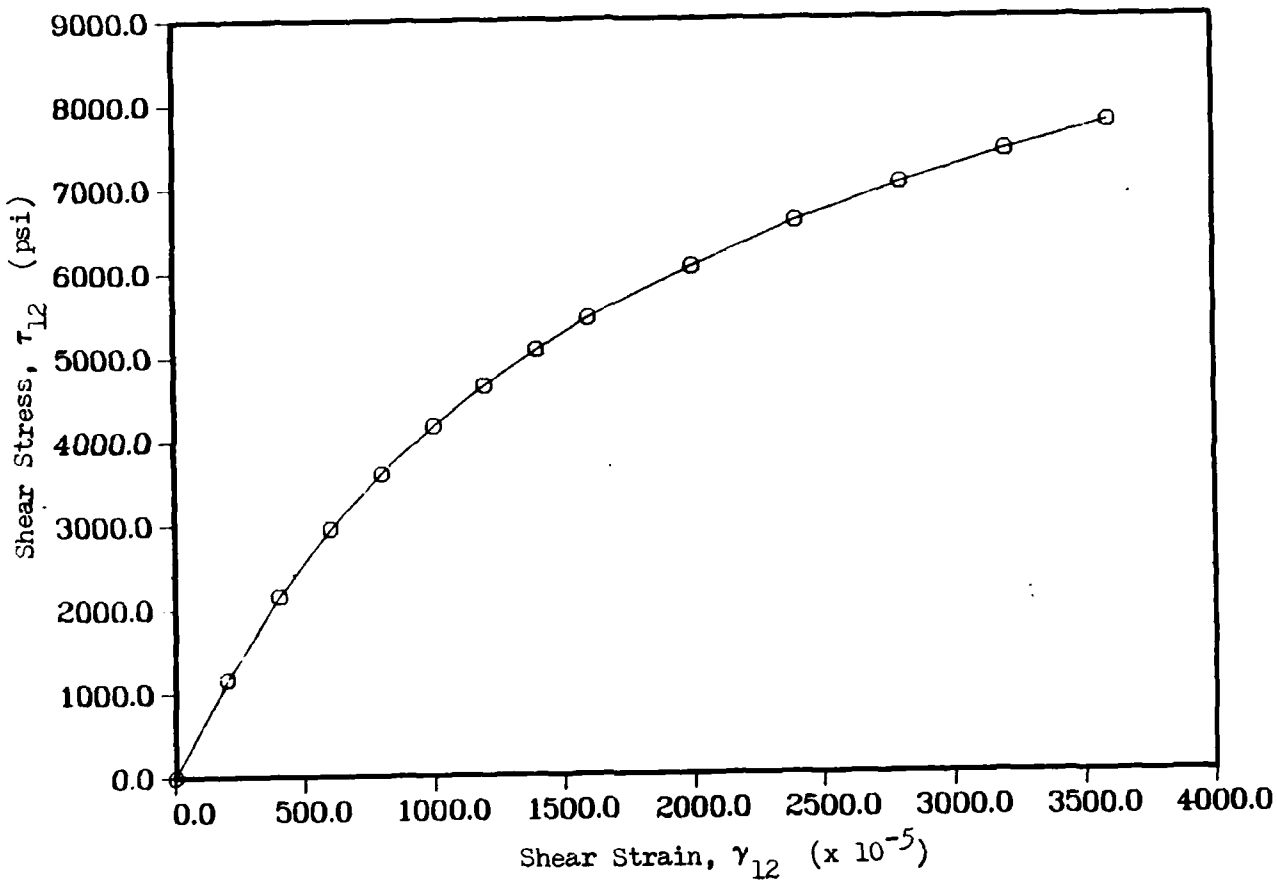

Fig. B.7 Experimental τ_{12} vs. γ_{12} for Glass/Epoxy

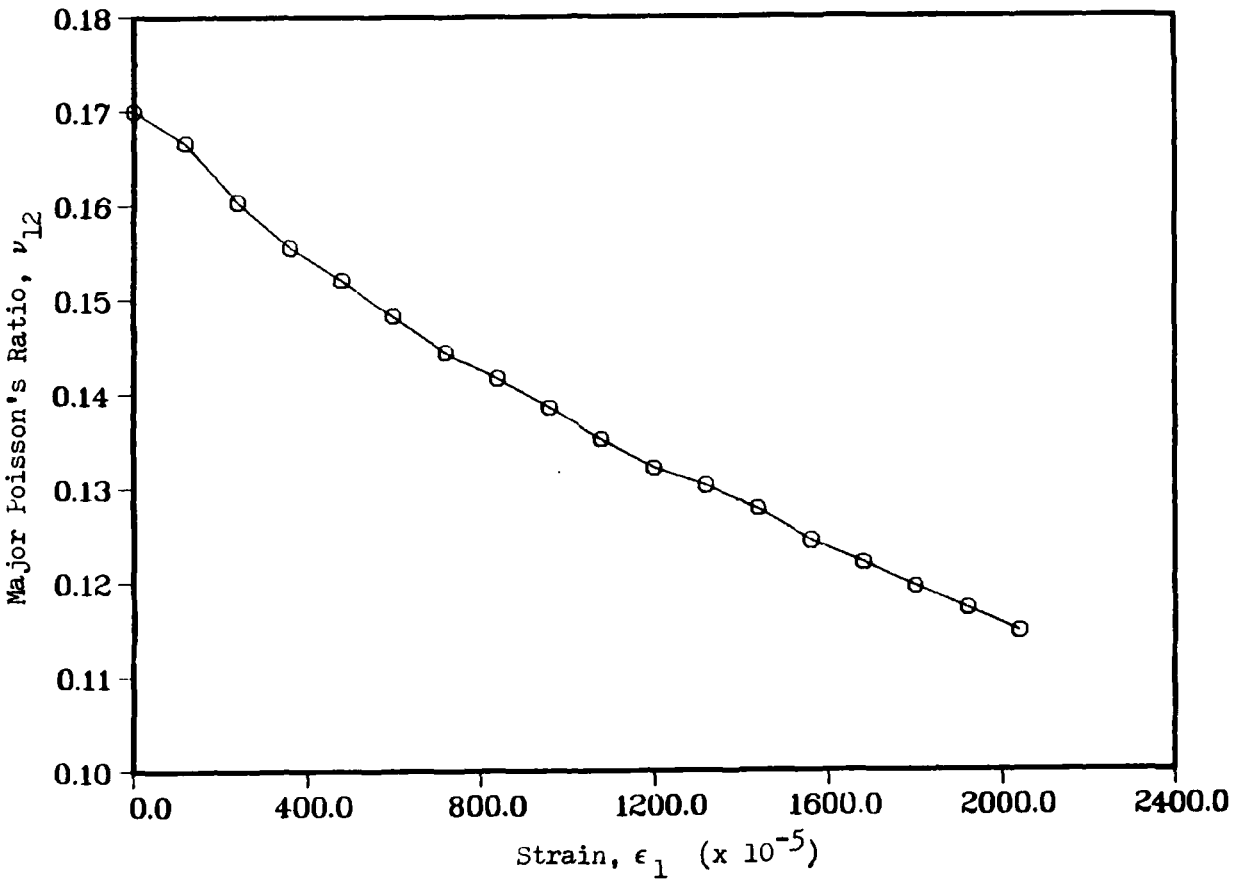

Fig. B.8 Experimental ν_{12} vs. ϵ_1 for Glass/Epoxy

Appendix C

Engineering Elastic Constants

AS4 3501-6 Graphite/Epoxy

$$E_1 = 18.844 \times 10^6 \text{ psi}$$

$$E_2 = 1.468 \times 10^6 \text{ psi}$$

$$G_{12} = 0.910 \times 10^6 \text{ psi}$$

$$\nu_{12} = 0.280$$

X, Longitudinal Tensile Strength = 285.6 ksi

Y, Transverse Tensile Strength = 6.194 ksi

S, In-Plane Shear Strength = 11.08 ksi

G-10 Glass/Epoxy

$$E_1 = 3.018 \times 10^6 \text{ psi}$$

$$E_2 = 2.890 \times 10^6 \text{ psi}$$

$$G_{12} = 0.588 \times 10^6 \text{ psi}$$

$$\nu_{12} = 0.170$$

X, Longitudinal Tensile Strength = 51.38 ksi

Y, Transverse Tensile Strength = 35.75 ksi

S, In-Plane Shear Strength = 7.740 ksi

Bibliography

1. Rizzo, R. R. "More on the Influence of End Constraints on Off-Axis Tensile Tests," Journal of Composite Materials, 3: 202-219 (April 1969).

2. Tsai, S. W., "Strength Characteristics of Composite Materials," NASA-CR 224, April 1965.

3. Azzi, V. D. and S. W. Tsai, "Anisotropic Strength of Composites," presented at the Spring Meeting, Society for Stress Analysis, May 1965.

4. Lauraitis, K.,"Tensile Strength of Off-Axis Unidirectional Composites," T. & A. M. Report No 344, Department of Theoretical and Applied Mechanics, University of Illinois, Urbana, Illinois, August 1971.

5. Pagano, N. J. and J. C. Halpin, "Influence of End Constraint in the Testing of Anisotropic Bodies," Journal of Composite Materials, 2 (1): 18-31 (January 1968).

6. Wu, E. M. and R. L. Thomas, "Off-Axis Test of a Composite," Journal of Composite Materials, 2 (4): 523-526 (October 1968).

7. Richards, G. L., T. P. Airhart, and J. E. Ashton, "Off-Axis Tensile Coupon Testing," Journal of Composite Materials, 3: 586-589 (July 1969).

8. Pipes, R. B. and B. W. Cole, "On the Off-Axis Strength Test for Anisotropic Materials," Journal of Composite Materials 7: 246-256 (April 1976).

9. Chamis, I. M. and J. H. Sinclair, "10^{o} Off-Axis Tensile Test for Interlaminar Shear Characterization of Fiber Composites," NASA TN D-8215, April 1976.

10. Chang, B. W., P. H. Huang, and D. G. Smith, "A Pinned-End Fixture for Off-Axis Testing," Experimental Techniques pp. 28-30 (June 1984).

11. Sandhu, R. S. and G. P. Sendeckyj, "On Design of Off-Axis Specimens," AFWAL-TR-84-3098, Air Force Flight Dynamics Laboratory, Wright-Patterson Air Force Base, Ohio, March 1984.

12. Sandhu, R. S., "Ultimate Strength Analysis of Symmetric Laminates," AFFDL-TR-73-137, AD 779927, Air Force Flight Dynamics Laboratory, Wright-Patterson Air Force Base, Ohio, 1974.

13. Sandhu, R. S., "Nonlinear Behavior of Unidirectional and Angle Ply Laminates," Journal of Aircraft, 13 (2): 104-111 (February 1976).

14. Whitney, J. M., I. M. Daniel, and R. B. Pipes. Experimental Mechanics of Fiber Reinforced Composite Materials. Englewood Cliffs NJ: Prentice-Hall, Inc., 1984.

15. Daniel, I. M. and T. Liber, "Lamination Residual Stresses in Fiber Composites," NASA CR-134826, 1975.

16. Nemeth, M. P., C. T. Herakovich, and D. Post, "On the Off-Axis Tension Test for Unidirectional Composites," Composites Technology Review, 5 (2): 61-68 (Summer 1983).

17. Kobayashi, A. S., ed., Manual on Experimental Stress Analysis, 4th ed., Brookfield Center Connecticut: Society for Experimental Stress Analysis, 1983.

18. Jones, R. M. Mechanics of Composite Materials. Washington D. C.: Scripta Book Company, 1975.

VITA

Steven M. Cron was born in Norwalk, California on 21 December 1961. He graduated from La Sierra High School in Carmichael, California in 1980. He then studied Mechanical Engineering at the University of Missouri, Columbia where he graduated in May 1984, Magna Cum Laude, with a Bachelor of Science in Mechanical Engineering. Upon graduation, he received a commission in the USAF through the ROTC program. He entered active duty in May 1984 when he started his study for a Master of Science in Aeronautical Engineering at the Air Force Institute of Technology.

Permanent address: 507 S. Juniper St.
Toppenish, WA 98948

UNCLASSIFIED

SECURITY CLASSIFICATION OF THIS PAGE AD-A164 321

REPORT DOCUMENTATION PAGE

1a. REPORT SECURITY CLASSIFICATION UNCLASSIFIED	1b. RESTRICTIVE MARKINGS
2a. SECURITY CLASSIFICATION AUTHORITY	3. DISTRIBUTION/AVAILABILITY OF REPORT Approved for public release; distribution unlimited
2b. DECLASSIFICATION/DOWNGRADING SCHEDULE	
4. PERFORMING ORGANIZATION REPORT NUMBER(S) AFIT/GAE/AA/85D-3	5. MONITORING ORGANIZATION REPORT NUMBER(S)
6a. NAME OF PERFORMING ORGANIZATION School of Engineering 6b. OFFICE SYMBOL (If applicable) AFIT/EN	7a. NAME OF MONITORING ORGANIZATION
6c. ADDRESS (City, State and ZIP Code) Air Force Institute of Technology Wright Patterson AFB, Ohio 45433	7b. ADDRESS (City, State and ZIP Code)
8a. NAME OF FUNDING/SPONSORING ORGANIZATION 8b. OFFICE SYMBOL (If applicable)	9. PROCUREMENT INSTRUMENT IDENTIFICATION NUMBER
8c. ADDRESS (City, State and ZIP Code)	10. SOURCE OF FUNDING NOS. PROGRAM ELEMENT NO. / PROJECT NO. / TASK NO. / WORK UNIT NO.
11. TITLE (Include Security Classification) See Box 19	
12. PERSONAL AUTHOR(S) Steven M. Cron, 2LT, USAF	
13a. TYPE OF REPORT MS Thesis 13b. TIME COVERED FROM _____ TO _____	14. DATE OF REPORT (Yr., Mo., Day) 1985 December 15. PAGE COUNT 133
16. SUPPLEMENTARY NOTATION	

17. COSATI CODES		
FIELD	GROUP	SUB. GR.
11	04	

18. SUBJECT TERMS (Continue on reverse if necessary and identify by block number)
Composite Materials, Test Method, Test Fixture, Failure Criteria, Nonlinear

19. ABSTRACT (Continue on reverse if necessary and identify by block number)

Title: Improvement of End Boundary Conditions for Off-Axis Tension Specimen Use

Thesis Advisor: Anthony N. Palazotto
Department of Aeronautics and Astronautics

Approved for public release: IAW AFR 190-1.
LYNN E. WOLAVER 16 JAN 86
Dean for Research and Professional Development
Air Force Institute of Technology (AFIT)
Wright-Patterson AFB OH 45433

20. DISTRIBUTION/AVAILABILITY OF ABSTRACT UNCLASSIFIED/UNLIMITED ☒ SAME AS RPT. ☐ OTIC USERS ☐	21 ABSTRACT SECURITY CLASSIFICATION UNCLASSIFIED
22a. NAME OF RESPONSIBLE INDIVIDUAL Anthony N. Palazotto	22b. TELEPHONE NUMBER (Include Area Code) 513-255-3517 22c. OFFICE SYMBOL AFIT/ENY

DD FORM 1473, 83 APR EDITION OF 1 JAN 73 IS OBSOLETE.

UNCLASSIFIED
SECURITY CLASSIFICATION OF THIS PAGE

Inaccuracies in using the off-axis tension test are caused by the nonuniform stresses produced by the end constraints. The purpose of this study is to show that these nonuniformities can be virtually eliminated by adjusting the amount of tab clamping and selectively locating the point about which the clamp may rotate. A second phase of the study is to conduct a limited verification of a strain energy failure criteria that can account for the material nonlinearity found in composites.

Determination of the ideal amount of clamping and point of rotation was carried out using a linear finite element method. The nonlinear behavior of the specimen was simulated using a nonlinear finite element method. The failure criteria was used in conjunction with the nonlinear finite element algorithm in determining failure. Experimentation was also carried out to verify the finite element solutions.

The results indicate that a nearly uniform state of stress can be produced with ideal tab clamping and rotation. The results indicate that the nonlinear behavior of the specimen was accurately predicted by the nonlinear finite element method but that the failure state predicted by the failure criteria was in error. Suggestions are made for improving the accuracy of the failure criteria.

END